α/β-Hydrolase Domain Containing Protein 15 (ABHD15)- Deeper Characterization and Functional Investigation of a Promising New Player of Adipogenesis

Dissertation

by

Dipl.-Ing. Evelyn Walenta

Graz University of Technology

Institute for Genomics and Bioinformatics

supervised by

Assoc.Prof. Mag.rer.nat. Dr.rer.nat. Juliane Bogner-Strauß

Graz, August 2013

STATUTORY DECLARATION

I declare that I have authored this thesis independently, that I have not used other than the declared sources / resources, and that I have explicitly marked all material which has been quoted either literally or by content from the used sources.

…… ……..

date (signature)

Acknowledgement

The last years, the time as a doctoral student, have been one of the most life changing and formative years of my life. For these years, I deeply want to thank my Professor and supervisor Juliane Bogner-Strauß. She supported me at every point of my thesis and made impossible things possible for me. Without her guidance, motivation, and help, this dissertation would not have been possible.

I would like to thank my thesis committee members, Professor Karin Athenstaedt and Professor Günter Hämmerle, who shared their great knowledge with me. Their ideas and also their help to see my experiments and the results from a different point of view opened new research opportunities.

Furthermore I want to thank Professor Dagmar Kratky and Madeleine Göritzer from the Institute of Molecular Biology and Biochemistry at the Medical University of Graz, who shared their wide knowledge of ER stress and apoptosis with me. I also want to give thanks to Alexander Deutsch from the Division of Hematology of the Medical University of Graz, who helped me with the apoptosis assays. For the help with HPLC-MS analysis, I want to thank Harald Köfeler from the mass spectrometry core facility of the Medical University of Graz, Christoph Magnes from the Institute for Bioanalytics and Metabolomics of Joanneum Research, and Gerald Rechberger from the Institute of Molecular Bioscience at the University of Graz. Further I deeply want to thank Franz Radner from the Institute of Molecular Bioscience at the University of Graz for the help to generate the knockout mice. I also want to give thanks to Jerrold Olefsky at the University of California San Diego, who let me collect experience in his laboratory, and also to DaYoung Oh, who supervised me during this year abroad. Furthermore, I thank the Public Library of Science for permission to include chapter eight of my dissertation, which is in revision for publication in PLOS ONE. Financially support was provided by the Graz University of Technology and the international PhD Program “Metabolic and Cardiovascular Disease”.

I’m also very thankful for the great support of my team at the Institute for Genomics and Bioinformatics, Ariane Pessentheiner, Andreas Prokesch, Helmut Pelzmann, Florian Stöger, Claudia Neuhold, and Thomas Schreiner. Not to forget, I want to thank Michael Maris for scientific and moral support, and all other friends I can’t name here. Finally, I want to thank my family. Without the inspiring example of my parents and siblings, who supported me in every possible way, I would not be the person I am today!

Abstract

Our knowledge about adipocyte metabolism and development is steadily growing, yet many players are still undefined.

This thesis clearly shows that α/β-hydrolase domain containing protein 15 (*Abhd15*) is a direct and functional target gene of peroxisome proliferator-activated receptor gamma **(**PPARγ), the master regulator of adipogenesis. Stable knockdown of *Abhd15* in 3T3-L1 cells evokes a striking differentiation defect, as evidenced by low lipid accumulation and decreased expression of adipocyte marker genes. In preconfluent cells, knockdown of *Abhd15* leads to impaired proliferation, which is caused by apoptosis, as we see an increased SubG1 peak, Caspase 3/7 activity, and pro-apoptotic regulation of the apoptosis marker proteins B-cell lymphoma protein 2 (BCL-2) and BCL-2-associated X protein (BAX). Furthermore, apoptosis-inducing concentrations of palmitic acid evoke a massive increase of *Abhd15* expression, proposing an apoptosis-protecting role for *Abhd15*. On the other hand, in mature adipocytes, physiological (i.e. non-apoptotic) concentrations of palmitic acid down-regulate *Abhd15* expression. Accordingly, we found that the expression of *Abhd15* in adipose tissue is reduced in physiological situations with high free fatty acid levels, like high-fat diet, fasting, and aging as well as in genetically obese mice.

Preliminary results of a *Abhd15-ko* mouse model however indicate increased adipose tissue mass, probably due to increased cell proliferation, and slight insulin resistance.

Taken together, our results position *Abhd15* as an essential component in the development of adipocytes, in apoptosis, and cell proliferation, thereby connecting three substantial factors in the regulation of adipocyte number and size. Together with its intricate regulation by free fatty acids, ABHD15 might be an intriguing new target in obesity and diabetes research.

Abstract (German)

Unser Wissen über den Metabolismus von Adipozyten wächst konstant. Trotzdem sind noch immer viele Gene, die in der Enstehung von Adipozyten eine Rolle spielen könnten, uncharakterisiert.

Diese Dissertation kann klar zeigen, dass *Abhd15* (α/β-hydrolase domain containing protein 15) ein direktes und funktionelles Zielgen von PPARγ (peroxisome proliferator-activated receptor gamma), dem sogenannten “Master Regulator” der Adipogenese, ist. Stabiles Silencing von *Abhd15* in 3T3-L1 Zellen führt zu einem schwerwiegenden Differenzierungsdefekt, reflektiert in niedriger Lipideinlagerung und reduzierter Expression von Adipogenese Markergenen. In prekonfluenten Zellen wiederum führt stabiles Silencing von *Abhd15* zur Beeinträchtigung der Proliferation, hervorgerufen durch erhöhte Apoptose. Die verstärkte Apoptose konnte klar durch den erhöhten SubG1 Peak, die erhöhte Caspase Aktivität, die erniedrigte Proteinexpression des Antiapoptosemarkers BCL-2 (B-Cell Lymphoma Protein 2) und die erhöhte Proteinexpression des Proapoptosemarkers BAX (BCL-2-associated X Protein) bewiesen werden. Des Weiteren führen Apoptose-induzierende Mengen von Palmitinsäure zu einem massiven Anstieg der *Abhd15* Expression, was darauf hindeutet, dass ABHD15 eine vor Apoptose schützende Rolle haben könnte. Auf der anderen Seite führen physiologische Konzentrationen von Palmitinsäure (sprich Konzentrationen, die keine Apoptose hervorrufen), zu einer negativen Regulation der *Abhd15* Expression in reifen Adipozyten. In Übereinstimmung damit ist die Expression von *Abhd15* in Fettgeweben unter phsyiologischen Bedingungen, die zu hohen freien Fettsäurewerten im Blut führen, wie z.B. eine fettreiche Diät, das Fasten, das Altern so wie in genetisch bedingt fettleibigen Mäusen, reduziert. Im Gegesatz zu den Zellkulturversuchen, weisen vorläufige Ergebnisse der Untersuchung von *Abhd15*-knockout Mäusen auf erhöhte Fettgewebsmasse hin, die durch erhöhte Zellproliferation entstehen könnten. Passend dazu, zeigen *Abhd15*-knockout Mäuse eine leichte Insulinresistenz.

Insgesamt deuten die Ergebnisse dieser Dissertation auf eine essentielle Rolle von ABHD15 in der Entwicklung von Adipozyten, in der Apoptose und der Zellproliferation hin. Dadurch verbindet ABHD15 drei grundlegende Faktoren die die Anzahl und die Größe von Adipozyten regulieren. Durch diese Tatsache, und dadurch dass die Regulation von *Abhd15* stark von der vorhandenen Menge freier Fettsäuren abhängig zu sein scheint, könnte ABHD15 ein vielversprechendes neues Zielgen für die Behandlung von Fettleibigkeit und Diabetes sein.

Contents

1 Abbreviations 3
2 Introduction 6
3 Materials & Methods 13
3.1 Animal studies 14
3.2 Promoter analysis 14
3.3 Luciferase reporter assays 14
3.4 Cell culture, differentiation, and lipid staining 15
3.5 Culturing of mouse epididymal fat pads and liver 15
3.6 Isolation of adipocytes and SVCs 16
3.7 RNA isolation, reverse transcription, and gene expression analysis 16
3.8 Silencing of Abhd15 using short hairpin (sh)RNA-lentivirus particles 17
3.9 Silencing of Abhd15 via electroporation using siRNA 18
3.10 Generation of recombinant retroviruses 18
3.11 Generation of mutated (T142A, S425A, S442A) and C-terminally FLAG-tagged Abhd15 18
3.12 Western blot analysis 19
3.13 Glucose uptake 19
3.14 Thin Layer Chromatography (TLC) 20
3.15 Lipid analysis with UPLC-QTOF-MS 20
3.16 HPLC-MS measurement of fatty acid precursors 21
3.17 Assessment of cell growth 21
3.18 BrdU cell cycle analysis 21
3.19 Caspase-Glo 3/7 assay 21
3.20 Southern blot analysis 21
3.21 Blood plasma FFA and TG measurement 22
3.22 Glucose and insulin tolerance test (GTT and ITT) 22
3.23 Statistical analysis 22
4 Results 23
4.1 Expression and regulation of Abhd15 24
4.1.1 *Abhd15* is a direct and functional target gene of PPARγ 24
4.1.2 *Abhd15* mRNA expression is decreased in adipose tissue dependent on free fatty acid levels 25
4.1.3 *Abhd15* expression is induced in macrophages upon inflammation 28
4.1.4 Potential secretion of ABHD15 29
4.2 Investigations of the function of ABHD15 34

4.2.1 *Abhd15* overexpression influences glucose uptake 34
4.2.2 Stable overexpression of *Abhd15* can influence the lipid profile 35
4.2.3 *Abhd15* is required for adipogenesis 42
4.2.4 *Abhd15* expression effects adipocyte development 44
4.2.5 *Abhd15* expression is tightly connected to apoptosis 50
4.3 Establishment of the Abhd15-ko mouse 54
4.3.1 Generation of *Abhd15*-deficient and loxP-tagged ES cells and birth of chimeric founders 54
4.3.2 Preliminary characterization of *Abhd15* whole body knockout mice 56
5 Discussion 76
6 Figure Legends 87
7 References 90
8 Appendix 97
8.1 Submitted Manuscript (PLOS ONE, PONE-D-13-25085) 98

1 Abbreviations

1 Abbreviations

Abhd15	α/β-hydrolase domain containing protein 15 gene
ABHD15	α/β-hydrolase domain containing protein 15 protein
APMAP	adipocyte plasma membrane associated protein
ARXES	adipocyte-related X-chromosome expressed sequence
ATF (3, 4, 6)	activating transcription factor (3, 4, 6)
BAT	brown adipose tissue
BAX	BCL-2-associated X protein
BCL-2	B-cell lymphoma protein 2
BMDC	bone marrow derived dendritic cells
BMDM	bone marrow derived macrophages
BSA	bovine serum albumin
cAMP	cyclic adenosine monophosphate
cGMP	cyclic guanosine monophosphate
CDK2	cyclin dependent kinase 2
cDNA	complementary DNA
C/EBP (α, β, δ)	CCAAT-enhancer-binding protein (α, β, δ)
CHOP	transcript factor homologous to CCAAT-enhancer-binding protein
CFP	cyan fluorescent protein
DMEM	Dulbecco's modified eagle medium
DMSO	dimethylsulfoxide
EDTA	ethylenediaminetetraacetate
ER	endoplasmic reticulum
ES cells	embryonic stem cells
eWAT	epididymal white adipose tissue
FA	fatty acid
FABP4	fatty acid binding protein 4
FAS	Fatty acid synthase
FBS	foetal bovine serum
FFA	free fatty acid
GAA	glacial acetic acid
GLUT4	glucose transporter type 4 protein
GTT	glucose tolerance test
HFD	high fat diet
HPLC-MS	high pressure liquid chromatography mass spectrometry
His-Tag	codon for six histidines in a row
IBMX	3-Isobutyl-1-methylxanthine
IL-6	interleukin 6

1 Abbreviations

IRE1	inositol-requiring enzyme 1
IRS1	insulin receptor substrate 1 protein
ITT	insulin tolerance test
ko	knockout
MCE	mitotic clonal expansion
ntc	non-targeting control
ob	obese gene
PBS	phosphate buffered saline
PDE3B	phosphodiesterase 3B
PERK	RNA-activated protein kinase (PKR)-like ER-resident kinase (PERK)
PGC-2	PPARγ coactivator 2 protein
PIC	protease inhibitor cocktail
pMSCV	murine stem cell virus plasmid
PPAR (α/γ2)	peroxisome proliferator-activated receptor (α/γ2)
PPRE	peroxisome proliferator-activated receptor response elements
pRB	pocket protein retinoblastoma
P/S	penicillin/streptomycin
qPCR	quantitative polymerase chain reaction
Rosi	rosiglitazone maleate
RXRα	retinoid X receptor alpha
shRNA	small hairpin RNA
siRNA	small interfering RNA
SIRT1	sirtuin 1
SK (1, 2)	sphingosine kinase
SREBP1c	sterol regulatory element binding protein 1c
sWAT	subcutaneous white adipose tissue
SVC	stromal vascular cells
TG	triglyceride
TLC	thin layer chromatography
TNFα	tumor necrosis factor α
TPA	12-O-tetredecanoylphorbol-13-acetate
TZD	thiazolidinedione
UCP1	uncoupled protein 1
WAT	white adipose tissue
wt	wild-type
Xbp1s	X-box binding protein 1 spliced gene

2 Introduction

2 Introduction

During the last decade, obesity became one of the major pandemics and is strongly associated with several diseases, such as type 2 diabetes, liver cirrhosis, cardiovascular diseases, and certain cancers.[1,2] Therefore obesity increases morbidity and mortality[2], but additionally socio-economic repercussions cannot be negligible[3,4].
As we live in a well-nourished society combined with a reduced requirement for physical exercise, we are exposed to ideal conditions for overweight. Nevertheless, many individuals are still lean while others become obese, hinting at an important influence of genetic factors that might predispose humans to obesity. Especially severe obesity is often a result of genetic disorders.[5,6] Consequently, it is of extreme importance to gain a better insight into adipocyte development and the link between adipose tissue biology and disturbed metabolism, especially as the further identification and enlightenment of molecules and genes that influence adipogenesis will possibly lead to new options for the treatment of obesity.

Obesity is characterized by an excessive increase in number and size of adipocytes, factors tightly regulated by the rate of proliferation of preadipocytes and the differentiation into mature adipocytes.[7] Despite a negative connotation of adipocytes in the context of obesity, they possess some highly important functions. Adipocytes are specialized in synthesis and storage of big amounts of triglycerides, and therefore, besides acting as thermal isolation layer[8], they are also essential regulators of whole-body energy homeostasis. Furthermore, beginning with the discovery of leptin nearly two decades ago, it was shown how adipocytes can coordinate energy balance and glucose homeostasis via secreted proteins.[9,10] Since then, the family of adipocyte derived signaling molecules grew, and so did their field of action. Many of those so called adipokines exert positive or negative actions on processes like adipogenesis and energy balance, but additionally haemostasis, blood pressure, and immune function.[10,11] So do leptin[9], adiponectin[12], and visfatin[13] promote insulin sensitivity, whereas resistin[14], retinol binding protein (RBP)4[15], and lipocalin2[16] induce insulin resistance.
As adipocytes play such a major role in energy metabolism, the process in which fibroblasts can differentiate into mature adipocytes, the so called adipogenesis, has been well investigated. [10] Adipogenesis can be divided into two main phases, the determination and the terminal differentiation phase. During the determination phase, pluripotent stem cells are converted into mutlipotent mesenchymal stem cells, and subsequently into preadipocytes. These steps do not include any morphological changes, whereas during the terminal differentiation, preadipocytes convert into mature adipocytes, including the characteristics like the machinery for lipid transport and synthesis, insulin sensitivity, and secretion of specific proteins.[10] This second phase of adipogenesis again can be divided into early and late terminal differentiation. Especially in 3T3-L1 cells, a preadipocyte model, the first steps

of early differentiation include growth arrest due to cell-cell contact, followed by two sequential rounds of mitosis, called mitotic clonal expansion (MCE).[17] MCE involves a transcription factor cascade, followed by the expression of adipocyte genes[18]. Thus, like growth arrest, MCE is a prerequisite for late differentiation.[17] Hence, early as well as late terminal differentiation are processes highly controlled through the sequential activation of several genes, most of them transcription factors.[19–21] The CCAAT-enhancer-binding protein (C/EBP) family, for example, contains three of the most important adipogenic transcription factors, C/EBPα, C/EBPβ, and C\EBPδ. Homodimers of the early differentiation marker C/EBPβ, but even more effectively heterodimers of C/EBPβ and C/EBPδ,[22] induce the expression of peroxisome proliferator-activated receptor gamma (PPARγ) and of C/EBPα.[20] In contrast to C/EBPβ and C/EBPδ, PPARγ as well as C\EBPα are required and sufficient for the adipocyte differentiation. The requirement of C/EBPα can be overcome by inducing agents, but nothing can rescue adipogenesis of cells lacking PPARγ.[10,20] Therefore and because many genes of the adipogenesis regulating cascade are either regulated by PPARγ or regulate PPARγ ,[10] this gene is called the "master regulator of adipogenesis".[19,23,24] PPARγ appears in a heterodimeric complex with retinoid X receptor alpha (RXRα) and acts as a ligand activated transcription factor.[11,25–27] Target genes of PPARγ include a cognate DNA element called PPAR response element (PPRE), which is transcriptionally activated during adipocyte differentiation and has been identified in a number of adipocyte genes.[11,20,25] On the other hand, the ligands of PPARγ have a critical role in induction and maintenance of the adipogenic differentiation process. Although the major endogenous ligand is not known yet, synthetic and natural activators were identified, including some possibly indirect acting ones. Interestingly, all naturally occurring ligands are derived from arachidonic acid.[11,20,25] Examples of synthetic activators are Thiazolidinediones (TZDs), which are used as drugs against type II diabetes.[28] TZDs have pro-adipogenic properties on fibroblasts and myoblasts, and the application increases insulin sensitivity.[11] The range of PPARγ ligands is very broad. It stretches from some long chain fatty acids over fatty acid metabolites to eicosanoids.[20,25] As diverse as the ligands are the "producers" of these ligands. One out of them is the sterol regulatory element binding protein 1c (SREBP1c), a protein which increases fatty acid and fat synthesis. Hence, it is hypothesized to be involved in the generation of endogenous ligands for PPARγ.[29] Therefore several players of adipogenesis, amongst them the hydrolase described in this thesis, are potential producers of PPARγ ligands and might thereby regulate adipogenesis as well.

Besides proliferation and adipogenesis, it has been demonstrated that apoptosis of pre-adipocytes as well as mature adipocytes is a potent player in the regulation of adipose tissue mass.[7] Therefore, reduction of adipocytes by induced/increased apoptosis may be an

additional treatment to other therapies.[30] Conversely, adipocyte apoptosis is increased in diet-induced obesity, and inhibition of apoptosis protects from adipose tissue macrophage recruitment, development of fatty liver, and insulin resistance of obese animals.[31] Due to this interesting contradiction, it will be of high interest to investigate apoptosis in the context of adipose tissue in more detail.

Apoptosis, as programmed cell death, has already been studied extensively in various cell lines. Nevertheless, especially in adipocytes no complete picture of the pathway could be unravelled until today. However, it is known that a cascade of activation of proteins is involved. Apoptotic pathways can be activated extrinsically via tumor necrosis factor (TNF) receptors, also called “death receptors”, or intrinsically via the endoplasmic reticulum (ER) and mitochondria.[32,33] In adipose tissue, the secretion of pro-apoptotic molecules from macrophages, during a status of inflammation, can lead to activation of cell surface-located “death receptors”, which thereafter bind specific ligands, and can thereby directly start the apoptotic cascade.[32] The intrinsic activation on the other hand is far more complex, and therefore unfortunately less solved. Also the death stimuli are more diverse, ranging from DNA damage, over metabolic stress, to ER stress.[34] The connecting factor is the mitochondria-ER crosstalk-mediating B-cell lymphoma 2 (BCL-2) protein family.[35] Although known to have very contrary functions, namely pro- and anti-apoptotic, the family members share a combination of α-helical regions, known as BCL-2 homology (BH) domains. These domains determine the function of each member. Generally known as “chief controllers of the mitochondrial outer membrane permeabilization (MOMP)”, and therefore assigned to mitochondria, some of the family members have thereof independent functions.[34] The pro-apoptotic BCL-2-associated X protein (BAX), for example, is able to regulate the levels of reactive oxygen species (ROS),[36] while BAX and BCL-2 homologous antagonist killer (BAK) together are able to regulate ER calcium homeostasis.[37] Importantly, BCL-2 family members are involved in ER stress and can trigger the ER stress response towards apoptosis.[35] Finally, all pathways, extrinsic and intrinsic, result in the activation of cysteine proteases, known as caspases. The active subunits, called cleaved caspases, can then either work as effectors or initiators of apoptosis.[33]

All three, proliferation, differentiation, and apoptosis are connected via signaling pathways. A main actor, linking these pathways, is the ER. The ER is the cell compartment where protein folding and other translational modifications take place. Especially adipocytes must be able to respond promptly to alterations of protein expression and processing during differentiation and thereby are challenging the ER.[38] However, excessive demand provoked e.g. by obesity or diabetes mellitus[39] leads to ER stress. As a protective strategy, the unfolded protein response (UPR) is activated, leading either to stress resolution or cell death by influencing

the activity of various pathways.[40] UPR can be roughly divided into three arms, depending on which one of the three major ER transmembrane receptors is activated. Those three are RNA-activated protein kinase (PKR)-like ER-resident kinase (PERK), transcription factor 6 (ATF6), and inositol-requiring enzyme 1 (IRE1). Each of them can lead to activation of a separate pathway, resulting in different downstream responses (Fig. 1).[41]

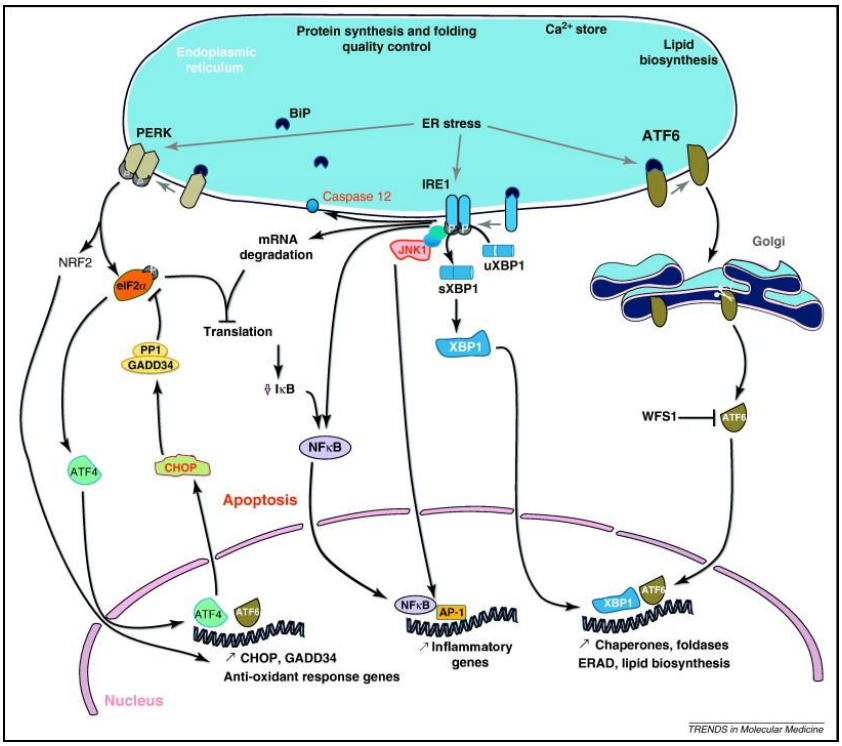

Fig. 1: Scheme of ER stress response. Due to UPR, three different pathways can be activated, the so called “three arms of ER stress”, which are named after each start protein, PERK, IRE1, and ATF6.[39]

Under acute ER stress, PERK is thought to be the first, followed by ATF6, and IRE1 is the last, to be activated.[41] Under prolonged ER stress, IRE1 activity is turned off, whereas PERK maintains its signaling, possibly to sensitize chronologically damaged cells to apoptosis.[35,42] The signal cascade of the PERK arm starts with its transphosphorylation, which makes it capable to phosphorylate the eukaryotic translation initiation factor 2-alpha (ELF2α). Thereby activated ELF2α in turn, leads to increased translation of mRNAs with internal ribosome entry sites, like transcription factor 4 (Atf4)[43], but also lowers the steady-state levels of inhibitors of kappa-light-chain-enhancer of activated B cells (IκB)[44]. This leads to activation and translocation of nuclear factor kappa B (NF-κB), leading to inhibition of PPARγ, thereby impairment of adipogenesis.[40] ATF4 on the other hand, is known for up-regulating the transcription factors Atf3 and CCAAT/enhancer-binding protein homologous protein (CHOP).[45] CHOP is one of the major elements in the decision of cell survival or death, and is

regulated on transcriptional as well as on translational level. Although mainly known for induction of gene expression of pro-apoptotic genes like *Bax*, CHOP also down-regulates pro-survival genes, like B-cell lymphoma 2 (*Bcl-2*).[41] Although both, PERK and ATF6, can lead to induced CHOP expression, no reports have linked ATF6 to ER stress-induced apoptosis, and it seems that ATF6 signaling is purely pro-survival.[41]

During the last years, we and others could show that α/β-hydrolase domain containing protein 15 (ABHD15) expression is strongly increased during adipogenesis of human and murine fibroblasts, as well as primary cell lines.[46,47] Further, it is highly expressed in adipose tissues, to a lower extend in liver, and barely in muscle tissues. Treatment of cells with the PPARγ agonist rosiglitazone (Rosi) leads to a strongly increased *Abhd15* expression, pointing out that *Abhd15* might be a PPARγ target gene.[47] Murine ABHD15 encodes a protein consisting of 459 amino acids with a predicted molecular weight of approximately 51 kDa, but it was detected with 47 kDa by others.[46,48] ABHD15 shows a potential to be secreted, as an N-terminally located signal peptide region of the size of 28 amino acids is predicted due to similarities to other signal peptides.[49] This signal peptide region can probably be spliced off. *Abhd15* orthologous gene sequences are highly conserved, e.g. murine and human ABHD15 exhibit 91% identity.[49] As it is already mentioned in its name, ABHD15 belongs to the α/β-hydrolase family, which is characterized by a similar tertiary protein fold of α-helixes and β-sheets. However, the family members do not share obvious sequence similarities, leading to a widespread variety of enzyme subclasses, such as carboxylesterases, lipases, esterases, dehydrogenases, dehalogenases, peroxidases, and epoxide hydrolases.[50] *Abhd15* shares most sequence similarity with *Abhd1* and *Abhd3*, but lacks both, a nucleophilic elbow and a HX_4D motif, therefore a chemical activity prediction is difficult.[51] Nevertheless, it is expected that ABHD15 possesses a hydrolytic active site, and inferences from electronic annotation using the InterPro protein sequence analysis and classification database proposed a carboxylesterase activity for the human ABHD15. However, a distinct function has not been proven by experiments to date.
Previous studies revealed that the insulin-activated protein kinase AKT phosphorylates ABHD15 in adipocytes and that ABHD15 associates with and regulates cyclic nucleotide phosphodiesterase 3B (PDE3B).[46,48,52] PDE3B is one out of several enzymes which are able to hydrolyze cAMP and cGMP, and thereby take part in the regulation of glucose and lipid metabolism.[53]

The knowledge of all the background data noted above, including its regulation during adipogenesis and in adipose tissues, and its possible features in glucose and lipid metabolism, motivated to have a deeper look at this so far barely characterized protein.

Regarding previous findings and findings presented in this thesis, ABHD15 is probably a new target for obesity and diabetes treatment.

3 Materials & Methods

3.1 Animal studies

Mouse experiments conformed to the Guide for Care and Use of Laboratory Animals of the US National Institutes of Health and were approved by the Austrian Federal Ministry of Science and Research, Division of Genetic Engineering and Animal Experiments.
Male C57BL/6 (age mentioned in figures and text) and 4 months old male ob/ob mice were used for this study. Animals were kept on a 12/12 hours light/dark cycle and were put on either chow or high fat diet (as mentioned either 60% or 40% calories in fat) with 8 weeks of age. Tissues were harvested from mice in *fed ad libitum* state or after fasting for 12 hours.

3.2 Promoter analysis

Genome organization around the *Abhd15* transcription start site was visualized using the UCSC genome browser (GRCm38/mm10). Custom tracks include data from chromatin immunoprecipitation (ChIP) followed by sequencing or microarray analysis, respectively, for PPARγ at day 6[54] and for PPARγ and C/EBPα at day 10[55] during 3T3-L1 adipocyte differentiation, as well as for PPARγ-RXRα direct repeats 1 (DR1) motifs (similarity score > 0.90) (potential binding sites on the plus strand are shown in red and on the minus strand in blue). *In silico* promoter analysis was performed with a Perl implementation of the MatInspector algorithm[56] using a 1133 element position weight matrix (PWM) as identified before [55]. Sequence logo was generated using http://icbi.at/logo.

3.3 Luciferase reporter assays

Three regions upstream of the *Abhd15* transcription start site (TSS) (F1 -1190-0bp, F2 -1190-530bp, and F3 -530-0bp from TSS) were cloned into luciferase reporter vectors (Promega, Madison, USA) either containing a minimal promoter (F2 into pGl4.26) or not (F1 and F3 into pGL4.21), and were cotransfected with *Pparγ2* and *Rxrα* containing pCMX expression vectors. As described before[57], renilla reporter vector pGl4.75 (Promega, Madison, USA) was cotransfected in all experiments in a ratio of 1:50 to luciferase reporter vectors as a control for varying transfection efficiencies. Transfection into Cos7 cells was performed in 96-well plates using MetafectenePro (Biontex, Martinsired, Austria) according to the manufacturer's protocol in a ratio of MetafectenePro to DNA 3:1 (µl:µg). 100 ng of luciferase reporter vector and either 50 ng of *Pparγ2* and *Rxrα* or 100 ng of the empty pCMX as a control were used. After 48 hours cells were lysed and assayed according to the

protocol provided with the Dual-luciferase assay system (Promega, Madison, USA). Luminescence read-outs were generated with a Berthold Orion II luminometer. Relative luciferase activity was calculated by referring renilla-normalized values to empty luciferase vector measurements.

3.4 Cell culture, differentiation, and lipid staining

3T3-L1 Cells were cultured as described before[58]. Fully differentiated 3T3-L1 cells (day 7 after differentiation start) were treated with 0.5 mM 3-isobutyl-1-methylxanthine, 10 µM isoproterenol, or 100 µM palmitic acid in serum-free high glucose DMEM containing L-glutamine (2 mM), penicillin (50 U/mL) and streptomycin (50 µg/mL) (P/S), and harvested after 2 hours of treatment. Preconfluent 3T3-L1 cells were treated with palmitic acid concentrations as indicated in the text, figures, and figure legends for 24 hours. Palmitic acid was resolved in 90% ethanol to a stock of 50 mM and added to serum-free high glucose DMEM containing L-glutamine, P/S, and 0.5% BSA. Plates were oil red O-stained as described earlier[59].

BNL-Cl2 and HepG2 cells were grown in high glucose DMEM containing FBS (10%), L-glutamine (2 mM), P/S (50 U/mL, 50 µg/mL). Fully confluent cells were harvested after 2 hours treatment with 0.5 mM 3-isobutyl-1-methylxanthine or 10 µM isoproterenol.

HEK-293A cells were cultured in as described before[60] in high glucose DMEM containing FBS (10%), L-glutamine (2 mM), P/S (50 U/mL, 50 µg/mL), and G418 (Geneticin, 500 µg/mL).

U937 cells were grown in RPMI 1640 medium supplemented with 10% fetal bovine serum, L-glutamine (2 mM), P/S (50 U/mL, 50 µg/mL). Cells were differentiated to macrophages with the treatment with 10 nM 12-O-tetredecanoylphorbol-13-acetate (TPA).[61]

3.5 Culturing of mouse epididymal fat pads and liver

100-300 mg fat pad and liver pieces of 6 months old male mice were harvested and cultured in 1 mL high glucose DMEM containing L-glutamine (2 mM) but no FBS or antibiotics. Medium was collected from 0-3 h, 3-9 h, 9-18 h, and 18-42 h, or 0-48 h and 48-96 h. To precipitated the proteins from each sample (1 mL), methanol (4 mL), chloroform (1 mL), and ddH_2O (3 mL) were added after each other and vortexed. After centrifugation (14000 x g, 3 min, 4°C), the top layer was removed (proteins remained in the mid-layer), and 4 mL methanol added and vortexed. Supernatant was removed after centrifugation (14000 x g, 2 min, 4°C), and pellets dried in a SpeedVac. Each sample was resolved in 25 µL lysis buffer

(50 mM Tris-HCl pH 6.8, 10% glycerol, 2.5% SDS, 1x protease inhibitor cocktail, 1 mM PMSF) and subjected to benzonase digestion before used for western blot analysis.

3.6 Isolation of adipocytes and SVCs

Epididymal fat pads of each mouse were minced in 1 mL PBS with 0.5% BSA, and in 10 mL collagenase (2 mg/mL in PBS, Sigma C0130) digested under shaking for 30 min, 37°C. Non digested parts were removed with a 100 µm cell strainer and remaining cells centrifuged at 1000 x g for 10 min and 20°C. Afterwards the top white layer was collected, containing the adipocyte fraction, and the supernatant discarded. The pellet was digested with 500 µL red blood lysis buffer (15.5 mM NH_4Cl, 1 mM $KHCO_3$, 10 µM EDTA, sterile filtered) for 5 min at room temperature. After adding of 500 µL of PBS with 0.5% BSA, cells were centrifuged at 1000 x g for 10 min and the supernatant discarded. The pellet contained the SVC fraction.

3.7 RNA isolation, reverse transcription, and gene expression analysis

Cells were washed with PBS and harvested using an RNA isolation kit (Marcherey-Nagel, Dueren, Germany). Tissue RNA was isolated with the TRIzol® reagent (Invitrogen, Carlsbad, USA) according to the manufacturer's protocol. Expression of genes was assessed by real-time reverse transcriptase-polymerase chain reaction (RT-PCR) using an ABI Prism 7700 Sequence Detector system utilizing SYBR Green PCR master mix (Applied Biosystems, Darmstadt, Germany). Gene expression was normalized using TFIIβ for murine tissues and cells and β-actin for human cells as reference genes. Relative mRNA expression levels were calculated using averaged 2^{-ddCt} values for each biological replicate as implemented before[62].

Primer sequences (h: human, m: murine):
mAbhd15 (TATGAACGTGGGTTCTTGCT, TTGGTGTGACAGAACAGGGT),
hAbhd15 (CCGTGCTGCGCTGCCGAGAGTGG, GGCTGTGGCATACCTGCTGAGGGCG),
hβ-Actin (CGCCGCATCCTCCTCTTC, GACACCGGAACCGCTCATT),
mAtf3 (CCCCGAGCGAAGACTGGAGCAAA, GGGACAATGGCGGTCGCACT)
mAtf4 (GCAAAGCCCCACAACATGAC, CCCCAAACCCGACTGGTC)
mAtf6 (TTATCAGCATACAGCCTGCG, CTTGGGACTTTGAGCCTCTG)
mC/ebpα (ATCTGCGAGCACGAGACGTC, TGTCGGCTGTGCTGGAAGA),
mC/ebpβ (GGACTTGATGCAATCCGGA, AACCCCGCAGGAACATCTTTA)
mC/ebpδ (CGACTTCAGCGCCTACATTGA, GAAGAGGTCGGCGAAGAGTT)

mCdk2 (CCTGCTTATCAATGCAGAGGG, TGCGGGTCACCATTTCAGC)
mChop (CTGCCTTTCACCTTGGAGAC, CGTTTCCTGGGGATGAGATA)
mCyclinA (GACAGAGCTGGCCTGAGTCATT, TGTGGCGCTTTGAGGTAGGT)
mCyclinE1 (GAAAAGCGAGGATAGCAGTCAG, CCCAATTCAAGACGGGAAGTG)
mE2F1 (GAGAAGTCACGCTATGAAACCTC, CCCAGTTCAGGTCAACGACAC)
mE2F2 (AGGTGCTGGATGTGCAAAAG, TTGGACTTCTTGCGGATGAGC)
mE2F3 (AGGAGGATTTACGACATCACCA, CCACTGGACGTTGTTCTTAGACT)
mE2F4 (CATGAGTGGGCCTATCGAGG, GACTCTGGAGTAGATCGTCAGG)
mE2F5 (ACTCAGGGCCTATCCATGTG, CTCAGGCAGGTTTTGAGCAG)
mFabp4 (CGACAGGAAGGTGAAGAGCATC, ACCACCAGCTTGTCACCATCTC),
mFasn (GCTGTAGCACACATCCTAGGCA, TCGTGTTCTCGTTCCAGGATC),
mIl-6 (CCTACCCCAATTTCCAATGCTC, TTGCCGAGTAGATCTCAAAGTGA)
mIre1 (CCCTGATAGGTTGAATCCTGGCTATGTG,
AATCTATGCGCTAATCTGCTGGCCTCTG)
mp107 (CCCGGAGCCGAAAACAGAG, ACCAATCATACGGAAATTCCCC)
mp130 (AACTTCCCCATGATTAGCGATG, GGTTAGAACACTGAAGGGCATTT)
mp27 (GGCCCGGTCAATCATGAAG, GAAATTCCACTTGCGCTGACTC)
mp53 (TGGAGGAGTCACAGTCGGAT, CGTCCATGCAGTGAGGTGAT)
mPde3B (ATTCAATGCCAAGGCCAATG, AATTTGATGCACACCTGGCAG)
mPparα (GGCGAACGATTCGACTCAAG, TCCAAAACGAATCGCGTTGT)
mPparγ2 (TGCCTATGAGCACTTCACAAGAAAT, CGAAGTTGGTGGGCCAGAA),
mRb (CGACATTTGGACCAGATTATGATG, GCAGTGACGATGATTTTGAACTTG)
mSirt1 (GCCGCGGATAGGTCCATATAC, CATATCATCCAGCTCAGGTGGAG)
mTFIIα (GTCACATGTCCGAATCATCCA, TCAATAACTCGGTCCCCTACAA)
mTnfα (CTTCTCATTCCTGCTTGTGGC, TAGAACTGATGAGAGGGAGGC)
mUcp1 (CTGAGTGAGGCAAAGCTGATTT, TAGGCTGCCCAATGAACACT)
mXbp1s (GACTATGTGCAGGCCCAGTTG, GCCCAAAAGGATATCAGACTCAGA)

3.8 Silencing of *Abhd15* using short hairpin (sh)RNA-lentivirus particles

One control non-targeting shRNA lentivirus and two shRNA lentiviruses directed against *Abhd15* were purchased from Sigma (MISSION shRNA lentiviral particles NM_026185). 3T3-L1 cells were seeded into 6-well plates 12 hours before transduction using $3*10^4$ cells/well (30% confluence). Cells were infected over night with 5 MOI (multiplicity of infection) in standard medium containing 8 µg/ml polybrene (Sigma). After 16 hours, the infection medium

was replaced with fresh medium containing 3 µg/mL puromycin (Sigma). 3T3-L1 cells were selected for stable expression for at least 5 days.

3.9 Silencing of *Abhd15* via electroporation using siRNA

Control non-targeting siRNA and siRNA directed against *Abhd15* were purchased from Sigma (MISSION siRNA NM_026185). 80,000 fully differentiated 3T3-L1 (day 8 after differentiation start) were electroporated per 10 µL reaction with siRNA (100 nM) using the Neon Transfection System (Invitrogen), at 1400 V, 20 ms, 1 pulse. Cells were harvested 2 days after transfection.

3.10 Generation of recombinant retroviruses

The coding sequence of mouse *Abhd15* was amplified by PCR from mouse adipose tissue cDNA using Pfu polymerase (Thermo Scientific). The primers were designed to create *Bgl*II and *Xho*I restriction sites and the product, containing the whole open reading frame, was ligated into *Bgl*II-*Xho*I digested Murine Stem Cell Virus vector (pMSCVpuro; BD Biosciences Clontech). To produce infectious, but replication-incompetent recombinant retroviruses expressing *Abhd15*, PhoenixEco packaging cells were transfected with pMSCV-*Abhd15* using Metafectene (Biontex Laboratories, Planegg, Germany). Supernatants containing viral particles were collected 48 hours after transfection. Viral supernatants were supplemented with 8 µg/mL polybrene and added to 3T3-L1 cells (30% confluence) for infections for 18–24 hours. Cells were selected with 3 µg/mL puromycin, expanded, and seeded for differentiation experiments. The empty pMSCVpuro vector was used as control.

3.11 Generation of mutated (T142A, S425A, S442A) and C-terminally FLAG-tagged *Abhd15*

Primers were designed to mutate *Abhd15* site specifically and further create *Sgf*I and *Mlu*I restriction sites. The coding sequence of mouse *Abhd15* was amplified by PCR from mouse adipose tissue cDNA using Pfx polymerase (Invitrogen). The product, containing the whole open reading frame, was ligated into *Sgf*I-*Mlu*I digested pCMV6-DDK (OriGene Technologies).

3.12 Western blot analysis

Control (ntc/pMSCV) and *Abhd15*-silenced/overexpressing (Abhd15_sil1/[MSCV-Abhd15) 3T3-L1 cells were harvested by scraping with lysis buffer (50 mM Tris-HCl pH 6.8, 10% glycerol, 2.5% SDS, 1x protease inhibitor cocktail, 1 mM PMSF) after two washing steps with PBS and benzonase (Merck, Vienna, Austria) digested. Protein concentrations were determined with the BCA protein assay kit (Pierce, Rockford, USA). For analysis of blood plasma, 2 µL were used. Protein samples were separated according to size by SDS-polyacrylamide gel electrophoresis (NuPAGE, Invitrogen). Resolved samples were transferred onto nitrocellulose or polyvinylidene difluoride membranes. Blots were incubated with primary antibodies at 4°C over night, and secondary antibodies at room temperature for 2 hours. Secondary antibody signals were visualized by enhanced chemiluminescence detection (ECL component from Pierce Clarity™ and Western ECL Substrate from Bio-Rad, Hercules, USA) using a ChemiDoc™ MP Imaging System (Bio-Rad).

1° and 2° antibodies: ABHD15, anti-goat polyclonal (Santa Cruz)
ABHD15, anti-rabbit polyclonal, 1:1000 (Eurogentec)
ABHD15, anti-rabbit polyclonal, 1:1 (Gift of Gustav Lienhardt)
Adiponectin, anti-rabbit polyclonal, 4 µg/mL (Thermo Scientific Pierce)
β-actin, anti-mouse monoclonal, 1:25,000 (Sigma)
β-actin, anti mouse monoclonal, 1:20,000 (Santa Cruz)
BAX, anti-rabbit polyclonal, 1:1000 (Cell Signaling)
BCL-2, anti-rabbit polyclonal, 1:000 (Cell Signaling)
horseradish peroxidase-conjugated goat anti-mouse (Dako)
1:2000 (ABHD15)/1:3000 (BAX, BCL-2)
horseradish peroxidase-conjugated rabbit anti-mouse, (Dako)
1:3000 (β-actin, Sigma)/1:1000 (β-actin, Cell Signaling)
1:5000 (adiponectin)

3.13 Glucose uptake

293A cells were transfected with empty vector, *Abhd15* wild-type, and *Abhd15* phosphorylation site mutants using lipofectamine (Invitrogen). 48 hours later, cells were serum deprived in low glucose DMEM containing L-glutamine (2 mM) and P/S (50 U/mL, 50 µg/mL) over night. After starving with hepes-salt buffer (7.67 g/L NaCl, 0.35 g/L KCl, 0.31 g/L MgSO4*7 H_2O, 0.18g/L CaCl*2 H_2O, 4.76g/L Hepes, 0.34 g/L NaH_2PO_4*H_2O, 1.0 g/L BSA, pH 7.4) for 1 hour, cells were incubated in absence (basal) or presence of insulin (100

ng/mL) for 30 min. Glucose uptake was determined in quadruplicates with 2-[^{3}H]deoxyglucose (0.2 µCi, 0.1 mM final concentration) for 10 min. To stop the uptake cells were washed three times with ice-cold PBS. Cell membrane was disrupted with 0.1 N NaOH, shaking, for 30 min, subsequently neutralized with 0.1 N HCL, and counted. Counts were normalized to protein concentrations.

3.14 Thin Layer Chromatography (TLC)

Thin layer chromatography on Silica Gel 60 plates (Merck) was used to separate lipids by polarity. For neutral lipids a solvent mixture of hexane, diethyl ether, and glacial acetic acid (70/29/1), followed by toluene (Roth). Polar lipids were separated with the solvent mixture chloroform, methanol, and water (85/25/2.5) (Merck). Lipids were visualized by incineration and with iodine. For HPLC-MS analysis of scratched bands, they were extracted several times with solvents mixes containing various rates of chloroform, methanol, water, and glacial acetic acid (GAA)*. Silica gel was removed by centrifugation (max. speed, room temperature, 20 min).

*	1.	Chloroform/methanol/H2O	(85/25/2.5)	room temperature, 2 h
	2.	Chloroform/methanol	(2/1)	4°C, over night
	3.	Chloroform/methanol/GAA	(2/1/0.1 Vol%)	room temperature, 2 h
	4.	Chloroform/methanol	(1/1)	room temperature, 2 h
	5.	Methanol		room temperature, 2 h

3.15 Lipid analysis with UPLC-QTOF-MS

Cells were differentiated to day 4 and lipids extracted by the MTBE method as described before[634]. For lipid analysis an AQUITY-UPLC system (Waters, Manchester, UK) equipped with a BEH-C18-column (2.1x150 mm, 1.7µm) (Waters) was used. A binary gradient was applied. Solvent A consisted of water/methanol (1/1, v/v), solvent B was 2-propanol. Both solvents contained phosphoric acid (8 µM), ammonium acetate (10 mM) and formic acid (0.1 Vol%). A SYNAPT™G1 qTOF HD mass spectrometer (Waters) equipped with an ESI source was used for analysis. Data acquisition was done by the MassLynx 4.1 software (Waters), for lipid analysis the “Lipid Data Analyser” software was used[64].

3.16 HPLC-MS measurement of fatty acid precursors

On day 3 and 4 after differentiation start, cells were washed twice with ice cold PBS. 4 mL PBS were used to scrape off cells of each T75 flask. Thereof, 200 µL were used for protein determination, and 3.7 mL were centrifuged (200 x g, room temperature, 5 min) and the pellet frozen in liquid nitrogen immediately. Samples were measured by Christoph Magnes of the Lipidomics research Center.

3.17 Assessment of cell growth

Cells were plated at a density of 1000 cells/96-well and cultured for 72 hours. Seven replicates of the CellTiter 96 AQueous One Solution Cell Proliferation Assay (Promega, Madison, USA) were measured using 3-(4,5-dimethylthiazol-2-yl)-5-(3-carboxymethoxyphenyl)-2-(4-sulfophenyl)-2**H**-tetrazolium, inner salt (MTS). Absorbance was recorded by a BioRad spectrophotometer at 490 nm.

3.18 BrdU cell cycle analysis

$1x10^6$ cells were incubated for 1 hour at 37°C with 10 µM BrdU solution. BrdU and 7-AAD staining was performed according to the BrdU Flow kit manual (Becton Dickinson, San Diego, USA). A total of 1×10^5 events were collected on FACScan and cellular DNA content was analyzed by FlowJo software (TreeStar, Ashland, USA).

3.19 Caspase-Glo 3/7 assay

14,500 cells/96-well (in 100 µL) were cultured for 18 hours and analyzed for caspase activation using the Caspase-Glo 3/7 assay (Promega Corporation, Madison, USA), according to the manufacturer's protocol. Luminescence was measured 30 min after adding the Caspase-Glo 3/7 reagent (Caspase-Glo substrate and buffer).

3.20 Southern blot analysis

The DNA of the manipulated clones was extracted with the DNeasy Blood and Tissue Kit (Qiagen) and afterwards digested with probe corresponding restriction enzymes (Fermentas). After separation of the DNA fragments by gel electrophoresis, the DNA

in the gel was depurinated (0.2 N HCl), denaturated (1.5 M NaCl in 0.5 M NaOH), neutralized (1.5 M NaCl, 1 M TrisHCl, pH7.5) and blotted overnight. The DNA was cross linked with the membrane (1600*100 µJ/cm^2) and dried. Probes binding to the DNA fragments were labeled and therefore visualized with radioactive ^{32}P-dATP (American Radiolabeled Chemicals).

3.21 Blood plasma FFA and TG measurement

4 µL blood plasma was used for measuring FFAs using the NEFA-HR (2) kit (Wako), and 2 µL blood plasma were used for the measurement of triglycerides using the triglyceride reagent from Thermo Scientific.

3.22 Glucose and insulin tolerance test (GTT and ITT)

For both, GTT and ITT, mice were fasted 6 hours, and then intraperitoneally injected with glucose or insulin in the concentrations mentioned in the Figures. Glucose blood levels were measured at time points mentioned in the Figures.

3.23 Statistical analysis

If not otherwise stated, results are mean values (± standard deviation) of at least three independent experiments, or results show one representative experiment out of at least three. Statistical significance was determined using the two-tailed Student's *t* test.
* $p \leq 0.05$, ** $p \leq 0.01$, *** $p \leq 0.001$

4 Results

4.1 Expression and regulation of *Abhd15*

4.1.1 *Abhd15* is a direct and functional target gene of PPARγ

We and others have shown before that *Abhd15* expression is strongly increased during adipogenesis of various human and murine cell lines.[46–48] Therefore a connection to PPARγ was likely, and could be proven by the fact that *Abhd15* expression during adipogenesis strongly depends on PPARγ activation before, during, and after adipogenesis.[47] To investigate this in more detail, published ChIP sequencing data sets that identified genome-wide PPARγ and C/EBPα binding sites in differentiating 3T3-L1 cells were analysed [54–56]. According to these studies, *Abhd15* possesses PPARγ and C/EBPα binding sites in its promoter region (Fig. 2). Further, motif search for peroxisome proliferator response element sequences (PPRE) revealed two putative binding sites of PPARγ and its dimerization partner retinoid X receptor alpha (RXRα), ~990 bp and ~440 bp upstream to the *Abhd15* transcription start site (TSS) (Fig. 2).

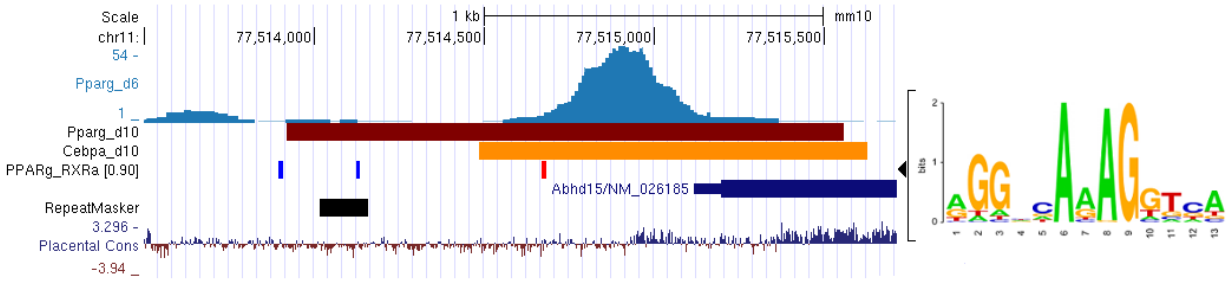

Fig. 2: Genome organization around the *Abhd15* transcription start side (TSS) of 3T3-L1 cells during differentiation with ChIP data of PPARγ (day 6 and day 10) and C/EBPα (day 10) binding, and PPARγ-RXRα direct repeat motif analysis. The data suggest putative PPARγ-RXRα binding ~990 bp and ~440 bp upstream to the *Abhd15* TSS.

In order to prove the direct binding of PPARγ and its dimerization partner RXRα to the *Abhd15* promoter region, luciferase reporter assays with three different sequences located upstream to the *Abhd15* TSS were performed. The segments contained either the predicted 990 bp PPRE (F2), or the 440 bp PPRE (F3), or both PPREs (F1) (Fig. 3A). *Abhd15* promoter activation could be clearly observed in the region ~440 bp upstream to the TSS, and could be further increased upon addition of Rosi (Fig. 3B). The region with the putative PPRE at ~990 bp seemed not to be involved in *Abhd15* promoter activation (Fig. 3B).

Taken together, these results proof that *Abhd15* is a direct and functional PPARγ target gene.

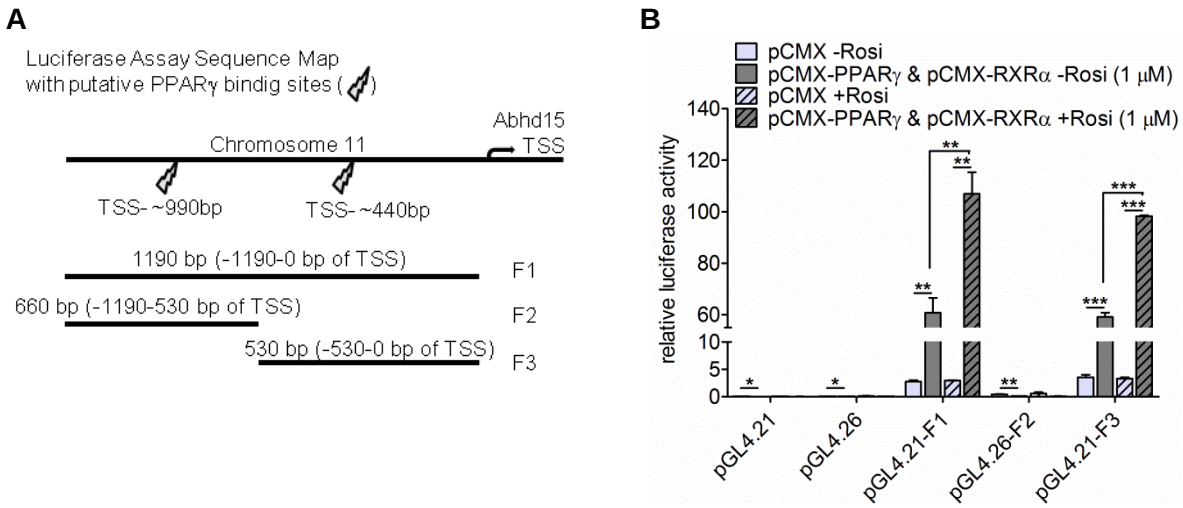

Fig. 3: Luciferase Assay of PPARγ binding. **A.** Sequence maps of the sequences containing either one (F2 and F3) or both (F1) of the putative PPARγ-RXRα binding sites evaluated in Fig. 2, used for the luciferase assay. **B.** 3 regions of interest located upstream of the *Abhd15* gene were cloned into luciferase reporter vectors (named pGL4.21-F1, pGL4.26-F2, pGL4.21-F3) and cotransfected with either Pparγ/Rxrα expressing vectors or an empty vector (pCMX) into Cos7 cells. The luciferase activity of pGL4.21-F1 and pGL4.21-F3, both containing the putative PPARγ-RXRα binding site ~440 bp upstream to the TSS, was significantly increased when compared to pCMX-transfected cells. Addition of Rosi to cells cotransfected with pGL4.21-F1 or pGL44.21-F3 and Pparγ/Rxrα, again significantly increased luciferase activity.

4.1.2 *Abhd15* mRNA expression is decreased in adipose tissue dependent on free fatty acid levels

In accordance to the increased expression during adipogenic differentiation, *Abhd15* is mainly expressed in murine brown (BAT) and white adipose tissue (WAT), and to a lower extent in liver,[47] suggesting a role in lipid synthesis. However, arguing against this, *Abhd15* mRNA expression was significantly decreased in WAT of genetically obese, leptin-deficient mice (*ob/ob*) when compared to their wild-type littermates (Fig. 4A). Moreover, already after 3 days on a high fat diet (HFD, 60% calories in fat), *Abhd15* mRNA expression was strongly down-regulated in WAT in comparison to chow-fed controls (Fig. 4B). This reduction of *Abhd15* mRNA expression in WAT was still evident after 15 weeks on HFD (Fig. 4B). Notably, 23 weeks old mice had strongly reduced expression levels compared to 8 weeks old littermates, suggesting that *Abhd15* mRNA expression is also reduced upon aging (Fig. 4B).

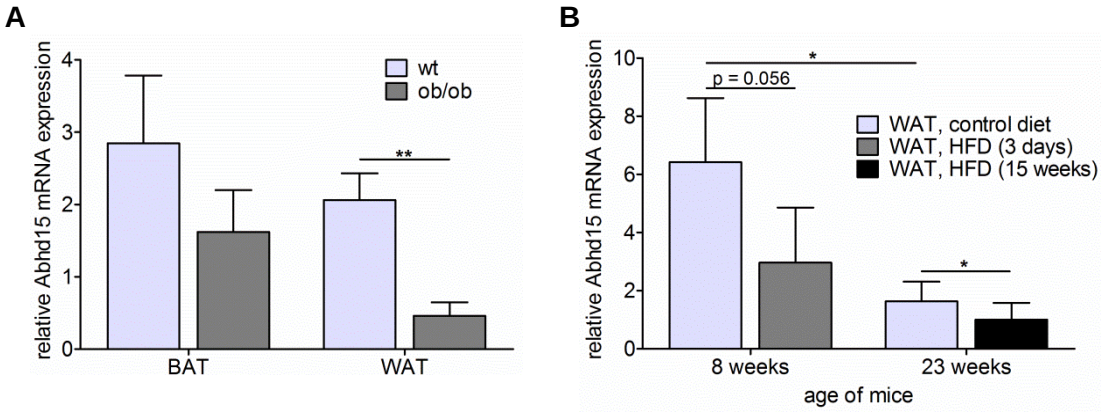

Fig. 4: *Abhd15* mRNA expression in adipose tissue of genetically obese mice, upon HFD and ageing. **A.** *Abhd15* mRNA expression was decreased in WAT and BAT of genetically obese mice (ob/ob, n=4) compared to wild-type (wt, n=3) mice. **B.** Mice fed a high fat diet (HFD, 60% calories in fat) showed a decreased *Abhd15* mRNA expression in WAT already after 3 days (n=4), but still after 15 weeks on this diet (n=6). Additionally, aging strongly decreased *Abhd15* mRNA levels.

Furthermore, overnight fasting decreased *Abhd15* mRNA expression levels in murine WAT and BAT (Fig. 5A). Accordingly, simulated fasting of mature adipocytes by short-term treatment (2 hours) of fully differentiated 3T3-L1 cells with isoproterenol or 3-isobutyl-1-methylxanthine (IBMX) also resulted in reduced *Abhd15* mRNA expression (Fig. 5B). Both components increase intracellular cAMP levels and thereby stimulate lipolysis.[65,66]

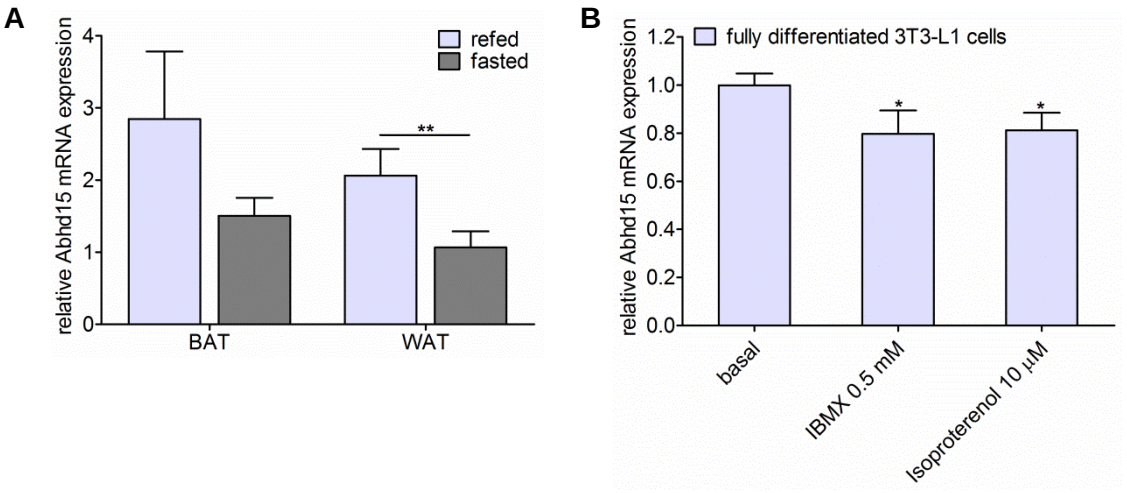

Fig. 5: *Abhd15* mRNA expression in adipose tissue and adipocytes upon fasting. **A.** In mouse tissues *Abhd15* mRNA expression is regulated depending on the nutritional status. Upon fasting, the expression is decreased in both BAT and WAT. (n=3) **B.** Simulated fasting of fully differentiated 3T3-L1 cells (day 7 of differentiation) with IBMX (0.5 mM) and isoproterenol (10 µM) for 2 hours resulted in reduced *Abhd15* mRNA expression.

The observations that *Abhd15* mRNA expression is reduced in obese mice, in mice fed HFD, but also upon fasting indicate that increased free fatty acids (FFAs), the common

denominator in these conditions, diminish *Abhd15* expression. In accordance, short-term treatment (2 hours) of mature adipocytes with 100 µM palmitic acid, a dose reflecting fasting levels without evoking toxic effects [67], strongly reduced *Abhd15* mRNA expression (Fig. 6).

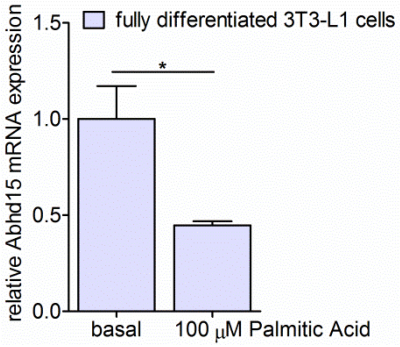

Fig. 6: Palmitic acid treatment. Treatment of fully differentiated 3T3-L1 cells (day 7 of differentiation) with palmitic acid (100 µM) strongly reduced *Abhd15* mRNA expression.

In liver cells, however, *Abhd15* seems to be regulated differently. In comparison to their wild-type littermates, liver samples from ob/ob mice (Fig. 7A) and mice on HFD (Fig. 7B) showed increased *Abhd15* mRNA expression. The increase on HFD in liver is even stronger than the decrease in adipose tissue (Fig. 4B, 7B). On the other hand, aging led to a decrease of *Abhd15* mRNA expression in the liver like it was observed in adipose tissues (Fig. 7C).

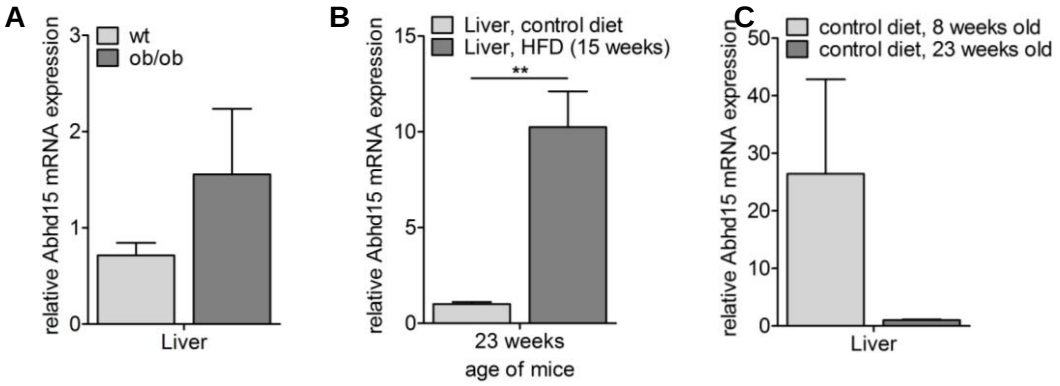

Fig. 7: *Abhd15* mRNA expression in liver of genetically obese mice, upon HFD and ageing. **A.** *Abhd15* mRNA expression was increased in liver of genetically obese mice (ob/ob, n=4)) compared to wild-type (wt, n=3) mice. **B.** After 15 weeks on a high fat diet (HFD, 60% calories in fat) mice showed massively increased *Abhd15* mRNA expression in the liver. (n=4) **C.** Aging decreased *Abhd15* mRNA levels. (n=4)

Also upon overnight fasting, liver *Abhd15* was regulated contrary to adipose tissue, as an increased expression was observed (Fig. 8A). On the other side, *in vitro* simulated fasting of fully confluent liver cells by short-term treatment (2 hours) with IBMX or isoproterenol did not

reflect this increase. Murine liver cells (BNL-CL2) showed no changes in *Abhd15* expression upon IBMX and isoproterenol treatment. In human liver cells (HepG2) a significant decrease upon IBMX stimulation and a slight decrease upon isoproterenol stimulation were observed for *Abhd15* mRNA levels (Fig. 8B).

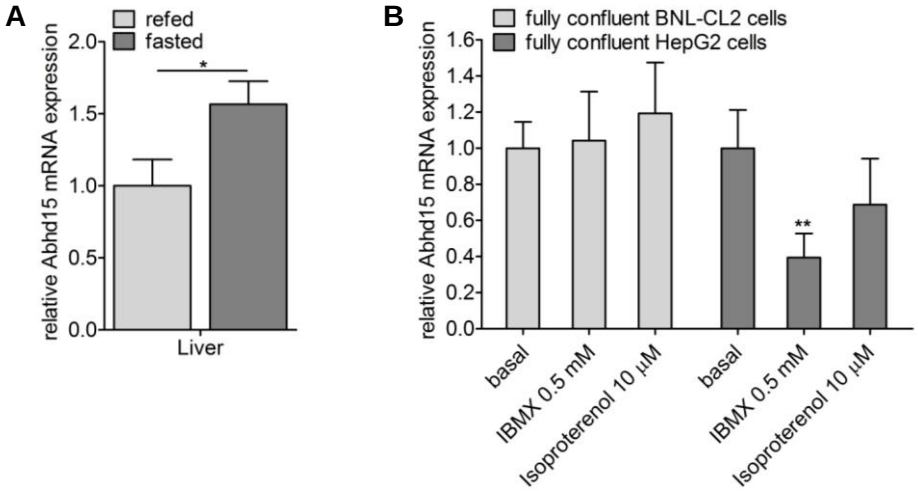

Fig. 8: *Abhd15* mRNA expression in liver and in liver cells upon fasting. **A.** *Abhd15* mRNA expression is increased in liver upon fasting. (n=3) **B.** Simulated fasting of fully confluent murine (BNL-CL1) and human (HepG2) liver cells with IBMX (0.5 mM) and isoproterenol (10 µM) for 2 hours showed no effect in murine liver cells, but decreased *Abhd15* mRNA expression in human liver cells.

4.1.3 *Abhd15* expression is induced in macrophages upon inflammation

As mentioned before, *Abhd15* expression in mice on HFD is decreased in adipose tissue (Fig. 4B). Interestingly, the decreased expression was only due to decreased expression in adipocytes, as the *Abhd15* expression is slightly increased in stromal vascular cells (SVC) of WAT (Fig. 9).

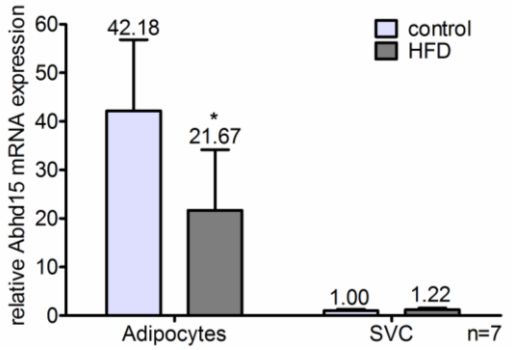

Fig. 9: *Abhd15* mRNA expression in adipocytes and SVC. *Abhd15* expression was decreased in adipocytes of WAT of mice after 15 weeks on HFD (60% cal in fat), whereas a slight increase in SVC could be seen. (n=7)

Due to the separation of adipocytes and SVC, which include the immune cells of WAT, the changed mRNA expression profile of the immune response can be investigated independently from adipocytes and blood cells. It is known that HFD leads to increased inflammation in adipose tissue,[68] and therefore results in a shift in the population of several immune cell types[69]. As a slight increase of *Abhd15* mRNA expression was observed (Fig. 9), the mRNA expression of *Abhd15* was investigated in various murine inflammatory cell types, kindly provided by DaYoung Oh. Compared to monocytes, which can be found in the blood plasma and migrate into the adipose tissue where they differentiate into macrophages[70], *Abhd15* expression is increased in RAW cells (a murine leukemic macrophage cell line), in bone marrow derived macrophages (BMDM), stated as M2 macrophages, and in bone marrow derived dendritic cells (BMDC), stated as M1 macrophages (Fig. 10A). *Abhd15* mRNA expression is massively increased, especially in the "activated" M1 macrophages [71] (Fig. 10A). Additionally, also differentiation of the human monocyte cell line U937 into macrophages led to increased mRNA expression of *Abhd15* (Fig. 10B).

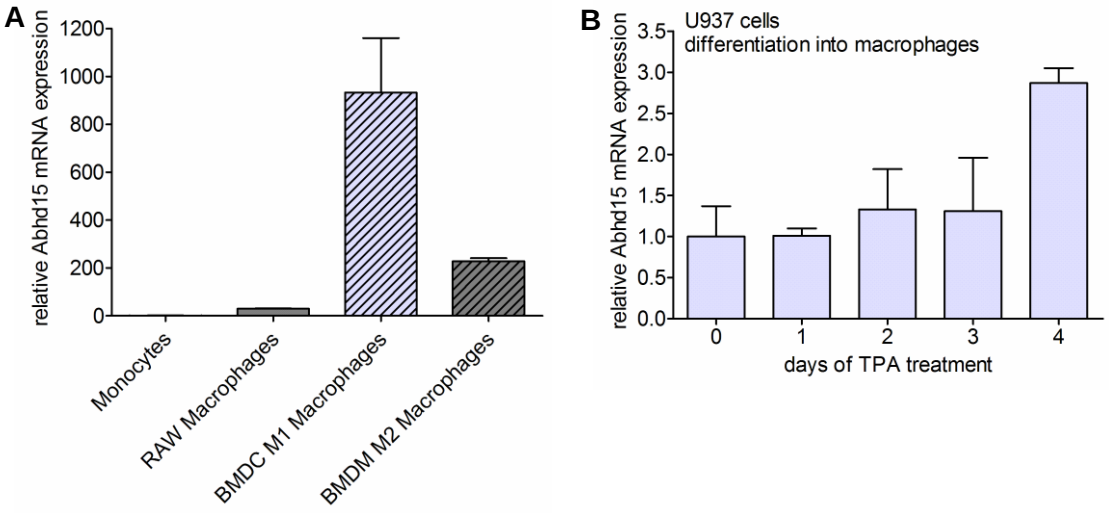

Fig. 10: *Abhd15* mRNA expression in immune cells. **A.** Compared to monocytes, *Abhd15* mRNA expression is increased in the macrophage cell line RAW, in bone marrow derived macrophages (BMDM), stated as M2 macrophages, and in bone marrow derived dendritic cells (BMDC), stated as M1 macrophages. (n=3) **B.** *Abhd15* mRNA expression increases during the differentiation of the human monocyte cell line U937 into macrophages. (n=3)

4.1.4 Potential secretion of ABHD15

As ABHD15 has the potential to be secreted due to a predicted signal peptide region, the localization was investigated in more detail. Our previous studies showed that in Cos7 cells overexpressed N-terminally His-tagged ABHD15 is located in the ER and can also be

detected in the supernatant of these cells.[47] In fully differentiated 3T3-L1 cells overexpressed C-terminally CFP-tagged ABHD15 was found in vesicle like structures, and localization at the lipid droplet could be excluded.[47,72] As both of these studies focused on overexpression models and detected tagged proteins, the size and the secretion potential of untagged/endogenous ABHD15 was investigated in more detail with antibodies directed against ABHD15.

Unfortunately none of the antibodies ordered revealed satisfying results. It was not possible to gain any useful signal with the antibody from Santa Cruz. The customized antibody ordered by Eurogentec detected one band at ~40 kDa. Using this antibody, the endogenous expression of ABHD15 (slot 1, 3, 5, and 7) expectedly increased during differentiation. However, the stable overexpression of untagged *Abhd15* (slot 2, 4, 6, and 8) did not show signals other than the ones seen for the endogenous expression, except for day 4 and day 6 (Fig. 11). Additionally, the protein detected in 3T3-L1 cells was smaller than the one in Cos7 cells overexpressing N-terminally His-tagged *Abhd15*. This could be due to cleavage of the N-terminally located signal peptide in 3T3-L1 cells and/or the His-tag that was expressed with *Abhd15* in cos7 cells, but not in 3T3-L1 cells (Fig. 11).

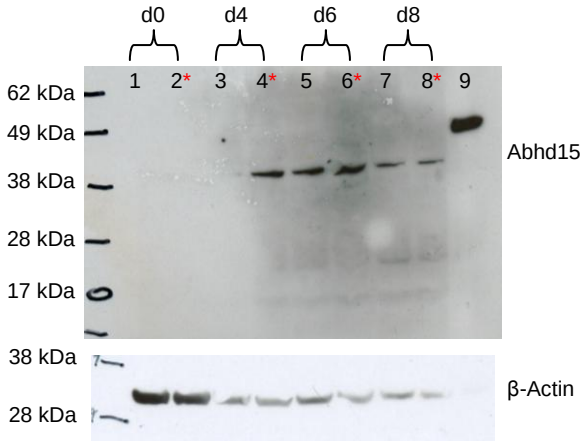

Fig. 11: Western blot analysis of 3T3-L1 cell lysates during differentiation. Stable overexpression of pMSCV-*Abhd15* (*) and empty control vectors (pMSCV, bands 1,3,5,7) showed a smaller protein size than cell lysates of pHisMaxC-*Abhd15*-transfected Cos7 cells (band 9), probably correlating to a cleavage of the signal peptide and/or the His-tag, as *Abhd15* was only His-tagged in Cos7 cells, but not in 3T3-L1 cells. β-Actin was used as loading control.

Using the Eurogentec antibody, unfortunately, no signal from endogenously expressed ABHD15 could be detected in the supernatant of 3T3-L1 cells, independent of the time point of differentiation (day 0, day 3, day 7), the time frame in which the medium was harvested (2 hours, 6 hours, 24 hours, 48 hours), or serum starvation (±FBS) (Data not shown). Therefore, epididymal fat pads were harvested from normal chow fed C57Bl6 mice, and 80-160 mg of tissue were cultured in DMEM, containing L-glutamine. The supernatants were collected after

short time incubation from the same well after 3 hours, 6 hours, 9 hours, and 24 hours, and for long incubation after 48 hours and another 48 hours. The Eurogentec antibody detected ABHD15 with a size of about 30 kDa in the first (3 hours) and second (6 hours) supernatant of the short time frame row, which means until about 9 hours after harvesting the tissue. Accordingly, ABHD15 could be detected only in the first supernatant (48 hours) of the long time frame row. In comparison, the known adipokine adiponectin[12] was secreted constantly during the first 48 hours, and to a reduced amount afterwards. (Fig. 12)

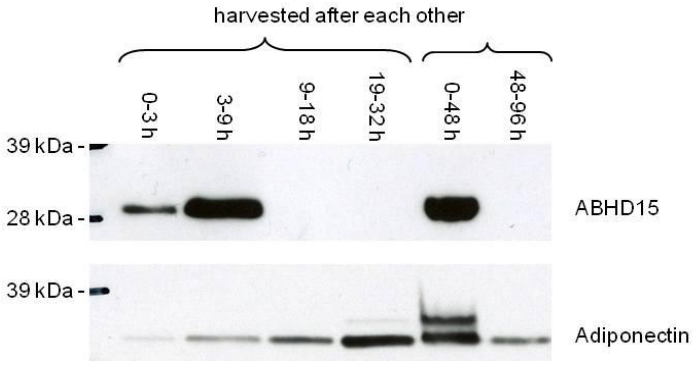

Fig. 12: Western blot analysis of the supernatant of cultured epididymal fat pads. Supernatants were harvested for a short time frame row and a long time frame row, in each case from the same well. The Eurogentec antibody detected ABHD15 with a size of about 30 kDa until about 9 hours after the tissue harvesting time point. The known adipokine adiponectin was used as a control and could be detected constantly during the first 48 hours, and to a reduced amount afterwards.

As seen with the western blot analysis of epididymal fat pads, the known adipokine adiponectin was constantly detectable over 96 hours after harvesting. ABHD15 on the other side was detectable only within the first 9 hours after harvest. It is conceivable that ABHD15 was only detectable due to dead cells that might arise during fat pad preparation and thereby proteins that usually locate inside the cell might be detectable in the supernatant. To investigate this point, fat pads and liver were cultured, and supernatants were additionally subjected to western blot analysis of an unsecreted protein. Hence, this blot was subjected to three antibodies, the Eurogentec ABHD15 antibody, an adiponectin antibody, and finally a β-actin antibody. In the cell lysate of 3T3-L1 cells the β-actin antibody detected only one distinct band at about 40 kDa (the predicted size for ß-actin is 42 kDa). This band could also be detected in the first and second supernatant fraction of the fat pad, whereas no band with this size could be detected in the supernatant of the liver. However, two other bands appeared at ~25 kDa and ~50 kDa. These bands could either be unspecific or fragments of β-actin. In any case, they show the same pattern as the ~30 kDa ABHD15 bands in the supernatants of the fat pad. Accordingly, in the liver the unspecific ß-actin bands could be clearly seen in the first fraction and decreased at later time points. However, the 42 kDa

specific ß-actin band was not visible as already shortly mentioned above. Therefore, β-actin could proof that proteins which are located inside of cells do show a different pattern than secreted proteins, like adiponectin. Adiponectin, being an adipokine, of course was not detected in liver cells. Assuming that the ~30 kDa band is ABHD15, it could be detected similarly to adiponectin within the first 9 hours of harvesting in the supernatant of the fat pad, and further it could be detected in all supernatants of the liver. This suggests that ABHD15 is secreted from fat pads, as well as liver. (Fig. 13)

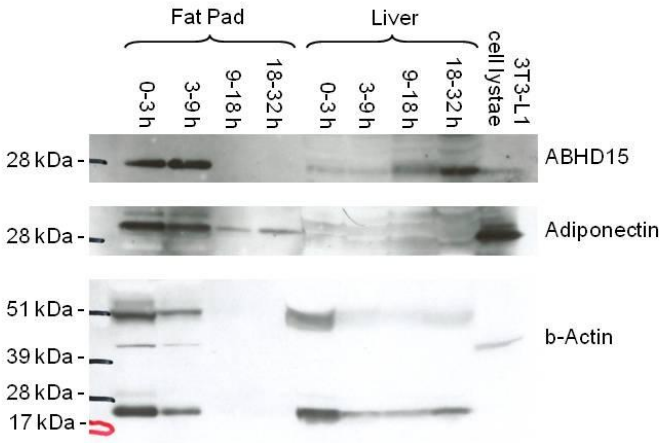

Fig. 13: Western blot analysis of the supernatants of cultured epididymal fat pad and liver, and cell lysate of differentiating 3T3-L1 cells as a control (day 6 after differentiation start). Supernatants were harvested after each other from the same well. The Eurogentec antibody detected ABHD15 with a size of about 30 kDa in fat pad and liver supernatants. In the supernatants of the fat pad, ABHD15 could be detected until 9 hours after tissue harvesting, whereas it could be detected in the liver for at least 42 hours. Adiponectin was used as a secretion control. Being an adipokine it was only detected in the supernatant of the fat pad. β-actin represents a not secreted protein, present in adipose tissue and liver cells.

Finally, the Eurogentec antibody could detect ABHD15 in murine (Fig. 14A) and in human (Fig. 14B) blood plasma at a size of about 40 kDa. Interestingly, ABHD15 was regulated depending on fed and fasted state (Fig. 14A), which fits to the decrease of *Abhd15* mRNA expression in brown and white adipose tissue of fasted mice (Fig. 5A), suggesting that the main source for secreted ABHD15 found in the blood is the protein produced in adipose tissues.

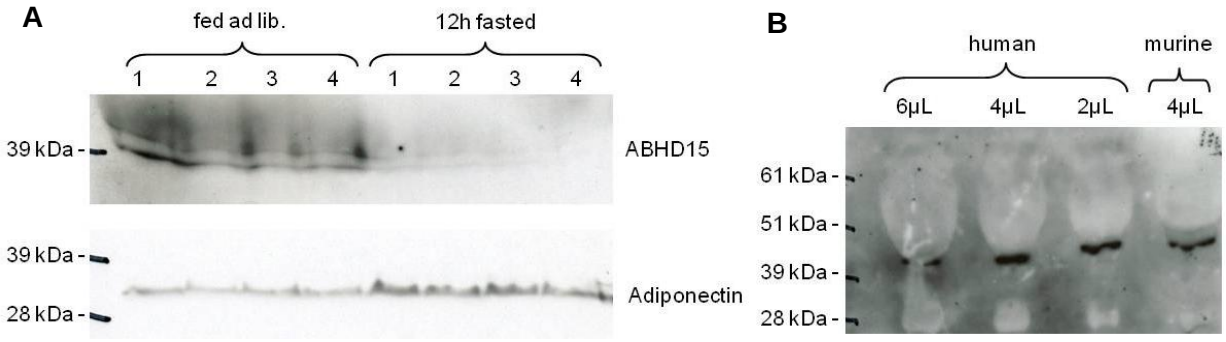

Fig. 14: Western blot analysis of blood plasma. **A.** Blood plasma of fed and fasted mice showed ABHD15 (Eurogentec antibody) to be decreased in fasted mice. The bigger protein size might be due to dimerization (~60 kDa) and following shifting by the high amount of albumin (66 kDa). Adiponectin was used as a loading control. **B.** ABHD15 could also be detected in human blood plasma.

However, the size of the protein bands detected by the ABHD15 antibody purchased from Eurogentec was not consistent. In 3T3-L1 cells, ABHD15 was detected with a size of ~40 kDa, and not detectable in the supernatant. In the supernatant obtained from cultured white adipose tissue and liver a strong band at ~30 kDa was detected. In blood plasma the antibody marked a protein band at ~40 kDa. To solve this problem, all three bands were subjected to protein sequencing by mass spectroscopy, carried out by Anita Sahu at the Institute of Pathology at the Medical University of Graz. Unfortunately, none of these three bands was positive for any fragments of ABHD15. This could be due to too low concentration of the protein in relation to other proteins found in adipocytes, adipose tissue supernatant, and blood plasma at the same size, or unspecific binding of the antibody. Unfortunately, the latter was proven by western blot analysis of adipose tissues, liver, and blood plasma of *Abhd15*-knockout (ko) mice. All of the bands detected in wild-type mice were also present in protein samples of *Abhd15*-ko mice. These results led to the conclusion that the antibody purchased from Eurogentec was not trustworthy neither. Therefore, a third antibody was tested. The group of Gustav E. Lienhard from Dartmouth Medical School (Hanover, NH, USA) published about ABHD15, including the usage of an antibody, in 2005[48] and 2006[46]. Kindly provided by Gustav E. Lienhard, this antibody was the only one that showed the silencing of ABHD15 in *Abhd15*-ko mice at a size of about 50 kDa (Fig. 15A). Further, it detected silencing in *Abhd15* stably silenced 3T3-L1 cells at the predicted size of ~50 kDa (Fig. 15B). Unfortunately, this antibody is already quite old, already diluted, and therefore the reuse is limited. Meanwhile, a further antibody has been ordered and will be tested in the future.

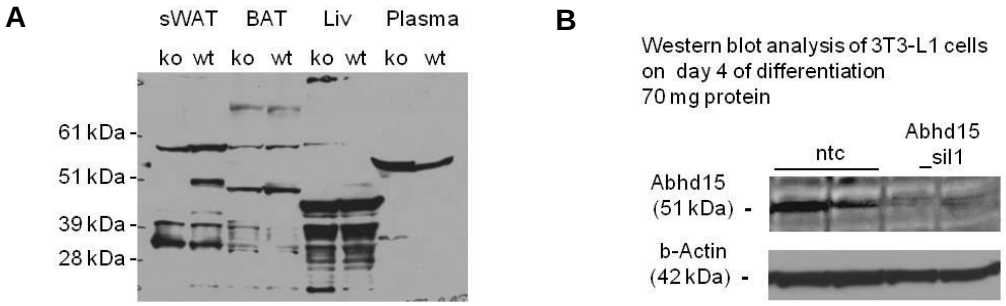

Fig. 15: Western blot analysis with the Lienhard anti-ABHD15 antibody. **A.** Tissues (subcutaneous (s) WAT, BAT, and liver) of wild-type and *Abhd15*-ko mice. ABHD15 could be detected in the wild-type mice at a size of ~50 kDa, and disappeared in ko mice. No ABHD15 band was detected in blood plasma. (n=2) **B.** Protein was harvested at day 4 of differentiation of control (ntc) and *Abhd15*-silenced 3T3-L1 cells (Abhd15_sil1) and subjected to western blotting. β-Actin served as loading control. ABHD15 protein expression is decreased in *Abhd15*-silenced 3T3-L1 cells compared to control cells. (n=2)

4.2 Investigations of the function of ABHD15

4.2.1 *Abhd15* overexpression influences glucose uptake

It was shown before that *Abhd15* becomes phosphorylated by AKT upon insulin stimulation.[46] Hence, the influence of *Abhd15* expression levels on glucose metabolism was investigated. Therefore, glucose uptake was implemented in a clean background cell model, namely 293A cells overexpressing glucose transporter type 4 (*Glut4*) and insulin receptor substrate 1 (*Irs1*).[60] This allows seeing also small effects, delicate to investigate in 3T3-L1 cells. To investigate especially the effect of insulin stimulated phosphorylation, the three identified phosphorylation sites[48] were mutated and overexpressed transiently by transfection, using the empty vector and the vector containing wild-type *Abhd15* as controls. Interestingly, under basal conditions overexpression of wild-type *Abhd15* led to a slightly increased glucose uptake, and the mutants T142A and S425A even showed a significant increase, while no trend could be seen overexpressing the mutant S442A when compared to the empty vector, respectively (Fig. 16A). Insulin stimulated cells though, did not show any differences in glucose uptake between wild-type or *Abhd15*-mutants when compared to the empty vector (Fig. 16A). To have a deeper look on the insulin stimulated uptake, levels for basal glucose uptake were set to one. This led to a significantly reduced glucose uptake in *Abhd15* wild-type and *Abhd15*-mutants overexpressing cells, compared to cells expressing the empty vector (Fig. 16B). Therefore, the effect of increased *Abhd15* expression on glucose uptake

was independent of the insulin-stimulated phosphorylation, as mutants of all *Abhd15* phosphorylation sites still showed the same effect (Fig. 16B).

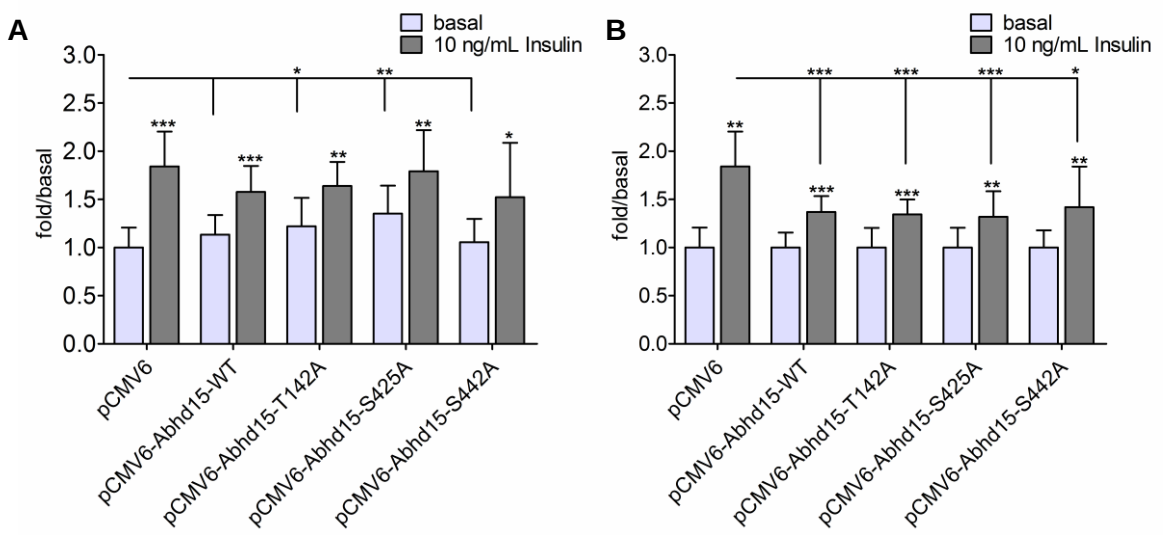

Fig. 16: Glucose uptake of 293A cells, overexpressing *Glut4* and *Irs1*. Insulin stimulation significantly increased the glucose uptake of all cells, independently whether they were transfected with the empty vector as a control (pCMV6), wild-type *Abhd15* (WT), or *Abhd15* with mutated phosphorylation sites (T142A, S425A, S442A) (**A & B**). **A.** Glucose uptake under basal conditions of mutants T142A and S425A were significantly increased compared to cells overexpressing the empty vector. **B.** When glucose uptake under basal conditions was normalized to one, cells transfected with the empty vector showed a 50% higher increased glucose uptake upon insulin stimulation than cells transfected with either *Abhd15* wild-type or *Abhd15*-mutants. Although it has been shown that those sites become phosphorylated upon insulin stimulation[46], no change of glucose uptake could be detected compared to WT.
Significance was calculated from 3 independent experiments, including 4 technical replicates.

4.2.2 Stable overexpression of *Abhd15* can influence the lipid profile

Due to the expression profile, and the prediction that ABHD15 might be a hydrolase, the lipid profile of *Abhd15* stably overexpressing 3T3-L1 cells was investigated. For this purpose, lentiviral vectors encoding *Abhd15* were used to generate 3T3-L1 cells stably overexpressing *Abhd15*. Control cells were transduced with empty vector constructs. After transduction and selection, the cells were grown to confluence and induced to differentiate using a standard hormonal cocktail.

Although *Abhd15* overexpression in preconfluent 3T3-L1 cells was 300-fold (Fig. 17A), no obvious differences between control and *Abhd15* overexpressing cells could be detected (Fig. 17B).

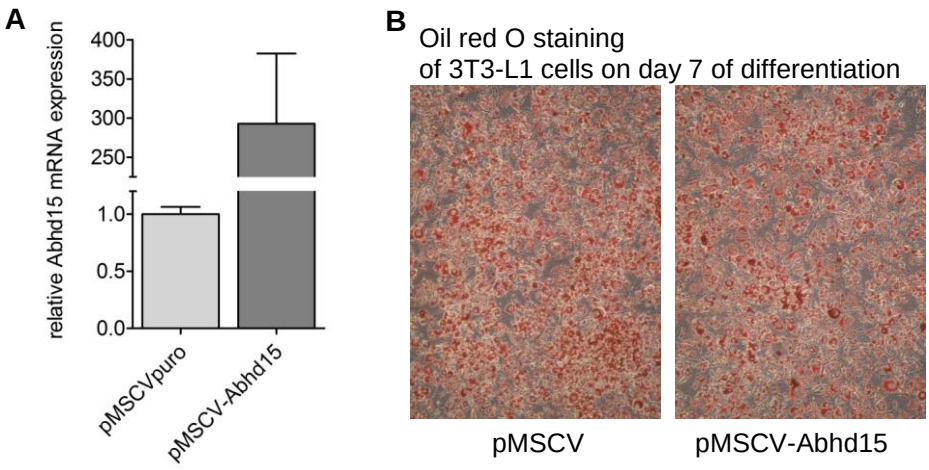

Fig. 17: Overexpression efficiency and Oil red O staining of stably *Abhd15* overexpressing 3T3-L1 cells. 3T3-L1 cells were infected with lentiviral particles obtained from phoenix cells transfected with either empty pMSCVpuro vector (pMSCVpuro) or a vector containing the *Abhd15* gene (pMSCV-Abhd15). After transduction, 3T3-L1 cells were selected with puromycin and expanded as a mixed population **A.** Relative mRNA expression of *Abhd15* in preconfluent 3T3-L1 cells stably overexpressing *Abhd15* compared to control cells. **B.** Overexpression of *Abhd15* did not affect adipogenesis when compared to control cells, indicated by similar neutral lipid staining on day 7 of differentiation.

As a slightly reduced lipid accumulation was vaguely perceptible in the overexpressing cells, thin layer chromatography (TLC) analysis of *Abhd15* overexpressing (4-fold on mRNA level on day 4 of differentiation compared to control cells) 3T3-L1 cells during differentiation was performed. Therefore lipids of *Abhd15* overexpressing and control cells were extracted on day 0, 2, 4, 6, and 8 of differentiation and separated due to polarity using TLC. It seemed that *Abhd15* overexpressing cells show a decrease in triglycerides already on day 4 of differentiation, which further could be seen on day 6 and 8 (Fig. 18). No differences could be examined in squalene, cholesterol ester, FFA, or cholesterol contents (Fig. 18).

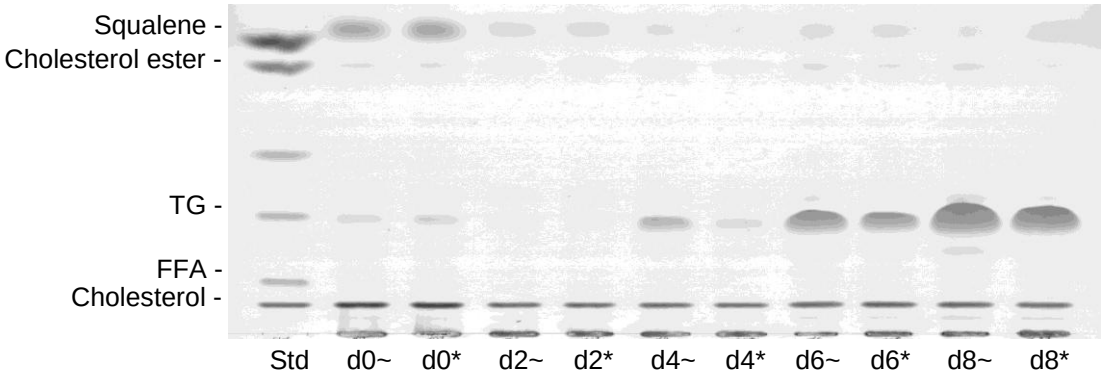

Fig. 18: Neutral lipid TLC of lipid extracts of 3T3-L1 cells during differentiation. Control samples overexpressing the empty transfection vector are marked with "~", *Abhd15* overexpressing samples with "*". *Abhd15* overexpressing cells (4-fold on mRNA level on day 4 of differentiation) showed a slightly decreased triglyceride content.

For further experiments day 4 was chosen for several reasons. First, cells are caught during differentiation, which means especially enzymes, which are required for lipid storage, are highly active.[10] Due to its expression profile during adipogenesis, which shows *Abhd15* to be highest expressed on day 4 of differentiation of 3T3-L1 cells[47], ABHD15 might be one of them. Second, lipid accumulation just started, which means high differences might be detected in a "zero-to-measurable" way. Third, due to already high endogenous *Abhd15* expression, overexpression was detected in a physiological, probably not stressful range of 2- to 4-fold.

Unfortunately, the repetition of the experiment of Fig. 18 with 4 biological replicates revealed no significant differences between overexpressing and control cells, as the variance within the two groups was too big (Fig. 19).

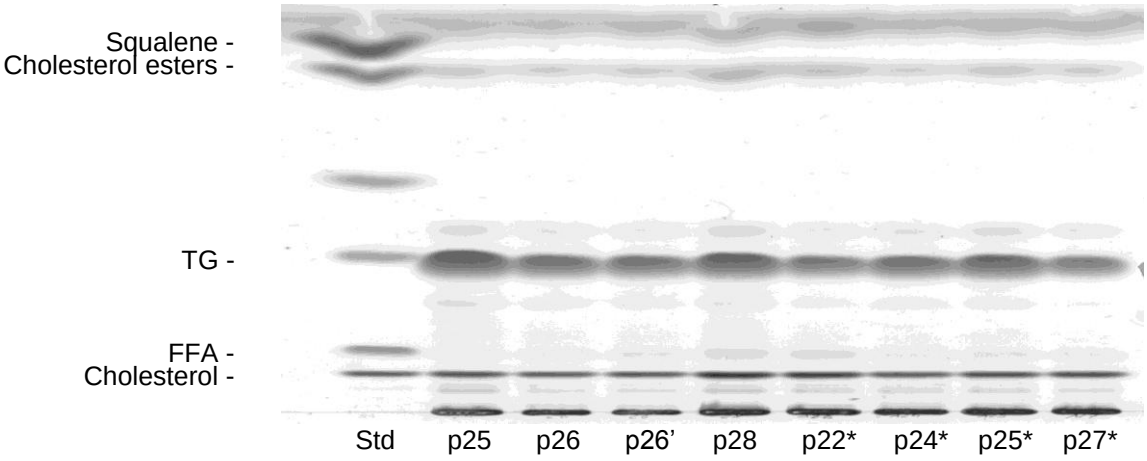

Fig. 19: Neutral lipid TLC of lipid extracts of biological replicates of 3T3-L1 cells at day 4 of differentiation. *Abhd15* overexpressing samples are marked with "*".The overexpression is physiological (p22* 4-fold, p24* 1.2-fold, p25* 2-fold, p27* 3-fold), but maybe not sufficient to bring out differences of the lipid profile, as no differences were visible when using TLC analysis.

Although not significant, a trend to reduced triglyceride content could be recognized, which encouraged to the examination of the lipid profile of *Abhd15* overexpressing 3T3-L1 cells in more detail. Therefore, lipid extracts of 3T3-L1 cells were harvested on day 4 of differentiation and handed over to Dr. Harald Koefeler for HPLC-MS analysis. Triglycerides, phosphatidylcholines, phosphatidylethanolamines, phosphatidylinositols, sphingomyelines, and phosphatidylserines were divided into subclasses depending on the length of their fatty acid chain, reflected by the number of carbons of the backbone, and the number of double bonds. 4 biological replicates overexpressing the empty vector were compared to 3 biological replicates overexpressing *Abhd15*, whereby 2-fold, 3-fold, and 4-fold overexpression on mRNA level was reached.

Analysis of the area of the signal peaks, reflecting the amount of lipids detected, revealed only one phosphatidylserine (32:1), which was significantly reduced in *Abhd15* overexpressing cells, depending on the overexpression-fold (Fig. 20). In healthy cells, phosphatidylserines are located on the inner layer of the cell membrane. If cells undergo apoptosis though, phosphatidylserines become exposed on the surface.[73] The exposure of phosphatidylserine in turn, is a signal for activated macrophages to remove those apoptotic cells.[74] Inside the cell, phosphatidylserines play an important role in various signaling pathways, and can contribute to non-specific electrostatic interactions, as they are very anionic phospholipids.[75]

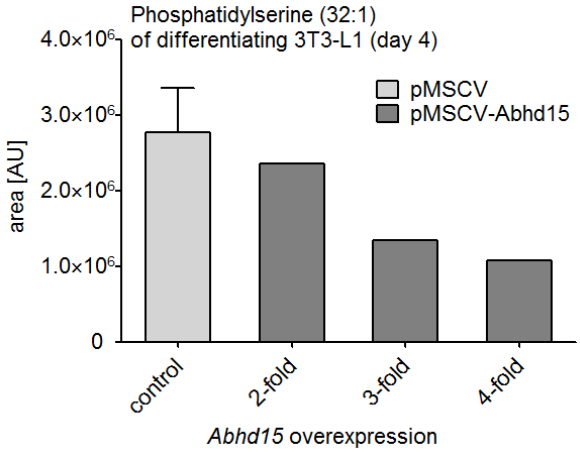

Fig. 20: Phosphatidylserine 32:1 content measured by HPLC-MS. HPLC-MS analysis of lipid extracts of 3T3-L1 samples (of day 4 of differentiation) stably overexpressing the empty vector (pMSCV, n=3)) or *Abhd15* (pMSCV-Abhd15). A decreased amount of phosphatidylserine 32:1, depending on the overexpression was detected.

Phosphatidylserine 32:1, which is the one significantly reduced in 3T3-L1 cell overexpressing 3T3-L1 cells, is present in very small amounts compared to the other phosphatidylserines (Fig. 21A). Therefore, normalization to the combined area of all phosphatidylserines led to a loss of significance (Fig. 21B), and the reduction has to be seen with caution, as it might be borderline to undetectable.

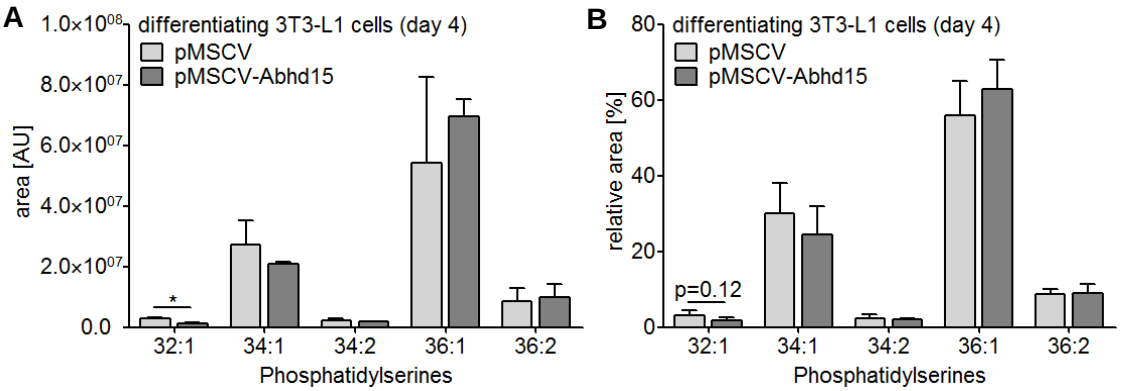

Fig. 21: Phosphatidylserines content measured by HPLC-MS. HPLC-MS analysis of lipid extracts of 3T3-L1 samples (of day 4 of differentiation) stably overexpressing the empty vector (pMSCV) or *Abhd15* (pMSCV-Abhd15). Phosphatidylserines with a chain length of 32 carbons including one double bond (32:1) showed a significant reduction in the consideration of area detected with mass spectrometry (**A**). Normalization to the total area of all phosphatidylserines led to loss of significance (**B**). (n=4)

To solve this problem, the same samples used for HPLC-MS were subjected to TLC, and after visualization with iodine, the bands at the level of phosphatidylserine, -ethanolamine, and –choline were scraped off and extracted. Following lipid analysis with UPLC-QTOF-MS measurement was performed by Dr. Gerald Rechnberger. Unfortunately, the amount of phosphatidylserine 32:1 was again very low, and barely detectable. One of the control samples and one of the *Abhd15* overexpression samples did not lead to any signal, the other samples to a very low signal with high deviation, and therefore no statement. As this experiment already included a long chain of separation and cleaning steps, a retry with an internal standard will be necessary in the future.

Unfortunately, analysis of all the other lipid classes mentioned above (triglycerides, phosphatidylcholines, phosphatidylethanolamines, phosphatidylinositols, and sphingomyelines) did not show any significant differences between *Abhd15* overexpressing and control cells (Fig. 22A-E).

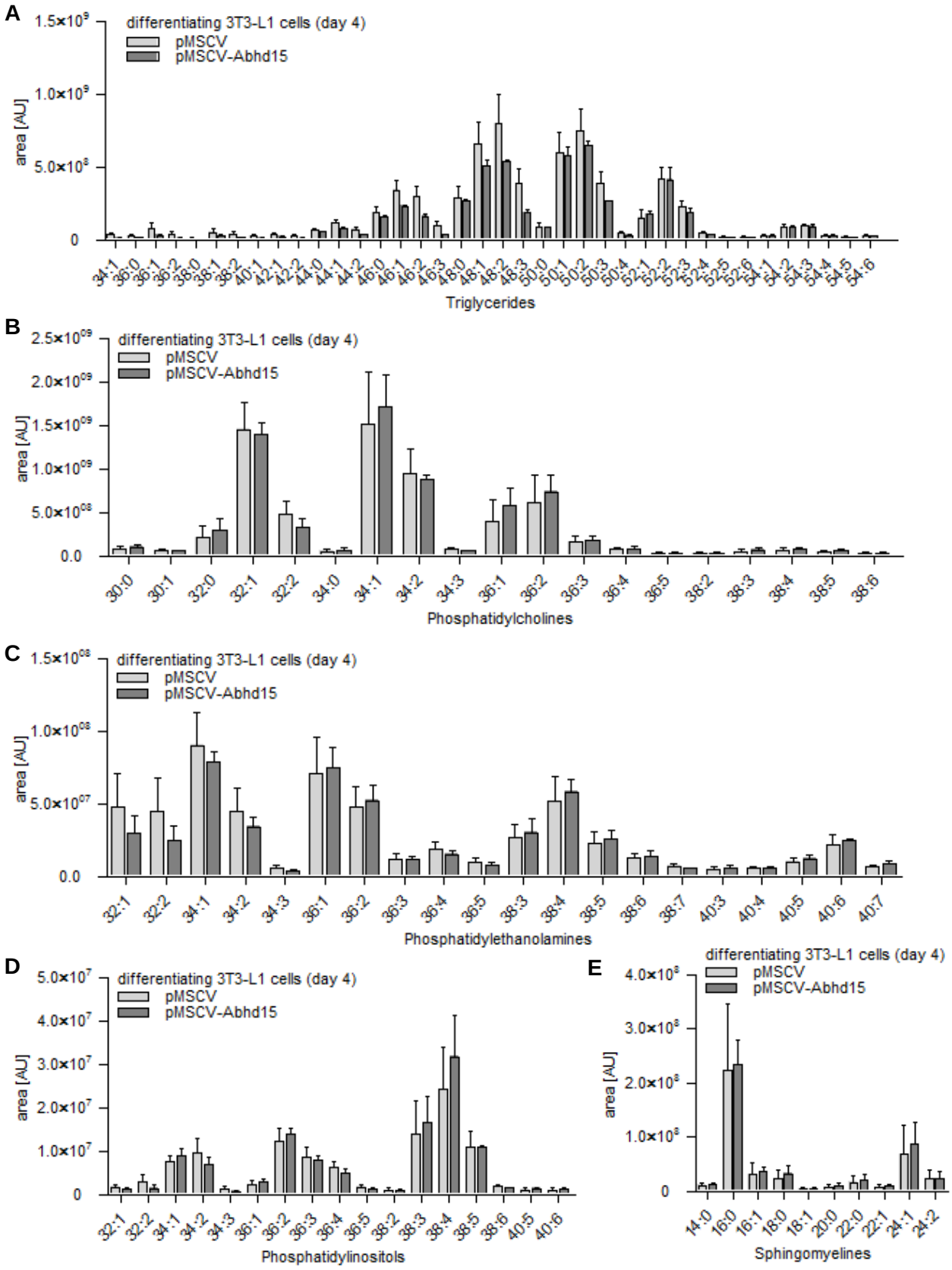

Fig. 22: HPLC-MS analysis of lipid extracts of 3T3-L1 samples (of day 4 of differentiation), revealed no significant differences between control (pMSCV) and *Abhd15* overexpressing (pMSCV-Abhd15) cells in the lipid classes triglycideries (**A**), phosphatidylcholines (**B**), phosphatidylethanolamines (**C**), phosphatidylinositols (**D**), and sphingomyelines (**E**). Within the lipid classes lipids could be distinguished due to their fatty acid carbon chain length (number before colon) and the number of double bonds (number after colon). (n=4)

Having a look on the total amount of the lipid classes, none of them showed a significant reduction or increase (Fig. 23). However, a trend to reduced triglycerides can be seen, as it was speculated before with the results from TLC experiments.

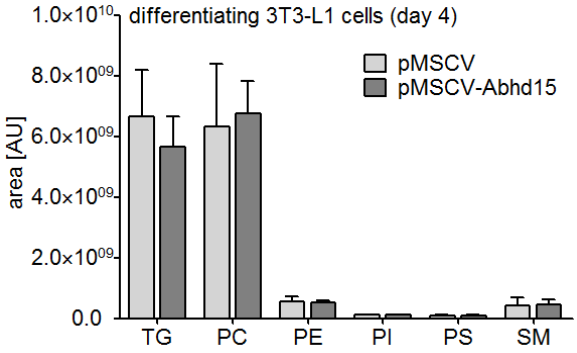

Fig. 23: HPLC-MS analysis of lipid extracts of 3T3-L1 samples (of day 4 of differentiation) stably overexpressing the empty vector (pMSCV) or *Abhd15* (pMSCV-Abhd15). No significant differences in the lipid classes triglycideries (TG), phosphatidylcholines (PC), -ethanolamines (PE), -inositols (PI), -serines (PS), or sphingomyelines (SM) could be detected. (n=4)

To evaluate if and where in fatty acid biosynthesis ABHD15 might be involved, the concentration of acetyl-CoA and malonyl-CoA, two major metabolites in lipid synthesis, as well as several intermediates of fatty acid synthesis, were measured in *Abhd15* overexpressing and control cells. Acetyl-CoA was measured on day 3 and day 4 of differentiation whereas all others were measured only on day 3. Acetyl-CoA was significantly decreased in *Abhd15* overexpressing cells on day 4 of differentiation, while no significant differences could be detected on day 3. Nevertheless, a trend to reduced C16-1-CoA and C18-1-CoA could be observed. (Fig. 24)

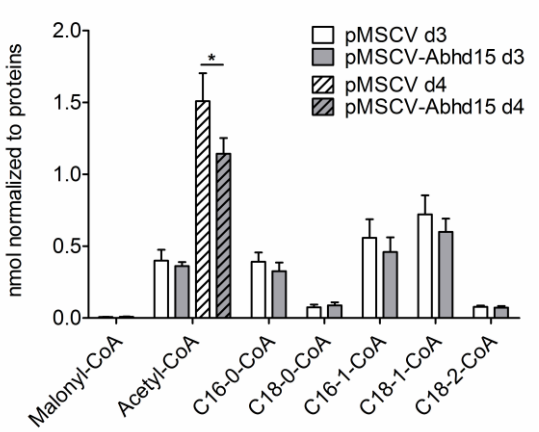

Fig. 24: HPLC-MS analysis of the precursors or intermediates of lipid synthesis of 3T3-L1 samples (of day 3 and day 4 of differentiation) stably overexpressing the empty vector (pMSCV) or *Abhd15* (pMSCV-Abhd15). Only acetyl-CoA was decreased in *Abhd15* overexpressing cells, and only on day 4 after differentiation start. On day 3 no significant differences between overexpressing and control cells were detected.

Taken these data together, it seems that *Abhd15* overexpression slightly decreased the production and thereby accumulation of triglycerides, but no significant proof can be presented. Furthermore, ABHD15 might degrade phosphatidylserine 32:1 and thereby either produce a signal molecule or impair the signal effect of phosphatidylserine 32:1.

4.2.3 *Abhd15* is required for adipogenesis

As stable overexpression of *Abhd15* did not lead to a conclusion concerning function of ABHD15, stable knockdown of *Abhd15* in 3T3-L1 cells was performed. For this purpose, an shRNA construct targeting *Abhd15*, encoded by lentiviral vectors, was used to generate 3T3-L1 cells with constitutive knockdown of *Abhd15* expression. After transduction and selection, the cells were grown to confluence and induced to differentiate using the standard hormonal cocktail. During differentiation, two *Abhd15*-targeting shRNA lentiviral constructs revealed a 80% reduced *Abhd15* mRNA expression compared to a non-targeting control shRNA (ntc) (Fig. 25). The silencing of the better shRNA lentiviral construct (Abhd15_sil1) was confirmed on protein level using western blot analysis (Fig. 15B).

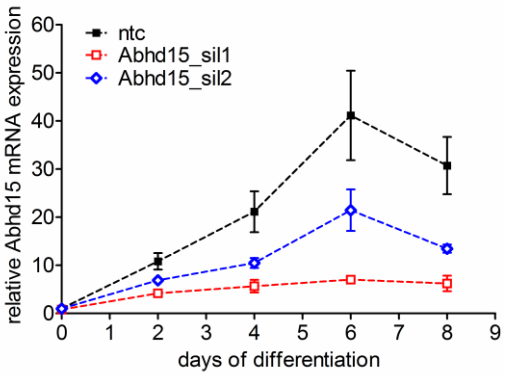

Fig. 25: *Abhd15* silencing during differentiation. 3T3-L1 cells were infected with lentiviral particles coding for *Abhd15* shRNA (Abhd15_sil) and for a non-target shRNA as control (ntc), selected for puromycin resistance, expanded as a mixed population and differentiated. Silencing efficiency during differentiation was determined by qPCR assay. (ntc n=4, Abhd15_sil n=2)

Knockdown of *Abhd15* drastically reduced the formation of lipid droplets, as revealed by Oil red O staining of fully differentiated 3T3-L1 cells (Fig. 26A). Additionally, mRNA expression levels of several adipogenic markers, such as *C/ebpα*, *Pparγ*, fatty acid binding protein 4 (*Fabp4*), and fatty acid synthase (*Fasn*), were strongly decreased in *Abhd15*-silenced compared to control cells at day 5 of differentiation (Fig. 26B).

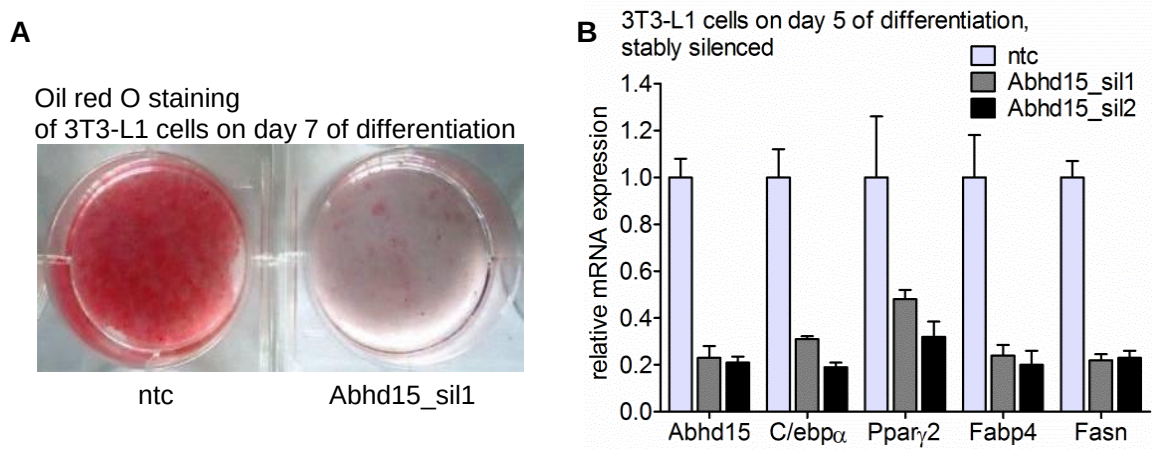

Fig. 26: Oil red O staining and adipogenic marker gene expression of stably *Abhd15*-silenced cells. 3T3-L1 cells were infected with lentiviral particles coding for *Abhd15* shRNA (Abhd15_sil) or for non-target shRNA as control (ntc), selected for puromycin resistance, expanded as a mixed population and differentiated. **A.** Silencing of *Abhd15* impairs adipogenesis, indicated by the strongly decreased amount of neutral lipids on day 7 of differentiation, stained with Oil red O. **B.** Stable silencing of *Abhd15* in 3T3-L1 cells showed high influences on the expression levels of various important adipogenic genes on day 5 of differentiation (*Cebpα*, *Pparγ*, *Fabp4*, *Fasn*).

In order to investigate a potential influence of *Abhd15* on mature adipocytes, *Abhd15* was transiently knocked-down in fully differentiated 3T3-L1 cells by means of siRNA introduced by electroporation. Although the expression level of *Abhd15* was reduced by 70% in mature adipocytes (Fig. 27), neither differences in lipid accumulation (data not shown), nor changes in expression levels of *C/ebpα*, *Pparγ*, *Fabp4*, and *Fasn* could be detected (Fig. 27).

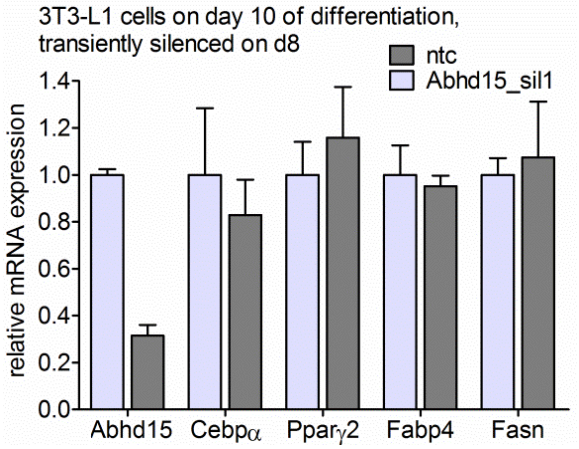

Fig. 27: Transient silencing of *Abhd15* by electroporation of siRNAs on day 8 of differentiation did not show any effects onto the mRNA levels of adipogenic genes in fully differentiated 3T3-L1 cells (day 10).

Together, these results point out that *Abhd15* is a required factor for adipogenic differentiation, whereas reduced *Abhd15* expression in mature adipocytes has no effect on the maintenance of the differentiated status.

4.2.4 *Abhd15* expression effects adipocyte development

To track the origin of the differentiation defect in *Abhd15*-silenced 3T3-L1 cells, three probable stages were investigated in more detail. To name them, *Abhd15* silencing could either disturb cells already before differentiation start, during the proliferation phase directly after induction of differentiation, or during the terminal differentiation.

Abhd15 silencing efficiency on mRNA level was best on day 6 of differentiation (Fig. 25). However, in preconfluent cells silencing of only 30% could be reached (Fig. 28A). *Abhd15* expression increased on mRNA level right after induction of fully confluent cells, but this increase was significantly lower in silenced cells, compared to control cells (Fig. 28B).

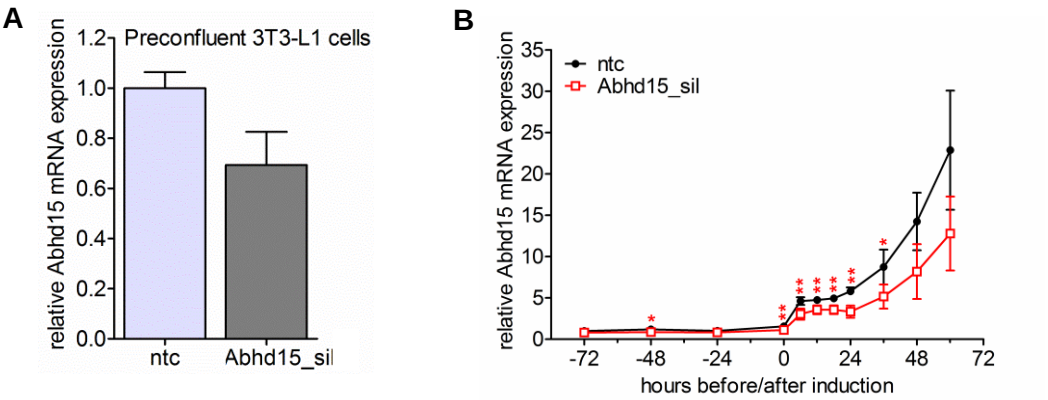

Fig. 28: Stable *Abhd15* silencing in preconfluent cells and during early differentiation. 3T3-L1 cells were infected with lentiviral particles coding for *Abhd15* shRNA (Abhd15_sil) or for a non-target shRNA as control (ntc), selected for puromycin resistance, and expanded as a mixed population. (n=4) **A.** Silencing of *Abhd15* reached only 30% silencing in preconfluent cells. **B.** After induction of 3T3-L1 cells to differentiate, *Abhd15* mRNA expression did not increase to the same extent in *Abhd15*-silenced cells as in control cells, leading to an increasing silencing efficiency upon differentiation.

The effect that the silencing efficiency was better during differentiation than in preconfluent cells, could be explained by the finding that *Pparγ* expression was also silenced in *Abhd15* stably silenced cells (Fig. 26B). Being a direct and functional PPARγ target gene, *Abhd15* expression could not be induced in silenced cells as in control cells. To have a closer look on this phenomenon, *Pparγ* mRNA expression was monitored especially during early differentiation. Right after induction, the expected increase of *Pparγ* mRNA expression was

reduced in *Abhd15*-silenced cells compared to control cells (Fig. 29A). The same effect could be observed for *C/ebpα* expression (Fig. 29B).

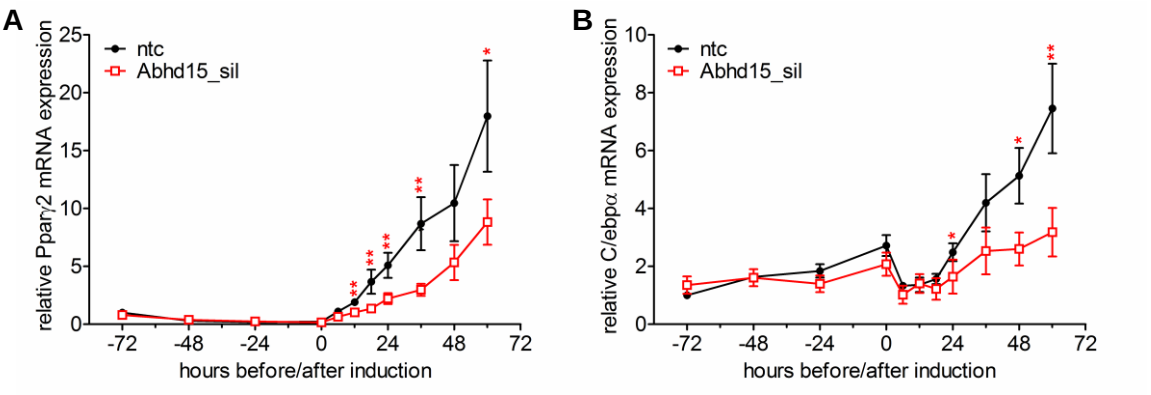

Fig. 29: *Pparγ* and *C/ebpα* mRNA expression in *Abhd15*-silenced cells. 3T3-L1 cells were infected with lentiviral particles coding for *Abhd15* shRNA (Abhd15_sil) and for a non-target shRNA as control (ntc), selected for puromycin resistance, and expanded as a mixed population. (n=4) **A.** After the growth arrest phase, induction of 3T3-L1 cells to differentiate did not increase *Pparγ* mRNA expression to the same extend in *Abhd15*-silenced cells as in control cells. **B.** Also, *C/ebpα* expression did not increase in *Abhd15*-silenced cells as it did in control cells.

In 3T3-L1 cells, the first steps before terminal differentiation include growth arrest due to cell-cell contact. Afterwards two sequential rounds of mitosis (called mitotic clonal expansion, MCE), which are necessary for terminal differentiation, are induced by treatment with the hormonal cocktail.[17] Mitotic clonal expansion involves a transcription factor cascade, followed by the expression of genes responsible for the adipocyte phenotype.[18] The reduced *Pparγ* levels upon *Abhd15* silencing started right during this phase of MCE, suggesting a cell cycle defect due to reduced *Abhd15* expression. *Pparγ* and *C/ebpα* are activated by C/EBPβ and C/EBPδ,[76] both expressed on mRNA level immediately after addition of the differentiation cocktail (Fig. 30A & B). Directly after induction of differentiation *C/ebpβ* expression was not as much increased in *Abhd15* silenced cells as in control cells (Fig. 30A). This effect was even stronger for *C/ebpδ* expression, especially at the time point of 6 hours after induction (Fig. 30B). Interestingly, a slight but significant reduced expression of *C/ebpβ* and *C/ebpδ* was detected already before induction start in *Abhd15*-silenced cells when compared to controls (Fig. 30A & B).

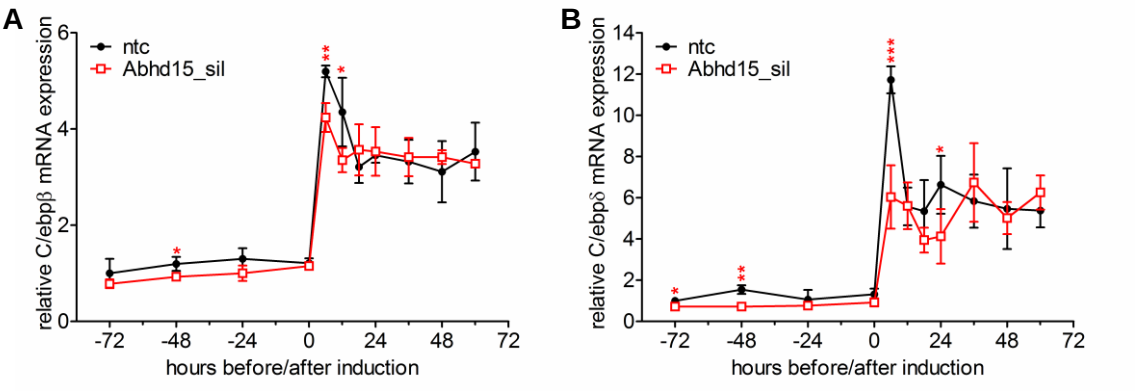

Fig. 30: *C/ebpβ* and *C/ebpδ* mRNA expression in *Abhd15*-silenced cells. 3T3-L1 cells were infected with lentiviral particles coding for *Abhd15* shRNA (Abhd15_sil) and for a non-target shRNA as control (ntc), selected for puromycin resistance, and expanded as a mixed population. (n=4) **A.** After the growth arrest phase, induction of 3T3-L1 cells to differentiate did not increase *C/ebpβ* mRNA expression to the same extend in *Abhd15*-silenced cells as in control cells. **B.** *C/ebpδ* expression did also increase less in *Abhd15*-silenced cells than in control cells.

When compared to control cells, both *C/ebpβ* and *C/ebpδ* mRNA expression levels were decreased in *Abhd15*-silenced cells 6 hours after induction of differentiation, and *Abhd15* expression seemed to be impaired anyway during the term of the first cell cycle of MCE (Fig. 31). Therefore, expression levels of several genes, which are specifically regulated during this first cell cycle of MCE, were investigated.

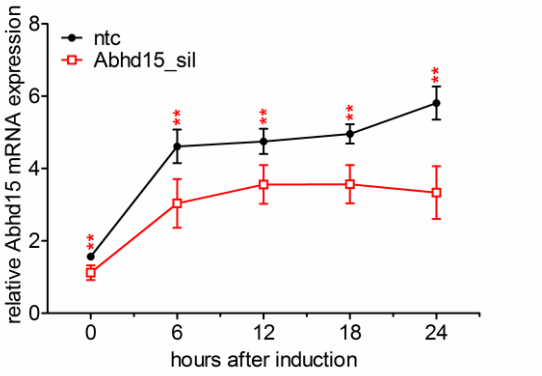

Fig. 31: *Abhd15* mRNA expression during MCE. 3T3-L1 cells were stably silenced using lentiviral particles coding for *Abhd15* shRNA (Abhd15_sil) and for a non-target shRNA as control (ntc). *Abhd15* mRNA expression increased after induction, but stayed at the same level during the first round (out of two) of the MCE. (n=4)

In the status of growth arrest, cells are in the G1 phase.[17] To passage into the S phase, several groups of genes, including activators and suppressors, are involved. During this passage, activator genes are up-regulated, while suppressors are down-regulated. One group of these genes are the *E2F* transcription factors. *E2F1* and *E2F2* are activators of the

cell cycle and therefore their expression increases at G1/S phase.[77] *E2F3b*, *E2F4*, and *E2F5* are suppressors and inhibit the cell cycle. Stably silencing of *Abhd15* led to a slight but significant increased mRNA expression of the cell cycle activators *E2F1* and *E2F2* (Fig. 32A & B), while the mRNA expression of the cell cycle suppressors *E2F4* and *E2F5* were slightly but significant decreased (Fig. 32D & E). *E2F3b* did not show significant differences (Fig. 32C). Together these data suggest a slightly activated cell cycle and therefore increased proliferation, which cannot explain the impaired differentiation that was observed in *Abhd15*-silenced cells (Fig. 26A). However, although significant, none of the influences of *Abhd15* silencing were striking.

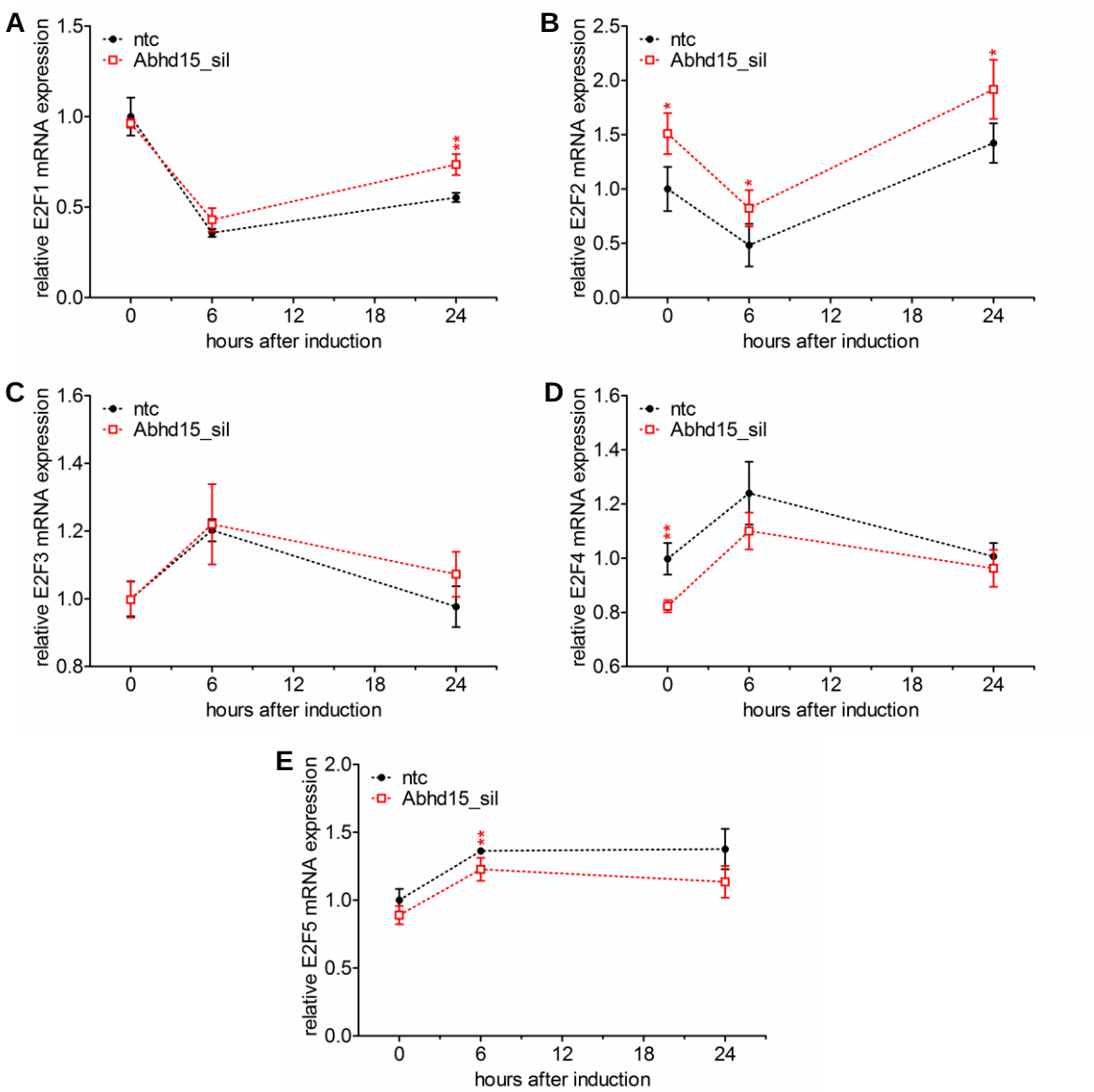

Fig. 32: mRNA expression of *E2F* transcription factors during MCE. 3T3-L1 cells were stably silenced using lentiviral particles coding for *Abhd15* shRNA (Abhd15_sil) and for a non-target shRNA as control (ntc). *Abhd15* silencing did not evoke any striking differences in any of the members of the E2F family. However, while the cell cycle activators *E2F1* (**A**) and *E2F2* (**B**) were slightly increased, the cell cycle suppressors *E2F4* (**D**) and *E2F5* (**E**) were slightly reduced. Expression of the suppressor *E2F3b* was unchanged (**C**). (n=4)

Further common for MCE are the down-regulation of the repressors *p27* and *CyclinE1*[78,79], and the activation of *CyclinA* and cyclin dependent kinase 2 (*Cdk2*)[17,80]. *p27* down-regulation was detected 6 hours after differentiation start, but silencing of *Abhd15* did not influence this (Fig. 33A). Although no decrease of *CyclinE1* could be shown in control cells, an increase could be detected in *Abhd15*-silenced cells (Fig. 33B). Interestingly, *CyclinA* mRNA expression was increased before, but decreased 24 hours after induction of differentiation in *Abhd15*-silenced cells compared to controls (Fig. 33C). The increase of *Cdk2* was relatively small, but *Abhd15*-silenced cells showed a significant decrease 6 hours after induction of differentiation (Fig. 33D).

Although none of the mentioned gene expressions were changed strikingly, at least a trend to decreased MCE could be perceptible. How and if those slight and not constant influences of *Abhd15*-silencing could lead to such a striking differentiation defect is questionable.

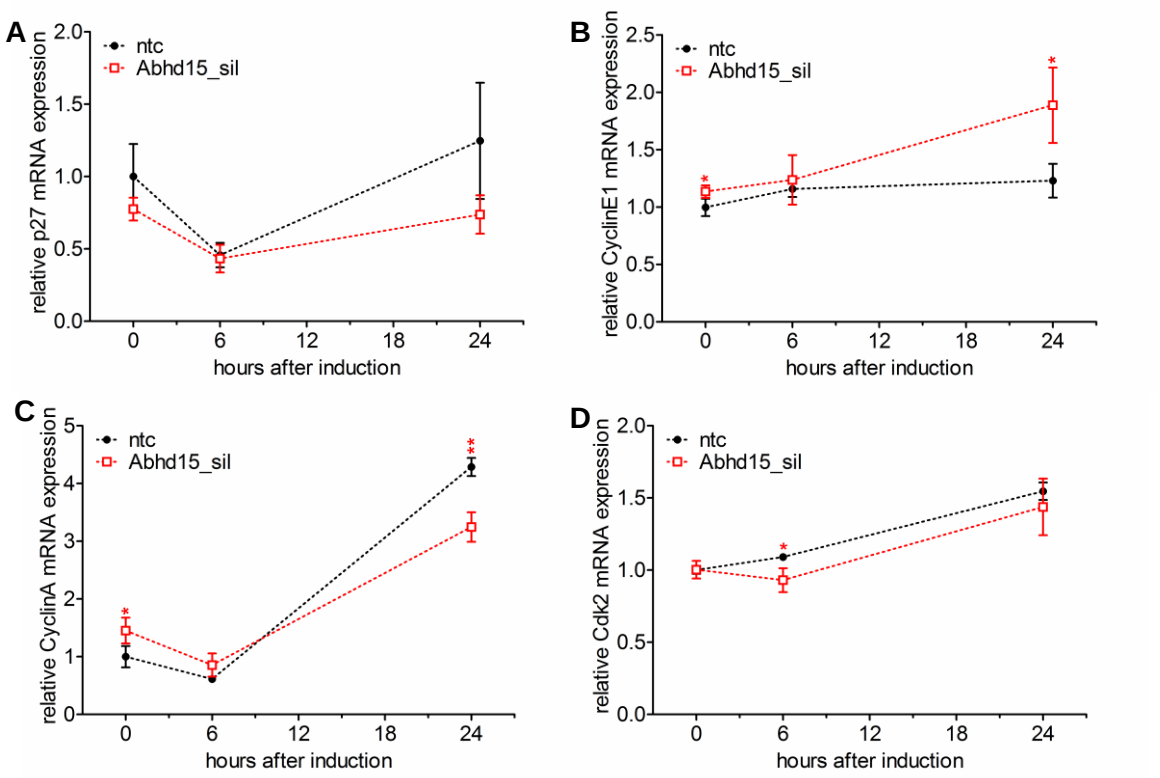

Fig. 33: mRNA expression of *p27*, *CyclinE1*, *CyclinA*, and *Cdk2* during MCE. 3T3-L1 cells were stably silenced using lentiviral particles coding for *Abhd15* shRNA (Abhd15_sil) and for a non-target shRNA as control (ntc). *Abhd15* silencing did not evoke any striking differences in the expression profile of the cell cycle suppressors *p27* (**A**) or *CyclinE1* (**B**), or activators *CyclinA* (**C**) and *Cdk2* (**D**). The expression profile of *CyclinE1* was slightly but significantly increased (**B**). *CyclinA* expression was unexpectedly slightly but significantly increased before, and reduced 24 hours after induction of differentiation (**C**). *Cdk2* expression was slightly reduced in *Abhd15*-silenced cells 6 hours after induction start (**D**). (n=4)

The next step, connecting E2F transcription factors, cyclins, and CDKs, was the investigation of pocket binding proteins i.e. retinoblastoma protein (pRb), p107, and p130. These pocket

binding proteins can bind to E2F factors and thereby keep them from activating or repressing the cell cycle. This binding is cleaved after phophorylation by CDKs, which in turn are regulated by cyclins.[81] As the investigation of neither *E2F* nor *cyclins* or *Cdk*s helped to explain the defect leading to impaired adipogenesis of *Abhd15*-silenced cells, the expression of these pocket proteins was investigated. *pRb* mRNA expression was slightly reduced in *Abhd15*-silenced cells (Fig. 34A), as was the mRNA expression of *p130* (Fig. 34B). The *p107* expression profile showed no differences between *Abhd15*-silenced and control cells (Fig. 34C). Unfortunately again, the results did not help to explain the impaired adipogenesis of *Abhd15*-silenced cells. No obvious regulations could be detected, as the significant differences measured seemed to be too small to be biologically relevant.

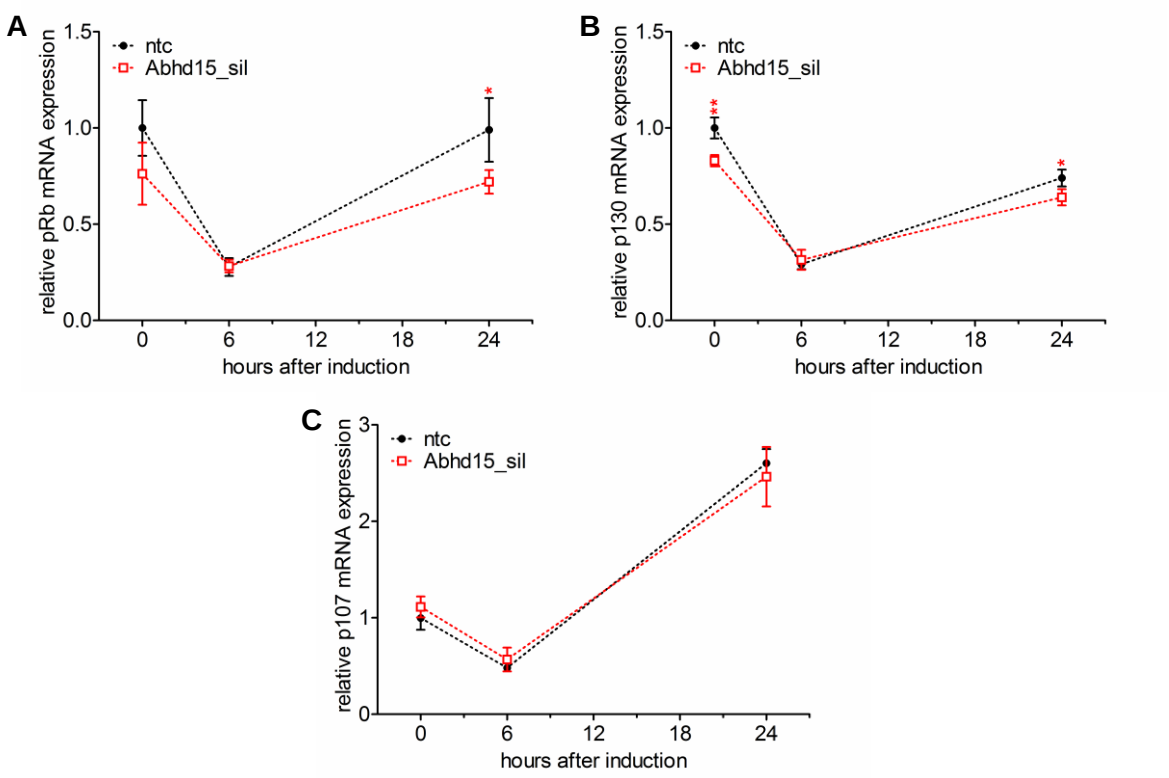

Fig. 34: mRNA expression of *pocket binding proteins* during MCE. 3T3-L1 cells were stably silenced using lentiviral particles coding for *Abhd15* shRNA (Abhd15_sil) and for a non-target shRNA as control (ntc). *Abhd15* silencing did not evoke any striking differences in the expression profile of pocket binding proteins *pRb* (**A**), *p130* (**B**), or *p107* (**C**). *pRb* and *p130* expressions were slightly decreased in *Abhd15*-silenced cells, whereas *p107* expression did not show any differences. (n=4)

These results indicate that the important early phase of differentiation is impaired in 3T3-L1 cells silenced for *Abhd15*, as the important adipogenic markers *Pparγ* and *C/ebpα* showed decreased mRNA expression. However, it seems that impaired MCE was not the reason for the differentiation defect, as none of the measured MCE markers is strongly affected by *Abhd15* silencing.

4.2.5 *Abhd15* expression is tightly connected to apoptosis

Preconfluent *Abhd15*-silenced 3T3-L1 cells only showed a ~30% decrease in Abhd15 mRNA expression (Fig. 28A), and noticeable did not show any decrease in *Abhd15* expression after 2 weeks of culturing (data not shown). Nevertheless, compared to control cells the cells with reduced *Abhd15* expression showed a slower proliferation rate, reflected by a decrease in cell count by 30-40% 48 hours after seeding a defined number of cells (Fig. 35A). In line with this, cells stably overexpressing *Abhd15* showed a slightly increased cell proliferation (Fig. 35B).

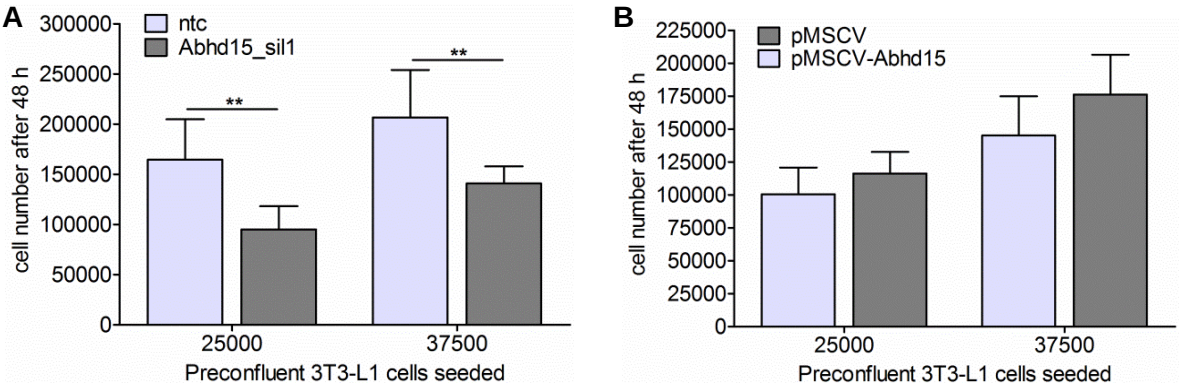

Fig. 35: Cell counting of *Abhd15*-silenced and overexpressing cells. **A.** 3T3-L1 cells were stably silenced using lentiviral particles coding for an *Abhd15* shRNA (Abhd15_sil) and for a non-target shRNA as control (ntc). Cell proliferation was reduced in *Abhd15*-silenced preconfluent 3T3-L1 cells, shown by the decreased cell number compared to control cells 48 hours after seeding. **B.** 3T3-L1 cells were infected with lentiviral particles obtained from phoenix cells transfected with either empty vector (pMSCV) or a vector containing the *Abhd15* gene (pMSCV-Abhd15). Cell proliferation was slightly increased in *Abhd15* overexpressing preconfluent 3T3-L1 cells, shown by an upwards trend in the cell number 48 hours after seeding.

With the help of Dr. Alexander Deutsch, this observation was confirmed by a colorimetric proliferation assay (MTS), revealing a highly significant reduction in proliferation of preconfluent *Abhd15*-silenced cells by ~20% (Fig. 36A). To get a better insight into the changed proliferation of *Abhd15*-silenced cells, their cell cycle was analyzed in more detail using BrdU FACScan. The analysis revealed an increased SubG1 peak (Fig. 36B), without any changes in the S phase (Fig. 36C), or G_1 or G_2 peak (data not shown) in *Abhd15*-silenced 3T3-L1 cells. As the SubG1 peak reflects apoptotic cells, whereas the S phase shows cells in the interphase, these results indicated increased apoptosis, rather than a defect in cell division, as a cause for the reduced cell number.

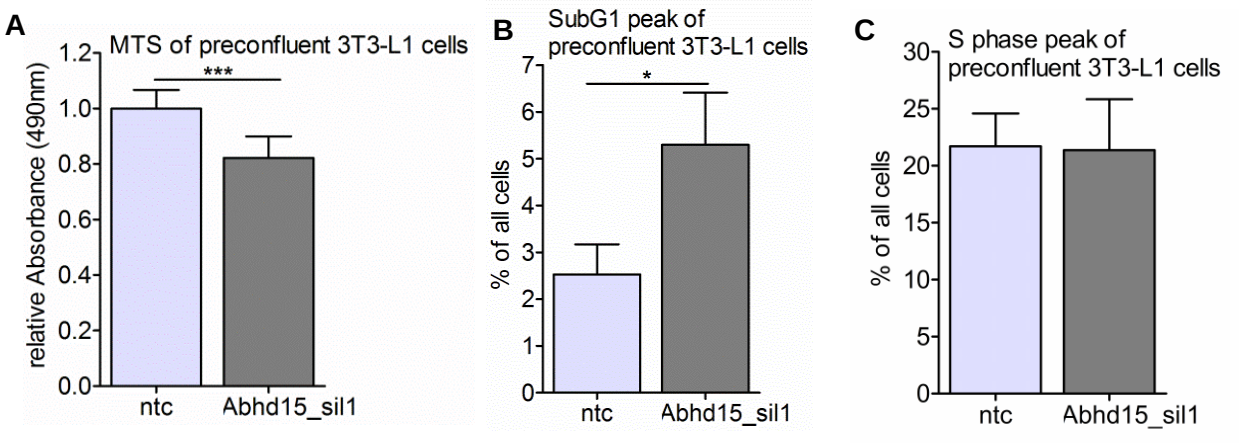

Fig. 36: MTS assay and cell cycle analysis of *Abhd15*-silenced cells. 3T3-L1 cells were stably silenced using lentiviral particles coding for an *Abhd15* shRNA sequence (Abhd15_sil1) and a non-target shRNA as control (ntc). **A.** The colorimetric proliferation assay (MTS) showed a reduction in proliferation of preconfluent *Abhd15*-silenced cells by ~20%. **B.** Analysis of preconfluent 3T3-L1 cells, using BrdU FACScan, showed a strongly elevated SubG1 peak, pointing towards increased apoptosis. **C.** BrdU FACScan Analysis revealed no differences in the S phase peak between preconfluent *Abhd15*-silenced and control cells.

Further, western blot analysis of B-cell lymphoma 2 (BCL-2) and BCL-2-associated X protein (BAX), both essential regulators of apoptosis [35], revealed decreased protein levels of the pro-survival regulator BCL-2, and increased protein levels of the pro-apoptotic regulator BAX (Fig. 37A & B). Finally, a caspase 3/7 assay, showing a more than 2-fold increased caspase activity in *Abhd15*-silenced cells (Fig. 37C), provided the last hint that apoptosis is increased in preconfluent *Abhd15*-silenced 3T3-L1 cells. Interestingly, annexinV staining, which is one of the most common assays to verify apoptosis[75], did not show any significant differences between control and *Abhd15*-silenced cells.

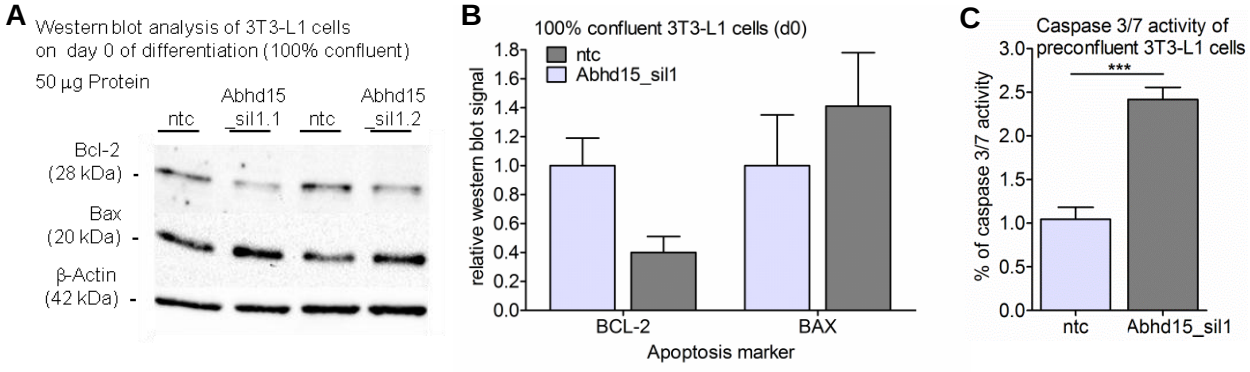

Fig. 37: Apoptosis analysis of *Abhd15*-silenced cells. 3T3-L1 cells were stably silenced using lentiviral particles coding for an *Abhd15* shRNA (Abhd15_sil1) and for a non-target shRNA as control (ntc). Western blot (**A**) and relative western blot signal (**B**) of the essential regulators of apoptosis BCL-2 and BAX. The protein expression of the pro-survival regulator BCL-2 was decreased, while the protein level of the pro-apoptotic regulator BAX increased. (n=2) **C.** Increased Caspase 3/7 activity could be measured in preconfluent *Abhd15*-silenced 3T3-L1 cells, proofing increased apoptosis.

In accordance with these findings, induced apoptosis (provoked by treatment of preconfluent 3T3-L1 cells with palmitic acid concentrations leading to conditions from non-apoptotic (100 µM) to highly apoptotic (500 µM) for 24 hours[82] resulted in a massive increase of *Abhd15* mRNA expression in a dose- dependent manner (Fig. 38).

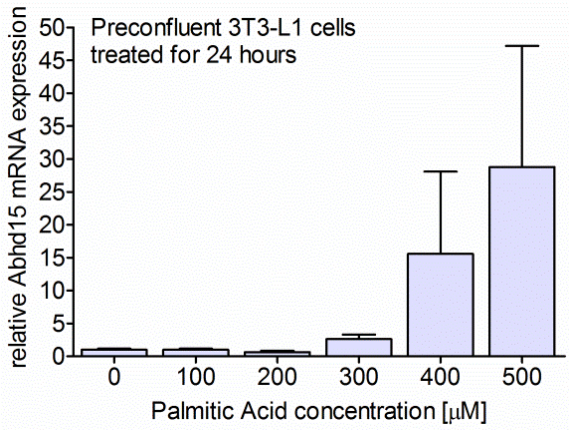

Fig. 38: Palmitic acid treatment of preconfluent 3T3-L1 cells. 24 hours treatment of preconfluent 3T3-L1 cells with palmitic acid concentrations, reaching from non-apoptotic (100 µM) to apoptosis-inducing (500 µM)[82], increased *Abhd15* mRNA expression dose dependently.

Together these results demonstrate a connection of *Abhd15* levels and apoptosis and suggest that a sufficient amount of *Abhd15* is necessary to keep apoptotic signaling in check.

The question why apoptosis is increased in *Abhd15*-silenced cells led us to investigate the adipogenesis-apoptosis linkage ER stress. Especially adipocytes have to be able to cope with ER stress and react to increased protein expression promptly.[83] Overflow of unfolded proteins leads to activation of one or more of the three major ER transmembrane receptors, namely PERK, ATF6, and IRE1, leading to a cascade of rescue mechanisms to reduce accumulation of unfolded proteins and restore normal ER function. However, chronic or too severe ER stress switches to apoptotic cell death.[41] In preconfluent *Abhd15*-silenced cells two of these three ER stress arms were slightly activated. The mRNA expression of the two PERK marker genes *Atf4* and *Atf3*, as well as *Atf6* itself were increased significantly. The third transmembrane receptor *Ire1* and its downstream marker gene X-box binding protein 1 spliced (*Xbp1s*) did not show any expression changes. (Fig. 39). Especially the PERK pathway is known to activate CHOP, which is well known to promote apoptotic cell death.[41] Indeed, also *Chop* mRNA expression was increased (Fig. 39). As it was already shown that the two CHOP regulated proteins, BCL-2 and BAX, were regulated pro-apoptotically, ER stress might be the missing link between *Abhd15* silencing and apoptosis.

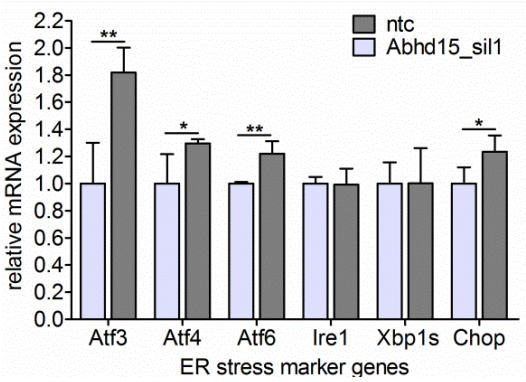

Fig. 39: Relative mRNA expression of endoplasmic reticulum (ER) stress marker genes of the PERK arm (*Atf3* and *Atf4*) and *Atf6* arm of UPR (unfolded protein response) were increased in preconfluent *Abhd15*-silenced 3T3-L1 cells. The third ER stress response arm, activated by increased *Ire1* and *Xbp1s* expression, was not stressed. *Abhd15* knockdown in preconfluent 3T3-L1 cells also led to increased *Chop* expression, an important element of the switch from pro-survival to pro-death signaling[41].

Another factor that might lead to the phenotype of *Abhd15*-silenced cells is that *Abhd15* silencing also influences the *Pde3B* expression.[46] The ~30% silencing of *Abhd15* in preconfluent cells (Fig. 28A) was sufficient to reduce *Pde3B* mRNA expression nearly to the same extent (Fig. 40). As PDE3B hydrolyzes cAMP and cGMP, and thereby takes part in the regulation of glucose and lipid metabolism,[53] it has to be kept in mind that the impaired adipocyte phenotype might partly result from the reduced *Pde3B* expression, especially, as reduced PDE3B could result in increased cAMP levels, which in turn can have pro- or anti-apoptotic effects [84]. However, these effects depend on the cell type [84].

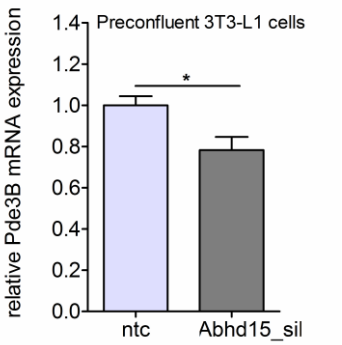

Fig. 40: Relative mRNA expression of cAMP and cGMP hydrolase *Pde3B* in preconfluent *Abhd15*-silenced 3T3-L1 cells. *Pde3B* was shown do be associated to and regulated by *Abhd15* expression[46].

4.3 Establishment of the *Abhd15*-ko mouse

4.3.1 Generation of *Abhd15*-deficient and loxP-tagged ES cells and birth of chimeric founders

To manipulate *Abhd15*, a targeting vector for the homologous recombination in murine HM-1 embryonic stem (ES) cells[85] was designed. The targeting vector removed exon 2 of the *Abhd15* gene, which harbours the predicted active site of the protein and therefore should prevent a functional gene product. The targeting vector was designed with a “long” and a “short” region of homology to *Abhd15* genomic sequences, a loxP recombination site within the first intron of *Abhd15*, a neomycin resistance gene flanked by loxP sequences[86], and a diphtheria toxin fragment A for enrichment of correctly targeted ES cell clones[87] (Fig. 41).
To generate the short arm of the targeting vector, a sequence 1.5 kb downstream to exon 2 was amplified by PCR using HM-1 ES cell genomic DNA as template. Subsequently this fragment was cloned into a pBlueKS- vector, harbouring a loxP flanked neomycin resistance cassette[86], which enables the selection of positive clones with G418. Next, a 2.7 kb genomic sequence encompassing *Abhd15* exon 2 and 0.5 kb each, up- and downstream of exon 2, was amplified by PCR and also cloned into the pBlueKS- vector, already containing the short arm, neomycin resistance cassette, and loxP sites. Subsequently the whole construct was cloned into a pBlueKS- vector already harbouring a loxP site. Furthermore, a long homologous region was generated by the amplification of a 3.9 kb fragment of intron 1 and cloned into the pBlueKS- vector, prepared in the step before. Finally, the whole construct was introduced 3’ to a diphtheria toxin A cassette into a pUC vector to generate the final targeting vector (Fig. 41).

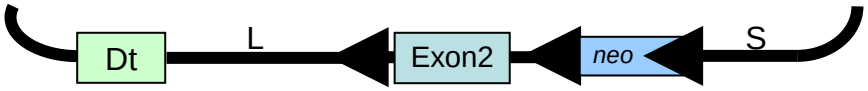

Fig. 41: *Abhd15*-ko mouse targeting vector. The targeting vector was designed with a “long” (L) and a “short” (S) region of homology to *Abhd15* genomic sequences around exon 2, a loxP recombination site (LoxP) within the first intron of *Abhd15*, a neomycin resistance gene (neo) flanked by loxP sequences, and a diphtheria toxin fragment A (Dt) for enrichment of correctly targeted ES cell clones.

The linearized targeting vector was transfected into 129 HM-1 ES cells by electroporation. G418 resistant clones were picked and expanded. Two probes (I and II) and fitting restriction sites (Fig. 42A) were used to perform southern blot analysis for identification of clones, which underwent homologous recombination and therefore contained the first loxP site (Fig. 42B) as well as the neomycin resistance gene (Fig. 42C). Further, to detect whether the targeting

vector operated not only by homologous recombination, but also by non-directional insertion, a probe detecting neomycin cassettes proved that only one cassette was included in the clones (Fig. 42C).

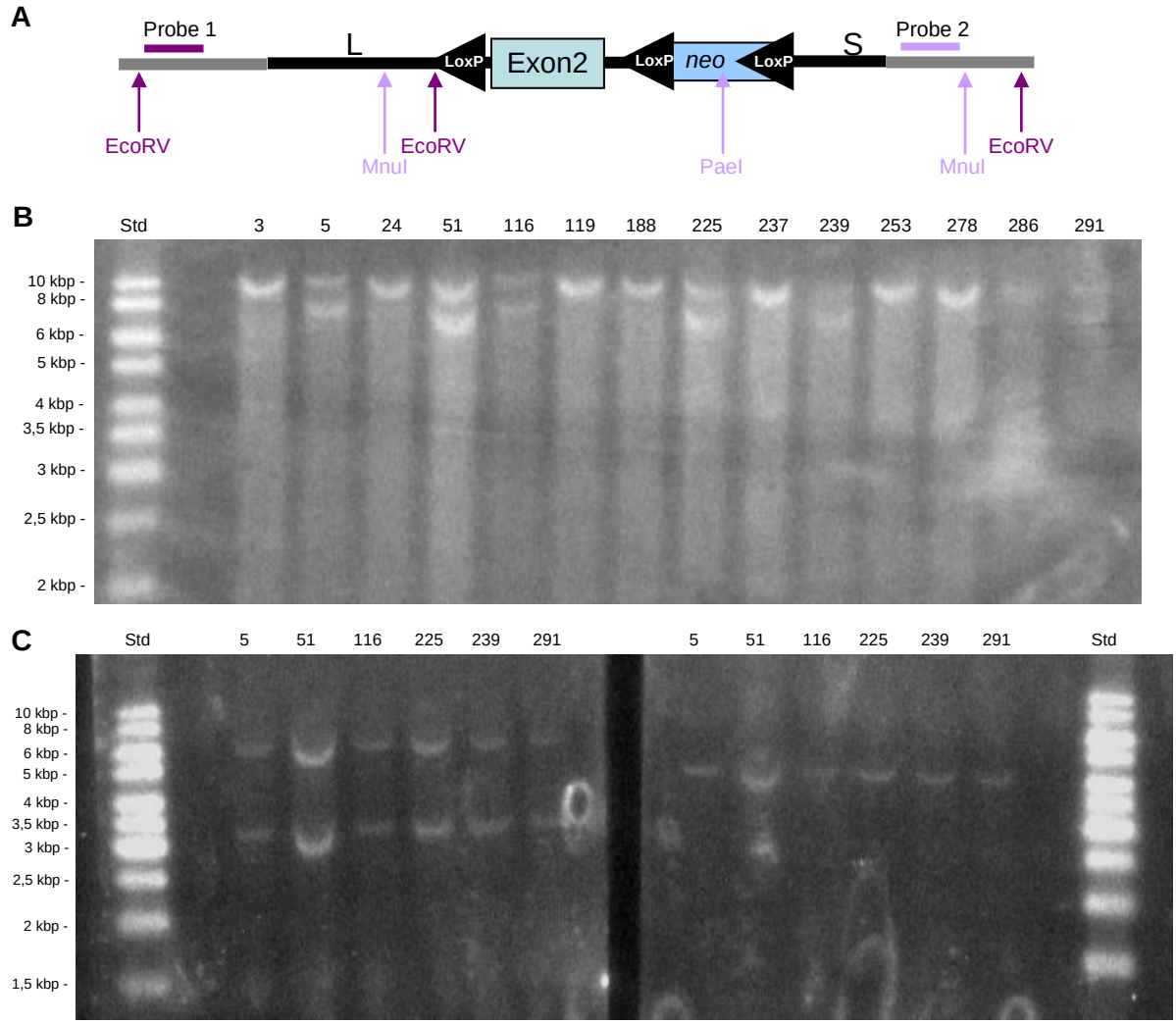

Fig. 42: Southern blot analysis to examine ES cell clones containing the loxP sites (LoxP) and the neomycin cassette (neo). **A.** Location of the Southern blot probes and restriction sites, to identify clones which contain the loxP site in intron1 and the neomycin cassette. **B.** Southern blot using probe I. DNA restriction with *EcoR*V evaluated the clones 5, 51, 116, 225, 239, and 291 to contain the loxP site in intron1. **C.** Southern blot using probe II. DNA restriction with *Mnu*I and *Pae*I evaluated the clones 5, 51, 116, 225, 239, and 291 to include the neomycin cassette after the homologous recombination (left side). To detect whether the targeting vector operated not only by homologous recombination, but also by non-directional insertion, a probe detecting neomycin cassettes proved that only one cassette was included in the clones (right side).

Two homologous recombined clones (#239 and #291) were used for Cre-mediated manipulation of the loxP flanked region as previously described[86]. ES cell clones with either a deleted (missing the neomycin resistant cassette and exon 2) or a floxed (missing the neomycin resistant cassette) *Abhd15* allele were further verified by PCR (data not shown) and southern blotting (Fig. 43).

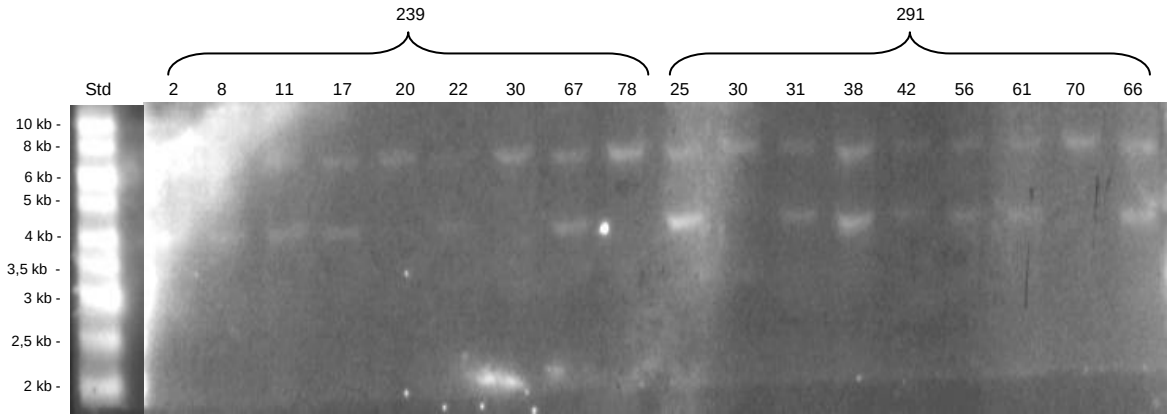

Fig. 43: Southern blot analysis to indentify floxed and knockout ES cell clones. DNA restriction with *Mnu*I and *Pae*I and southern blotting using probe II evaluated the clones 239-8, -11, -17, -22, -67, and 291-25, -31, -38, -42, -56, -61, -66 to be total knockout clones, whereas the clones 239-2, -20, -30, -78 and 291-30, -70 were floxed clones. All clones lacked the neomycin cassette.

After checking for normal karyotype appearance, the clone 239-78 was used for blastocyst injection and transferred into pseudo-pregnant mice, carried out by Univ.-Prof. Dr. Thomas Rülicke at the Institute of Laboratory Animal Science at the University of Veterinary Medicine Vienna. 12 chimeric mice were born, whereof 5 were used for breeding because of their high chimerism (≥80%). Only 2 of the mice were fertile, one male and one female, and only the male's litters were 100% agouti. These litters were mated with CMV-Cre and wild-type C57Bl6 to generate total knockout and floxed mice on a clean C57Bl6 background. Breeding of floxed *Abhd15* mice with transgenic mice expressing the Cre-recombinase under the control of a tissue specific promoter should yield mice that lack *Abhd15* in a specific tissue.

4.3.2 Preliminary characterization of *Abhd15* whole body knockout mice

As mentioned above, the generation of mice bred from the chimera mice were not on clean background. This is due to the use of 129 HM-1 ES cells, obtained from 129/ola mice, in combination with a C57Bl6 foster mouse. As C57Bl6 mice are a general multipurpose model, used for diet-induced obesity, transgenic/knockout model development, safety and efficacy testing, as well as immunology, it was chosen to be the better model than 129/ola. For final characterization of the mice, backcrossing for 10 generations is common usage.[88] The following experiments were performed with mice of generations F4-5, which means definitely not on clean background. However, although preliminary, these results should help to find the directions for further investigations.

Keeping in mind that *Abhd15* is expressed age dependently, it was tried to separate mice not only in male and female groups, but also in age groups. First the weight of *Abhd15*-ko mice was compared to wild-type littermates. It seems that *Abhd15*-ko did not influence weight gain of mice, as no differences were detected (Fig. 44A). HFD (40% calories in fat) though, did not lead to a weight gain in knockout mice (Fig. 44B). However, this experiment was performed only with one cohort of 8 wild-type and 4 *Abhd15*-ko mice, of which one mouse died at 6 months of age.

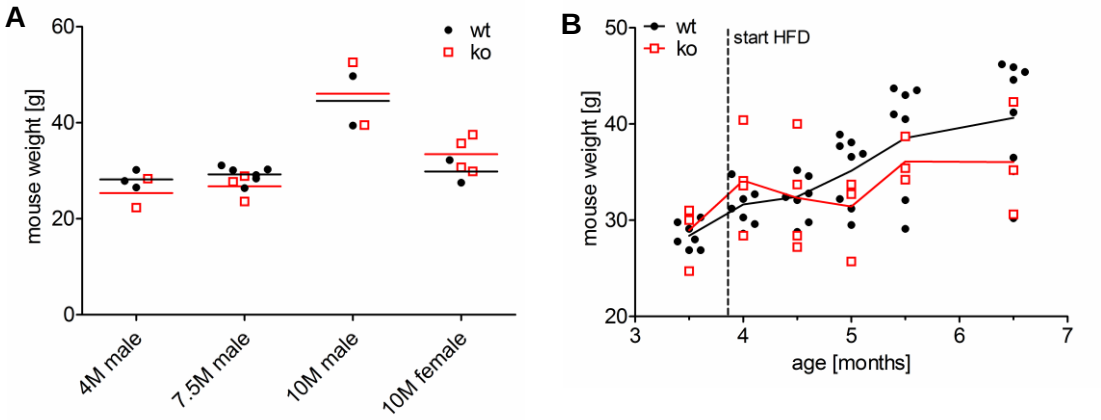

Fig. 44: Weight measurement of wild-type (wt) and *Abhd15*-ko (ko) littermates. **A.** No differences could be detected between ko and wt mice on a chow diet, independently of age (4 months (4M), 7.5 months (7.5M), 10 months (10M)), or sex. **B.** Upon HFD (40% calories in fat) ko mice did not gain as much weight as wt mice did.

Silencing of *Abhd15* in adipocytes led to impaired adipogenesis (Fig. 26A). Surprisingly, *Abhd15*-ko mice had more subcutaneous and epididymal WAT (sWAT and eWAT), than their wild-type littermates (Fig. 45A & B). This effect seemed to be bigger in young male and female mice than in old male mice (Fig. 45A & B). The same slight trend, but to a lower extend, could also be seen in BAT (Fig. 45C). The weights of livers of knockout and wild-type littermates were the same, except of the livers of old male mice, whose liver weights were slightly increased in knockout mice (Fig. 45D). However, the data of the 10 months old male and female mice have to be considered with caution, as only 2 mice were left to be sacrificed per group.

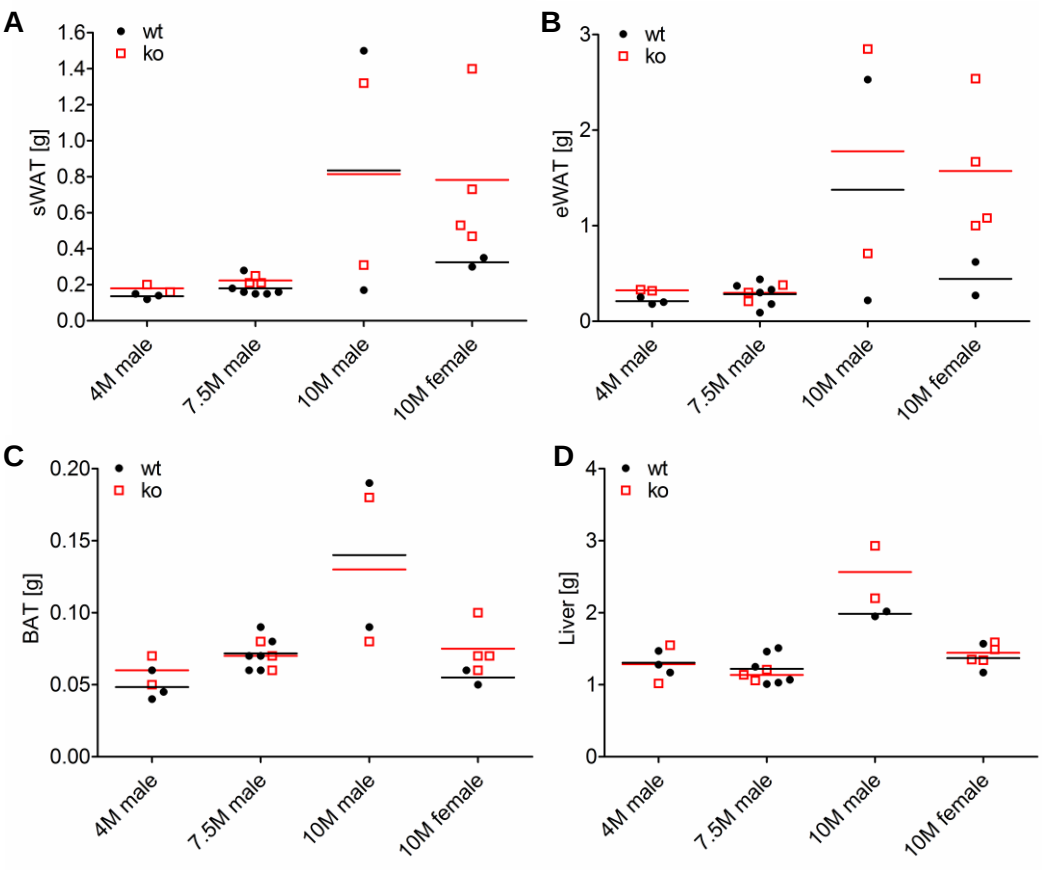

Fig. 45: Tissue weight of wild-type (wt) and *Abhd15*-ko (ko) littermates at different ages (4 months (4M), 7.5 months (7.5M), 10 months (10M)). **A.** sWAT weight was increased especially in younger or in female ko mice. **B.** As seen in sWAT, also the eWAT was increased in younger or in female mice. **C.** A slight trend to increased BAT was detected in young male and in female mice. **D.** Old male ko mice might tend to increased liver weight.

Having in mind that *Abhd15* was regulated upon levels of free fatty acids, and the additional fact that it is a predicted hydrolase, the question was asked whether knockdown of *Abhd15* might influence the levels of FFAs. Therefore, *Abhd15* FFA levels were measured in the blood of male and female mice in fed and fasted state. Unfortunately no significant differences between knockout and wild-type mice could be detected (Fig. 46A). However, the mice were at least 4 months old. As *Abhd15* expression was higher in younger mice (Fig. 4B & 7C), the difference between knockout and wild-type mice might be bigger in young mice as a trend to increased FFA level in 4 months old male knockout mice was observed. Further *Abhd15* mRNA expression was also reduced in adipose tissue of fasted mice (Fig.5A) and mice on HFD (Fig. 4B), which could explain why no changes were detected in mice when they were fasted and on HFD (40% calories in fat) (Fig. 46B).

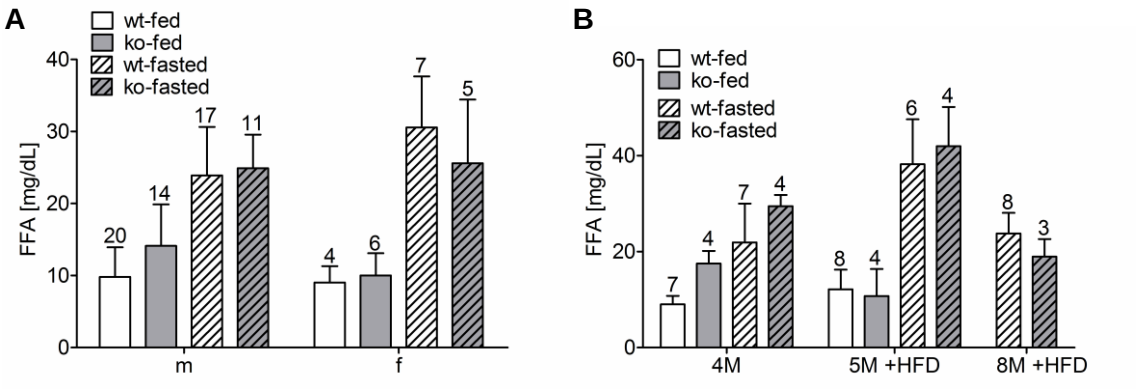

Fig. 46: Measurement of FFAs in the blood plasma of wild-type (wt) and *Abhd15*-ko (ko) littermates. Mice numbers are mentioned over the bars. **A.** No differences could be measured in male (m) and female (f) mice in fed and fasted status when mice of all ages were analyzed together. **B.** 4 months old male knockout mice showed a trend to increased FFA levels, compared to their littermates. The same mice did not show any differences in FFA levels when fed a HFD (40% calories in fat) afterwards.

Due to the predicted function of being a hydrolase, and due to the fact that *Abhd15*-ko mice seemed to have increased adipose tissue mass, differences in triglyceride levels in the blood plasma of *Abhd15*-ko mice were expected. Surprisingly, no differences in triglyceride concentrations of male and female mice in fed or fasted status could be detected (Fig. 47A). Even feeding of HFD did not lead to any differences in the triglyceride blood levels (Fig. 47B).

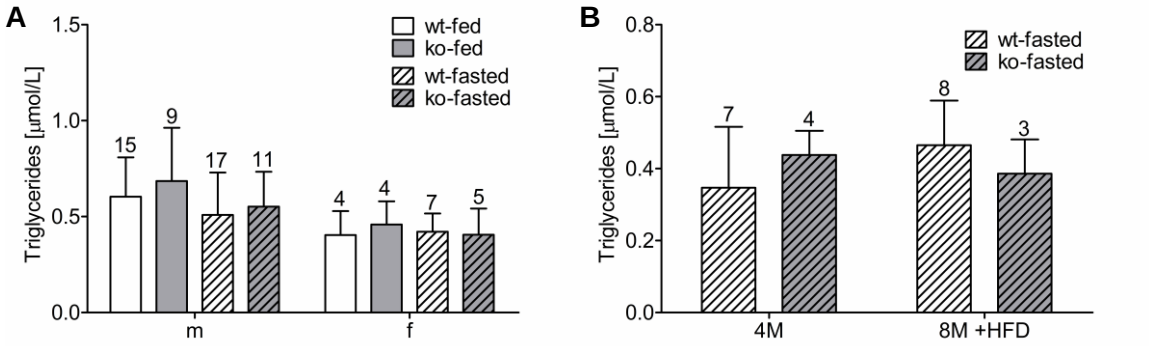

Fig. 47: Measurement of triglycerides in the blood plasma of wild-type (wt) and *Abhd15*-ko (ko) littermates. Mice numbers are mentioned over the bars. **A.** No differences could be measured in male (m) and female (f) mice in fed and fasted status, when mice of all ages were analyzed together. **B.** Triglyceride levels of mice at the age of 4 months (4M) and of the same mice after 4 months of HFD (40% calories in fat) at the age of 8 months (8M +HFD) did not reveal any differences between wt and ko mice in fasted status.

Finally blood glucose levels were measured. Although no significant differences between wild-type and *Abhd15*-ko mice were detected, male and female mice showed a trend to

reduced blood glucose levels in fasted status (Fig. 48). In fed status no differences were observed (Fig. 48).

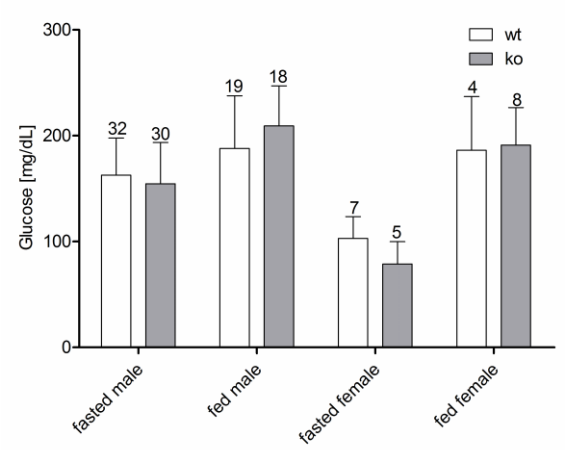

Fig. 48: Blood glucose levels of wild-type (wt) and *Abhd15*-ko (ko) littermates revealed a trend to reduced blood glucose in fasted male and female mice. No differences could be detected in fed mice. Mice numbers are mentioned over the bars.

To have a deeper look onto this effect, three cohorts of male mice were tested for their blood glucose levels several times at different ages. Interestingly cohorts 1 and 3 showed the trend to reduced glucose levels upon fasting, while cohort 2 did not (Fig. 49A). Although the glucose levels changed within the groups during aging, the trend stayed the same (Fig. 49A). Again no changes between *Abhd15*-ko and wild-type mice were detected in fed mice (Fig. 49B).

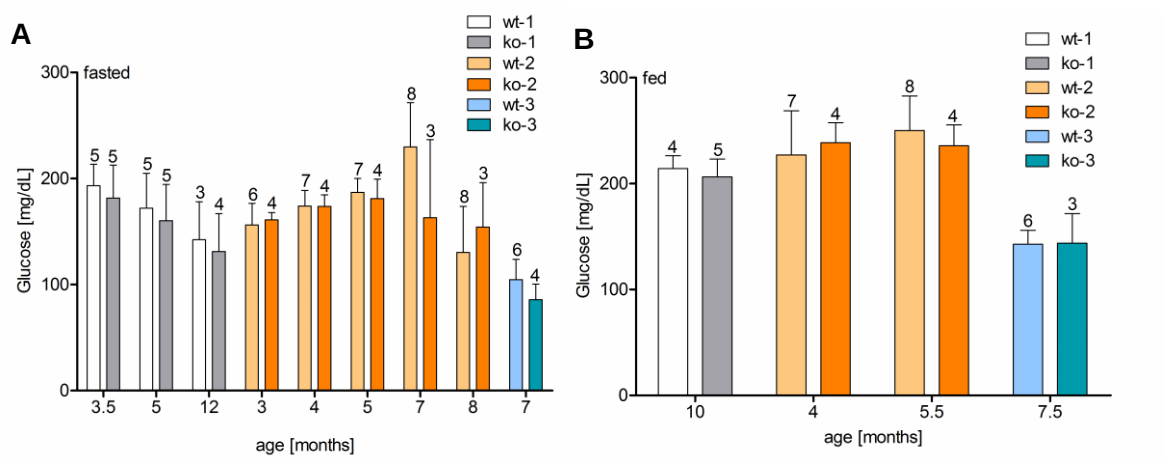

Fig. 49: Blood glucose levels of male wild-type (wt) and *Abhd15*-ko (ko) littermates. Mice number is mentioned over the bars. **A.** A trend to reduced blood glucose levels in fasted mice was detected in cohorts 1 (grey) and 3 (green). The trend was age-independent within the cohorts. Cohort 2 (orange) did not show any trends. **B.** No differences between wt and ko mice were detected in the fed status.

To investigate the glucose metabolism of *Abhd15*-ko mice, glucose and insulin tolerance were tested for three male and one female cohort of mice at different ages.

The first cohort did not show any abnormalities in glucose levels when challenged with a glucose tolerance test (GTT) (Fig. 50A & B). Challenging the mice with an insulin tolerance test (ITT) though, revealed that *Abhd15*-ko mice seemed slightly more insulin resistant than their wild-type littermates (Fig. 50C & D). At the age of 12 months the same mice were challenged with a low dose of insulin, which still was too high for one of the remaining wild-type mice and therefore led to death. Due to the low dose a very small effect was observed in wild-type mice, while no effect could be observed in *Abhd15*-ko mice. (Fig. 50E & F).

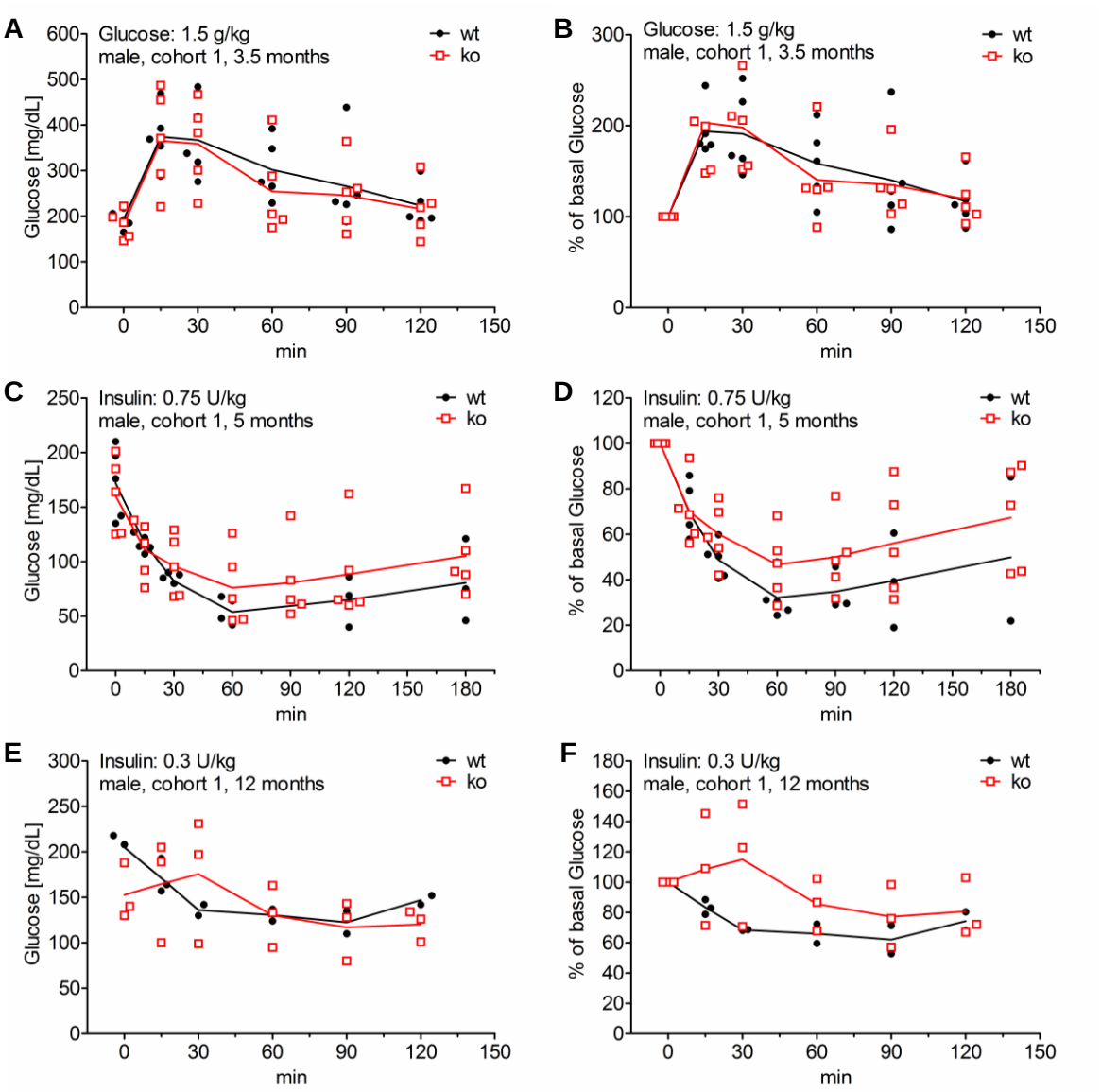

Fig. 50: GTT and ITT of cohort 1. 3.5 months old male *Abhd15*-ko (ko) and wild-type (wt) mice did not show any differences in glucose tolerance, neither in direct values (**A**), nor in values normalized to the basal levels (**B**). The same mice challenged with an ITT at 5 months of age showed that ko mice were slightly insulin resistant, reflected by direct measured (**C**), and normalized to basal blood glucose levels (**D**). At 12 months of age 1 out of 3 wild-type mice died already when challenged with the low dose of 0.3 U/kg insulin, which made the use of a higher dose impossible. Due to the low dose wild-type mice showed only a slight response, while *Abhd15*-ko mice showed no reduced plasma glucose level in directly measured (**E**) as well as normalized values (**F**).

The second cohort of male mice was treated with HFD after 4 months of age. Right before the start of HFD, the GTT revealed, like in the first cohort, no differences in glucose tolerance between *Abhd15*-ko and wild-type littermates (Fig. 51A & B). Also like the first cohort of mice, the second cohort again showed a slightly increased insulin resistance of *Abhd15*-ko mice, this time at the age of 3 months.

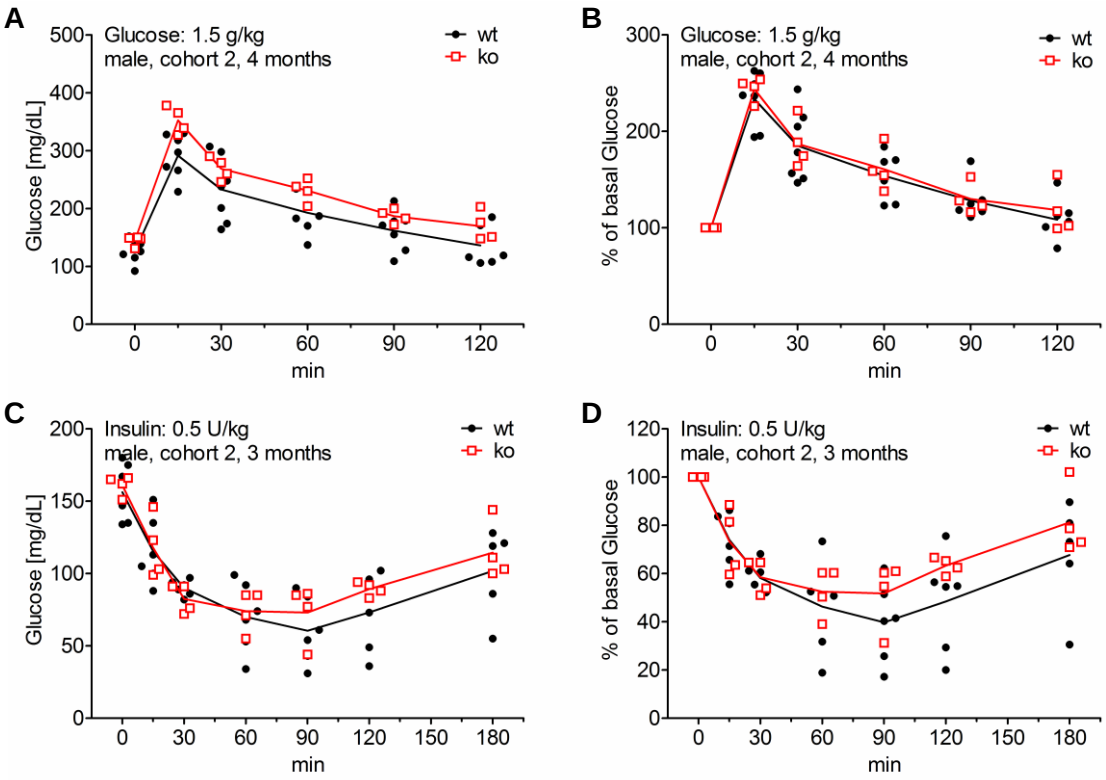

Fig. 51: GTT and ITT of cohort 2. At the age of 4 months male *Abhd15*-ko (ko) and wild-type (wt) mice did not show any differences in glucose tolerance, neither in direct values (**A**), nor in values normalized to the basal levels (**B**). ITT of these mice at the age of 3 months again showed, like the first cohort, that ko mice seemed to be slightly more insulin resistant than their wt littermates, shown in direct measurement data (**C**), but better in to basal glucose level normalized values (**D**).

Upon HFD though, wild-type mice gained weight, while *Abhd15*-ko mice did not (Fig. 44B). Therefore, it was not surprising that after 3 months of HFD, knockout mice were more insulin sensitive than their wild-type littermates (Fig. 52A & B).

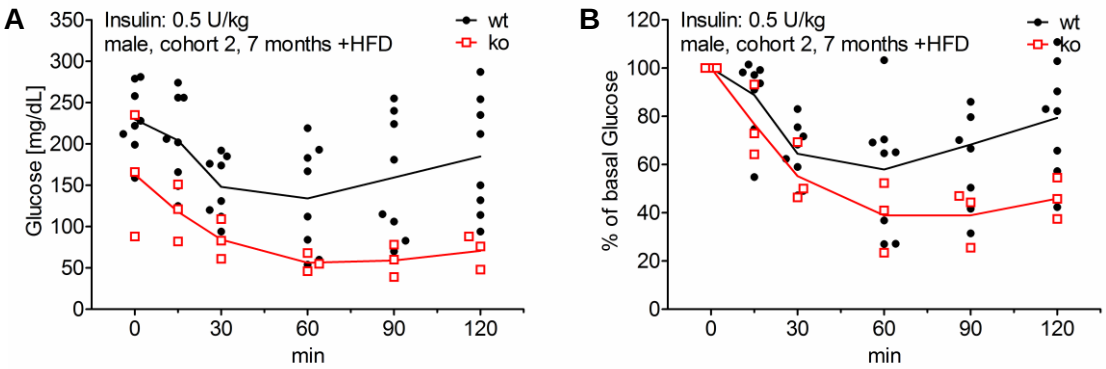

Fig. 52: ITT of cohort 2 after HFD. 7 months old male *Abhd15*-ko (ko) and wild-type (wt) mice on HFD showed ko mice to be more insulin sensitive than wt in direct measured values (**A**) and in values normalization to basal levels (**B**).

The third cohort again did not show any differences between wild-type and *Abhd15*-ko mice when challenged with a GTT at 7 months of age (Fig. 53A & B). Interestingly, in contrast to cohort 1 and 2, these mice seemed to be slightly more insulin sensitive (Fig. 53C & D) as seen for the second cohort after HFD. However, it is very unlikely that the reason for this change of insulin sensitivity is ageing, as the first and the third cohort measurement happened only one month apart.

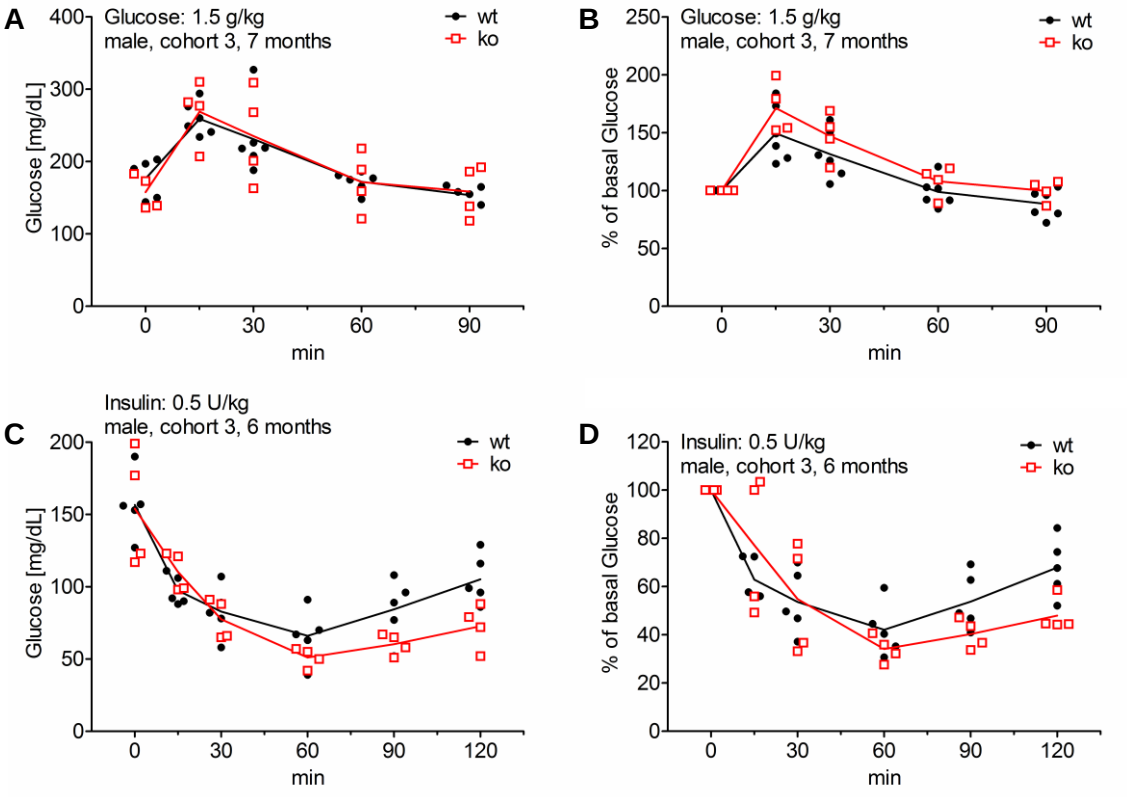

Fig. 53: GTTand ITT of cohort 3. 7 months old male *Abhd15*-ko (ko) and wild-type (wt) mice did not show any differences in glucose tolerance, neither in direct values (**A**), nor in values normalized to the basal levels (**B**). ITT of those mice at the age of 6 months showed, contrary to the first and second cohort, that ko mice seemed to be slightly more insulin sensitive than their wt littermates, shown in direct measurement data (**C**), and in to basal glucose level normalized values (**D**).

GTT of 7 months old female mice again did not show any differences between wild-type and *Abhd15-ko* mice (Fig. 54A & B). However, in this case the reduced glucose levels of *Abhd15-ko* mice upon fasting could be observed (Fig. 54B). The ITT of those mice at 7 months of age, showed again a slight insulin resistance (Fig. 54C & D), as it was observed before in cohort one and cohort two of males on chow diet.

This means that we saw increased insulin resistance in cohort one, and young mice of cohort two, as well as in the female cohort. Contrary to that, we saw increased insulin sensitivity in mice on HFD, as well as in cohort 3. Taken together it can be suggested that there are differences in knockout mice compared to wild-type mice, but definitely more experiments, especially with bigger cohorts with a clean background at various ages will be necessary.

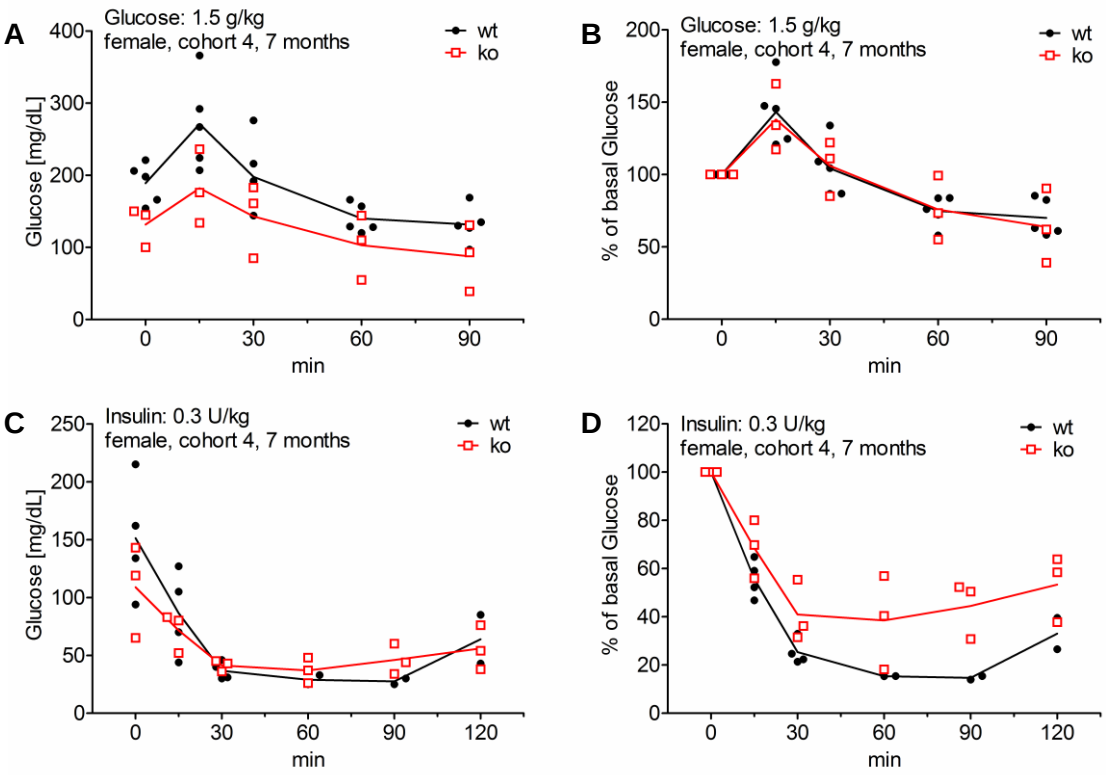

Fig. 54: GTT and ITT of cohort 4. 7 months old female *Abhd15*-ko (ko) and wild-type (wt) mice showed reduced glucose values in ko mice before glucose injection (**A**), but no differences in glucose tolerance (**B**). ITT of those mice at the age of 7 months again showed, like the first and second cohort of male mice, that ko mice seemed to be slightly more insulin resistant than their wt littermates, shown in direct measurement data (**C**), but better in to basal glucose level normalized values (**D**).

Next in line, mRNA expression of marker genes of several pathways were screened, to get a hint where *Abhd15* knockdown might lead to a lack of function or which genes might take over its functions. Therefore, tissues of wild-type and *Abhd15*-ko mice of various age groups and of both sexes were subjected to qPCR analysis.

First, *Abhd15* expression was examined in eWAT and liver, the tissues in which it is expressed highly in wild-type mice[47]. Thereby it was confirmed, additionally to southern blot and PCR analysis, that *Abhd15* was not expressed on mRNA level in *Abhd15*-ko mice (Fig. 55A & B). Interestingly, the variance of *Abhd15* within the cohorts was pretty big, and also the age dependent decrease of *Abhd15* on mRNA level could not be seen between 4 and 10.5 months old mice (Fig. 55A).

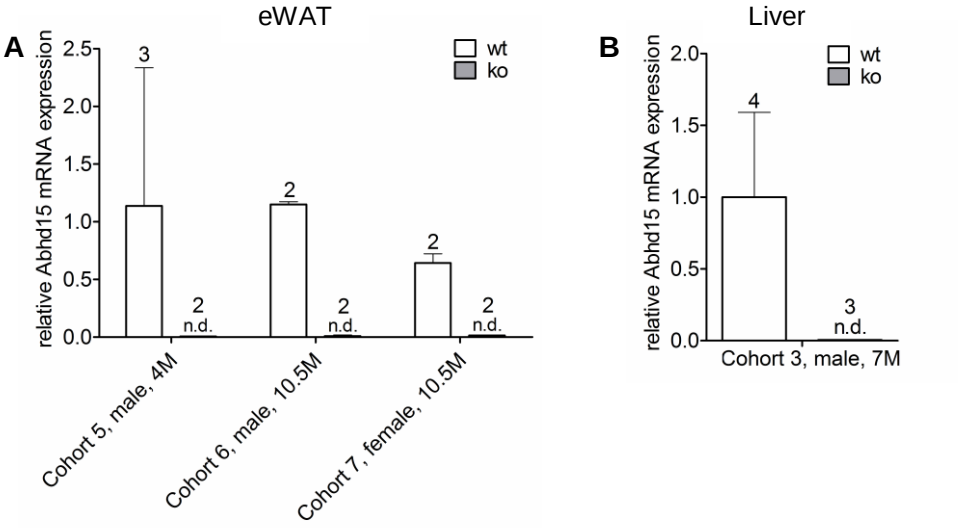

Fig. 55: mRNA expression of *Abhd15* in eWAT and liver. qPCR analysis of tissues of wild-type (wt) and *Abhd15*-ko (ko) mice of several ages (4 months (4M), 7 months (7M), 10.5 months (10.5M)). Mice numbers are mentioned over the bars, and mice with the same cohort numbers are littermates **A.** *Abhd15* was not detectable (n.d.) in eWAT of *Abhd15*-ko mice. **B.** *Abhd15* was also not detectable (n.d.) in liver of *Abhd15*-ko mice.

BAT is the tissue which shows the highest *Abhd15* expression on mRNA level.[47] For a fast screen, the genes *Fabp4*, *Pparα,* uncoupling protein 1 (*Ucp1*), *Atf3*, *Tnfα*, and *Pde3B* were chosen. *Fabp4* was investigates as a general adipogenesis marker[11], and *Pparα* and *Ucp1* as brown adipogenesis markers[89]. Further *Atf3* was chosen to uncover probable ER-stress[41] and due to its increased expression in *Abhd15*-silenced 3T3-L1 cells. To investigate the inflammatory status of BAT, *Tnfα*[90] was measured, and finally, due to its *Abhd15*-coupled expression in 3T3-L1 cells, *Pde3B*[46]. None of the marker genes investigated did show any clear expression differences between wild-type or *Abhd15*-ko mice (Fig. 56A-F). However, a slight trend to decreased *Fabp4* (Fig. 56A) and increased *Tnfα* (Fig. 56E) could be seen in *Abhd15*-ko mice.

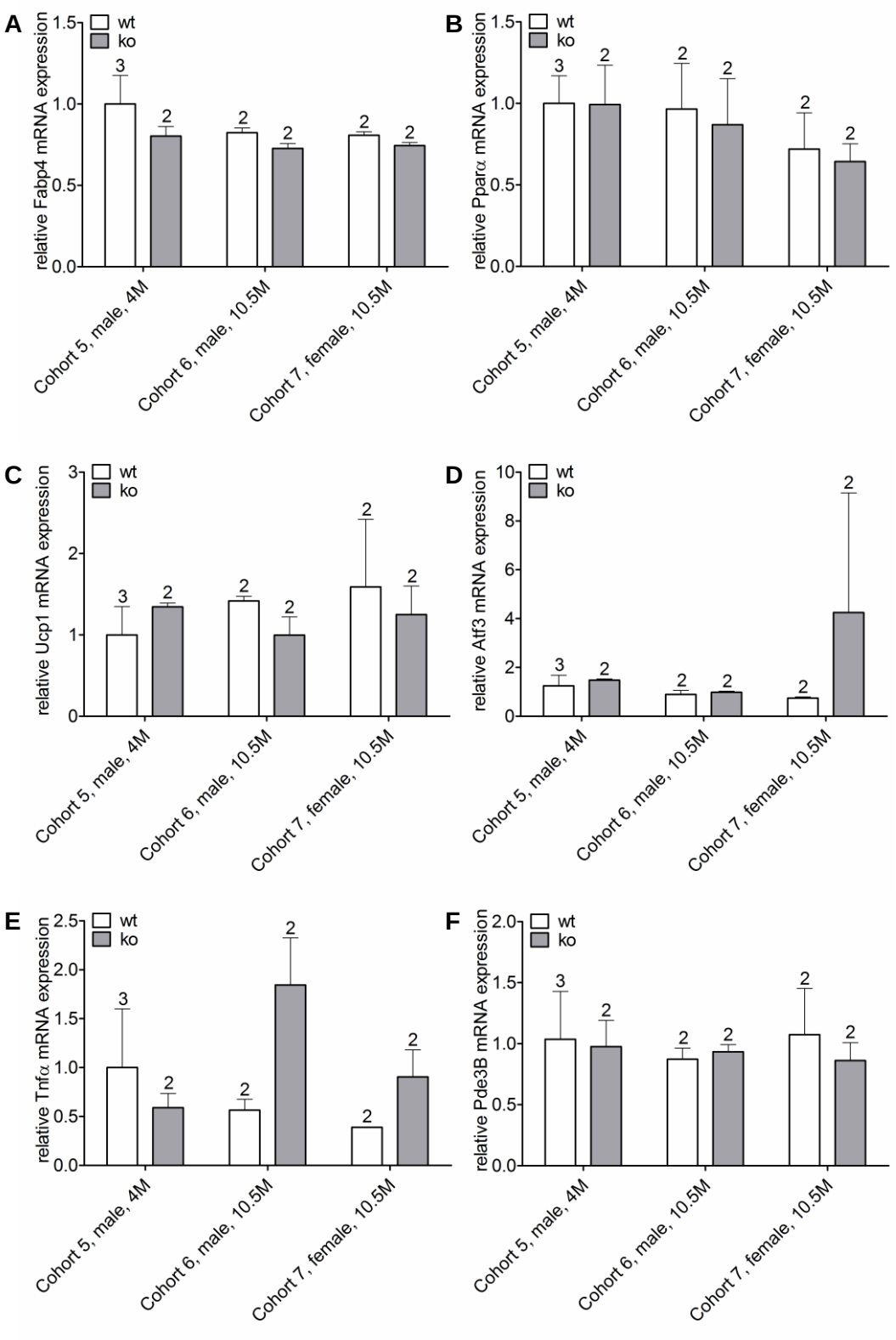

Figure 56: qPCR analysis of BAT of wild-type (wt) and *Abhd15*-ko (ko) mice of several ages (4 months (4M), 10.5 months (10.5M)). Mice numbers are mentioned over the bars, and mice with the same cohort numbers are littermates. Expression of the genes *Fabp4* (**A**), *Pparα* (**B**), *Ucp1* (**C**), *Atf3* (**D**), *Tnfα* (**E**), and *Pde3B* (**F**) was investigated.

The second highest *Abhd15* expression on mRNA level[47] and the highest on protein level[46] can be found in eWAT. As sWAT and eWAT masses were increased in *Abhd15*-ko mice (Fig. 45A & B), some differences in the expression pattern of *Abhd15*-ko mice were expected.

For sWAT, additionally to *Fabp4* a second marker of adipogenesis, *Pparγ* was investigated.[11] Further, due to the increased fat mass, the transcription factor *E2F1*, which is a cell cycle activator[77], and again the ER stress marker *Atf3*[41], the inflammation marker *Tnfα*[90], and *Pde3B,* as a probably *Abhd15* expression dependent gene[46], were investigated. Unfortunately, especially in sWAT the deviation within the cohorts and between the cohorts was immense, which made a detection of small differences between wild-type and *Abhd15*-ko mice impossible. No striking differences in any of the named marker genes were observed (Fig. 57A-F), but *E2F1* showed a slight trend to be increased in *Abhd15*-ko mice (Fig. 57C).

Also eWAT was screened for the expression of the adipogenesis marker *Pparγ*[11], the ER stress marker *Atf3*[41], the inflammation marker *Tnfα*[90], and the probably *Abhd15* expression dependent gene *Pde3B*[46]. Again the deviation within and between the cohorts was high, and made the examination of trends difficult. With these results, also in eWAT no significant differences between wild-type and *Abhd15*-ko mice were detected (Fig. 58A-D).

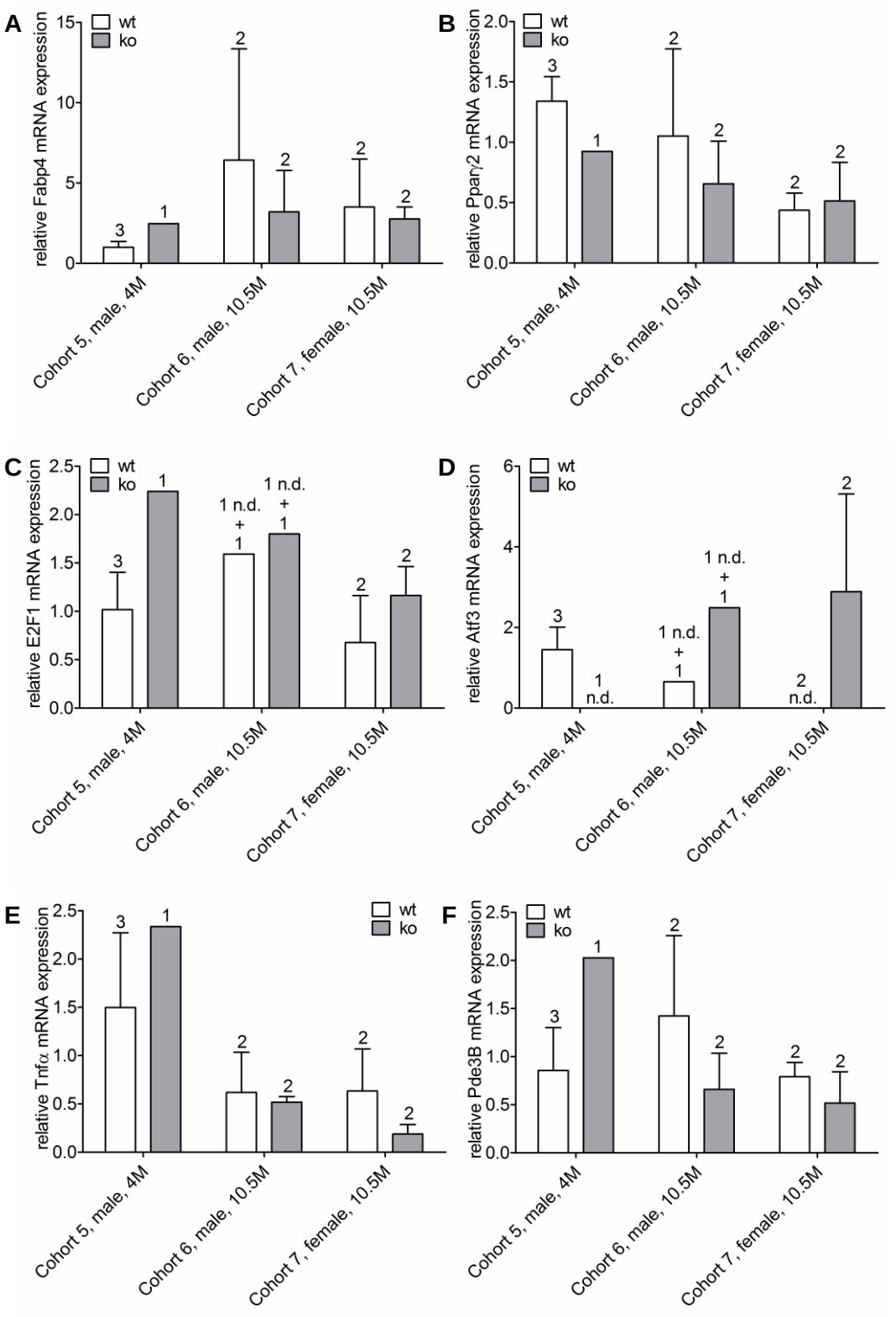

Fig. 58: qPCR analysis of sWAT of wild-type (wt) and *Abhd15*-ko (ko) mice of several ages (4 months (4M), 10.5 months (10.5M)). Mice numbers are mentioned over the bars, and mice with the same cohort numbers are littermates. Expression of the genes *Fabp4* (**A**), *Pparγ* (**B**), *E2F1* (**C**), *Atf3* (**D**), *Tnfα* (**E**), and *Pde3B* (**F**) was investigated.
The Cq values of *E2F1* and *Atf3* were very high, implementing a very low expression. In some samples the signal was not even detectable (n.d.).

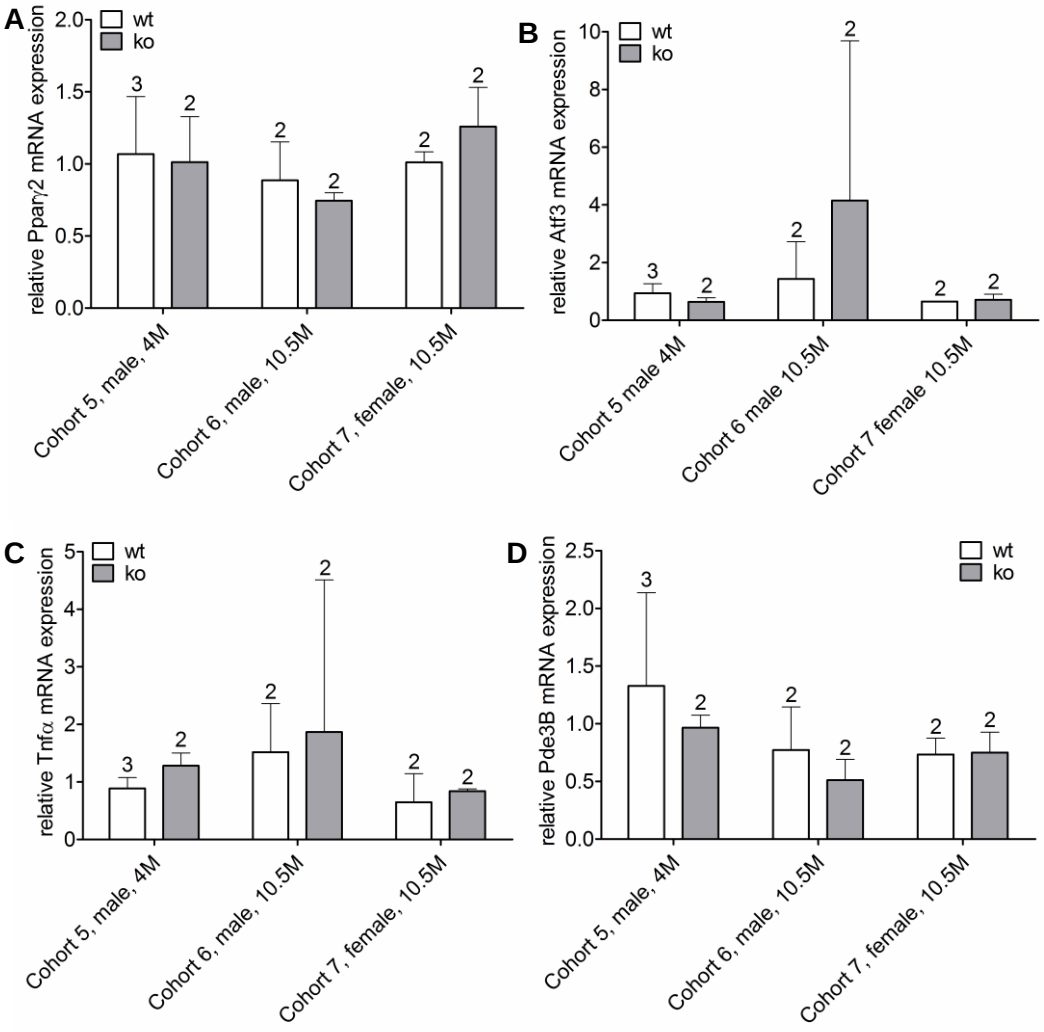

Fig. 59: qPCR analysis of eWAT of wild-type (wt) and *Abhd15*-ko (ko) mice of several ages (4 months (4M), 10.5 months (10.5M)). Mice numbers are mentioned over the bars, and mice with the same cohort numbers are littermates. Expression of the genes *Pparγ* (**A**), *Atf3* (**B**), *Tnfα* (**C**), and *Pde3B* (**D**) was investigated.

Although adipose tissue consists mostly of adipocytes, the influences of stromal vascular cells (SVC) on mRNA expression cannot be neglected.[91] Therefore, to find the reason for the increased mass of WAT in *Abhd15*-ko mice, adipocyte fraction and stromal vascular fraction (SVC) were extracted from eWAT, and adipocytes were subjected to qPCR analysis separately. Again, the adipogenesis markers *Fabp4* and *Pparγ*,[11] as well as the early differentiation marker and proliferation suppressor *C/ebpδ*[11,92], and the cell cycle activator *E2F1*[77] were measured (Fig 59A-D). Further, the ER stress marker *Atf3*[41], and the ER stress and apoptosis connecting factor *Chop*[41] were investigated, as well as the inflammation marker *Tnfα*[90], and the probably *Abhd15* expression-dependent gene *Pde3B*[46]. Additionally, the proliferation suppressor and apoptosis initiator *p53*[93], and sirtuin 1 (*Sirt1*) were examined

(Fig. 60A-F). *Sirt1* has been shown to be down-regulated upon insulin resistance[94], which in turn is a likely phenotype of *Abhd15-ko* mice.

Unfortunately, one out of three *Abhd15*-ko mouse samples did not show any signal, which reduced the group of knockout mice to the number of two. Keeping that in mind, still trends to increased *E2F1* (Fig. 59D) and *Tnfα* (Fig. 60D) were recognized in *Abhd15-ko* mice, which would hint to increased cell proliferation of adipocytes, accompanied by increased inflammatory signaling. None of the other genes screened showed any expression differences between wild-type and knockout mice (Fig. 59 A-C & Fig. 60 A-C & E-F).

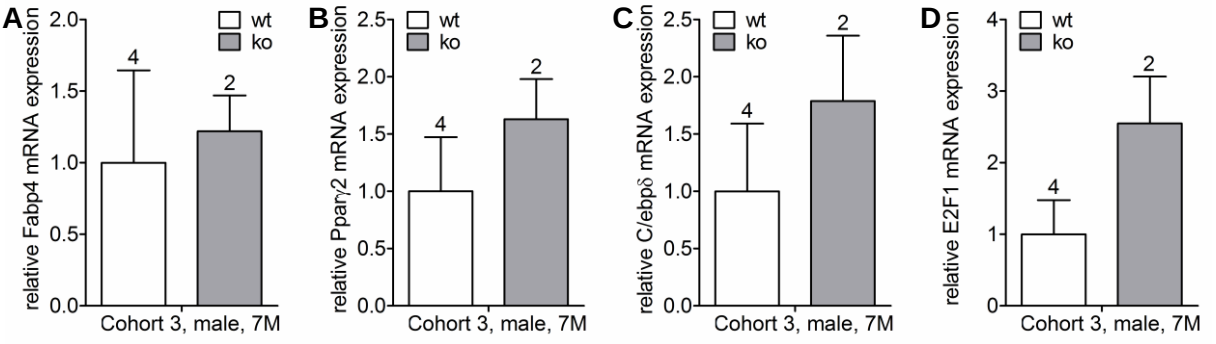

Fig. 60: qPCR analysis of adipocytes of eWAT of male wild-type (wt) and *Abhd15*-ko (ko) mice of 7 months (7M) of age. Mice numbers are mentioned over the bars. The genes *Fabp4* (**A**), *Pparγ* (**B**), *C/ebpδ* (**C**), and *E2F1* (**D**) were investigated.

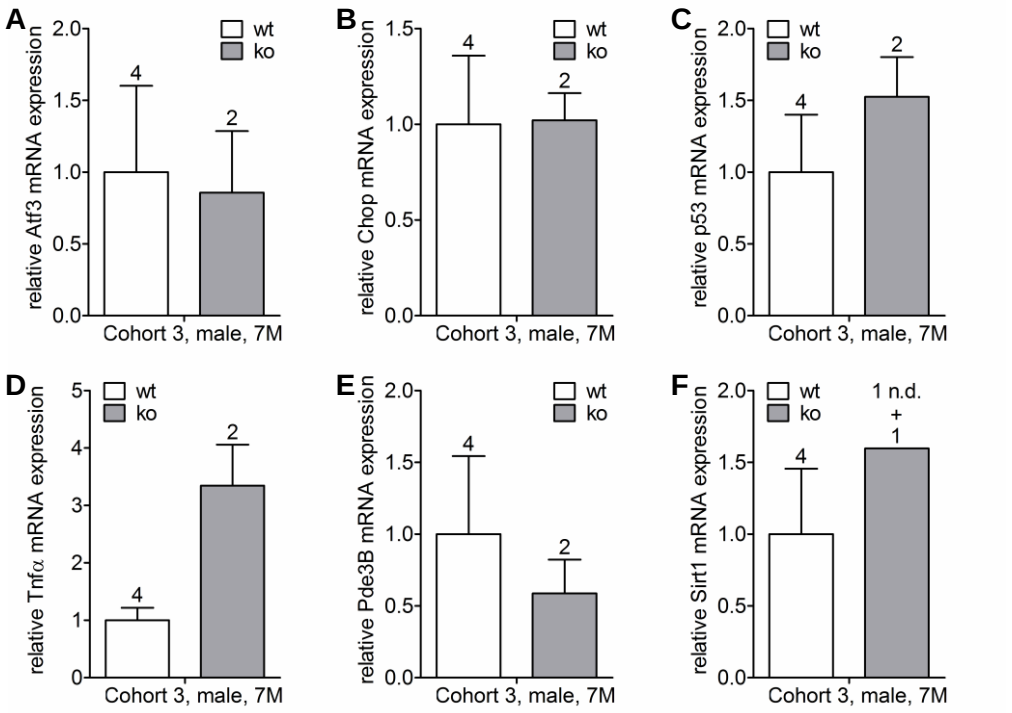

Fig. 61: qPCR analysis of adipocytes of eWAT of male wild-type (wt) and *Abhd15*-ko (ko) mice of 7 months (7M) of age. Mice numbers are mentioned over the bars. The genes *Atf3* (**A**), *Chop* (**B**), *p53* (**C**), *Tnfα* (**D**), *Pde3B* (**E**), and *Sirt1* (**F**) were investigated.

Especially due to the finding that *Abhd15* expression is high in macrophages compared to monocytes (Fig. 10A), and that it is increased during the differentiation to macrophages (Fig. 10B), differences between the phenotypes of immune cells from wild-type and *Abhd15*-ko mice would be expected. Therefore, the SVC fractions were subjected to qPCR analysis too. SVC samples were screened for the M1 marker gene interleukin 6 (*IL-6*)[95] and the inflammation marker *Tnfα*[90] (Fig. 61A-B). Further, expression of the cell cycle activator *E2F1*[77], the ER stress marker *Atf3*[41], and the ER stress and apoptosis connecting factor Chop[41] were measured (Fig. 62A-C). Finally, mRNA expression of *Pde3B*, *p53*, and *Sirt1* was examined (Fig. 62D-F).

For the next screening, more cDNA has to be used for SVC qPCR, as none of the Cq values was lower than 30, which led to a loss of signals due to not sufficient template gene concentration. Therefore, a clear answer to the question whether *Abhd15*-ko mice show differences in SVC expression profiles or not, cannot be given at this point. Additionally, the deviations within the groups were very high. Nevertheless, it seemed like if *Pde3B* mRNA expression was increased in *Abhd15*-ko mice (Fig. 62D).

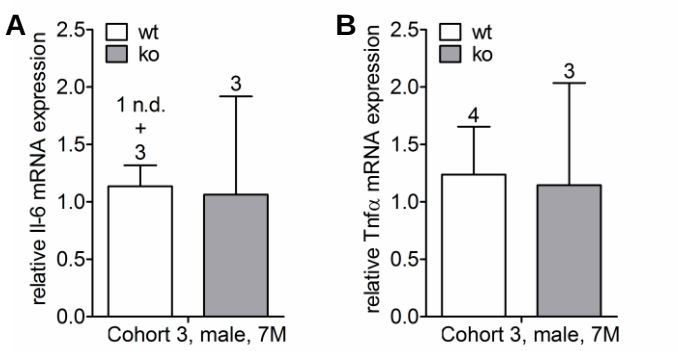

Fig. 62: qPCR analysis of SVCs of eWAT of male wild-type (wt) and *Abhd15*-ko (ko) mice of 7 months (7M) of age. Mice numbers are mentioned over the bars. The inflammatory marker genes *IL-6* (**A**) and *Tnfα* (**B**) were investigated. Due to low gene concentration no signal of *IL-6* was detected in one of the wt mice (not detectable (n.d.)).

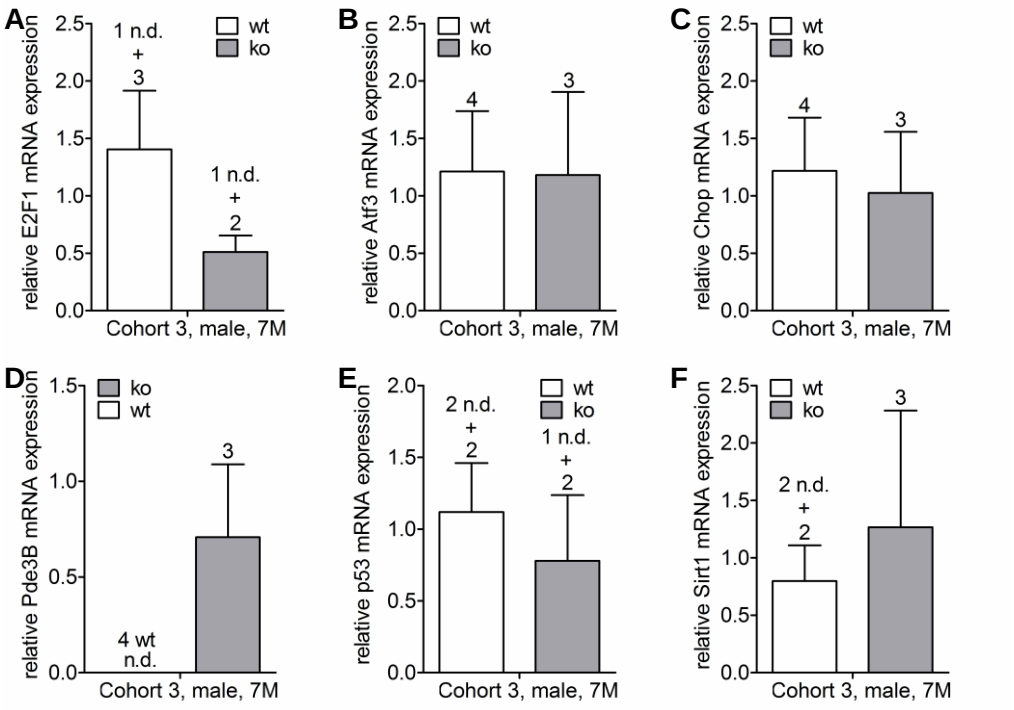

Fig. 63: qPCR analysis of SVCs of eWAT of male wild-type (wt) and *Abhd15*-ko (ko) mice of 7 months (7M) of age. Mice numbers are mentioned over the bars. The genes *E2F1* (**A**), *Atf3* (**B**), *Chop* (**C**), *Pde3B* (**D**), *p53* (**E**), and *Sirt1* (**F**) were investigated. Due to low gene concentrations some samples did not lead to any signals (not detectable (n.d.)).

Finally, the third major expression tissue[46,47], the liver, was investigated using qPCR analysis. Again, the two marker genes of adipogenesis, *Fabp4* and *Pparγ* were screened[11] (Fig. 63A-B), as well as the early differentiation marker and proliferation suppressor *C/ebpδ*[11,92], the ER stress and apoptosis connecting factor *Chop*[41], the ER stress marker *Atf3*[41], and the cell cycle activator *E2F1*[77] (Fig. 64A-D). Liver was also screened for the proliferation suppressor and apoptosis initiator *p53*[93], the insulin resistance regulated *Sirt1*[94], the inflammation marker *Tnfα*[90], and the probable *Abhd15* expression-dependent gene *Pde3B*[46] (Fig.65A-D).

As liver did not show any obvious phenotype differences, no differences were expected between the expression profile of *Abhd15*-ko and wild-type mice. Accordingly, it is not surprising that no obvious trends were observed (Fig. 63, 64, & 65). However, someone might see a slight trend to increased *E2F1* (Fig. 64D), and decreased *Atf3* (Fig. 64C) and *Tnfα* (Fig. 65C) mRNA expression levels.

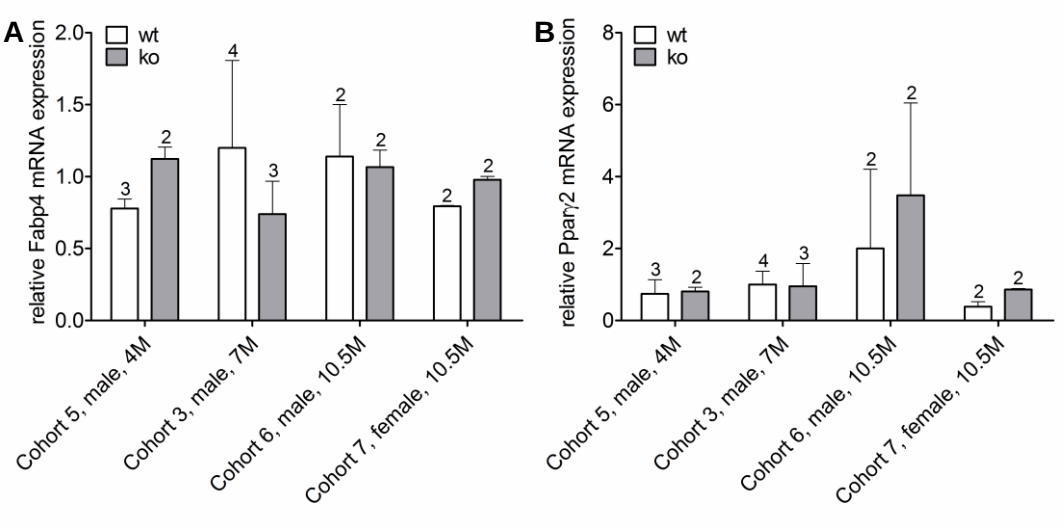

Fig. 64: qPCR analysis of liver of wild-type (wt) and *Abhd15*-ko (ko) mice of several ages (4 months (4M), 7 months (7M), 10.5 months (10.5M)). Mice numbers are mentioned over the bars, and mice with the same cohort numbers are littermates. The adipogenic marker genes *Fabp4* (**A**) and *Pparγ* (**B**) were investigated.

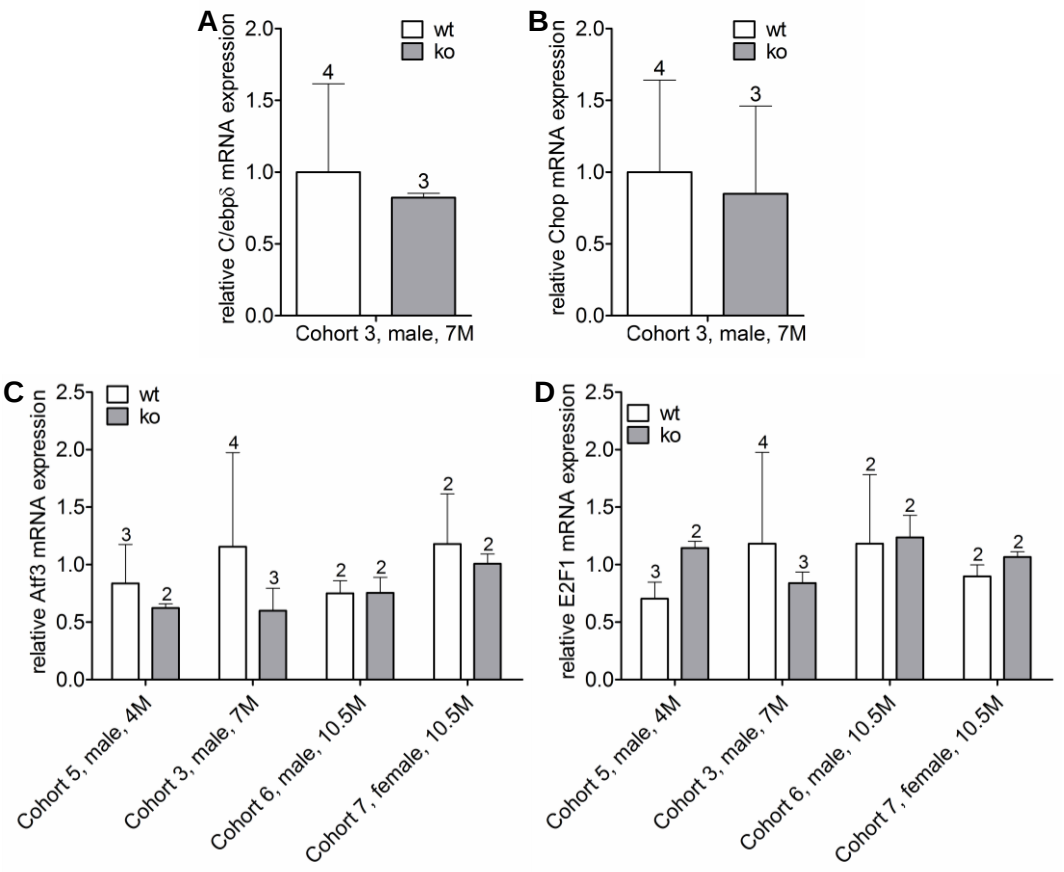

Fig. 65: qPCR analysis of liver of wild-type (wt) and *Abhd15*-ko (ko) mice of several ages (4 months (4M), 7 months (7M), 10.5 months (10.5M)). Mice numbers are mentioned over the bars, and mice with the same cohort numbers are littermates. The genes *C/ebpδ* (**A**), *Chop* (**B**), *Atf3* (**C**), and *E2F1* (**D**) were investigated.

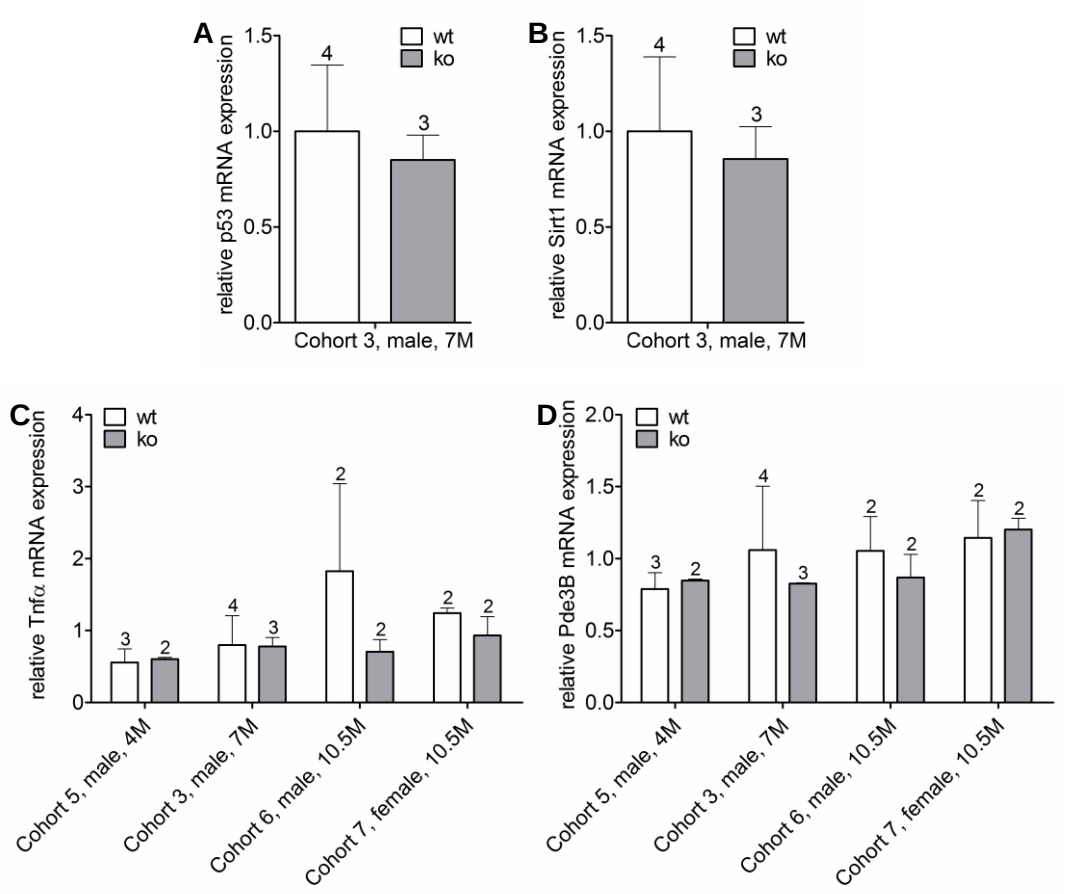

Fig. 66: qPCR analysis of liver of wild-type (wt) and *Abhd15*-ko (ko) mice of several ages (4 months (4M), 7 months (7M), 10.5 months (10.5M)). Mice numbers are mentioned over the bars, and mice with the same cohort numbers are littermates. The genes *p53* (**A**), *Sirt1* (**B**), *Tnfα* (**C**), *Pde3B* (**D**) were investigated.

In summary, the preliminary data of *Abhd15-ko* mice revealed that the knockout mice show increased WAT mass, in sWAT and eWAT. Further, fasted young mice seemed to have increased FFA in the blood, and fasted knockout mice of all ages showed a trend to reduced blood glucose. 3 out of 4 mouse cohorts hinted to increased insulin resistance in *Abhd15*-ko mice, but upon HFD knockout mice did not gain weight in the same amount like wild-type littermates did, which led to improved insulin sensitivity of knockout mice. Moreover, qPCR screening of several marker genes only pointed out trends, no striking differences between *Abhd15*-ko mice and wild-type littermates. The strongest effects were seen in adipocytes, which showed an increased expression of the cell cycle activator *E2F1* and the inflammatory marker *Tnfα.* The second very interesting finding was in SVC, which showed increased expression of the *Abhd15* expression dependent gene *Pde3B*.

Although some differences between *Abhd15*-ko and wild-type mice were found, no striking phenotype was observed so far. Therefore, to reduce the deviation within and between the cohorts, and to characterize the phenotype of these mice in more detail, all experiments will have to be repeated with mice on a clean background.

5 Discussion

In this study, conclusive evidence was provided that *Abhd15* is a direct and functional target gene of PPARγ and an essential factor for adipogenesis. Interestingly, while *Abhd15* expression increased during adipogenesis, it decreased in murine adipose tissues in the presence of high levels of FFAs, as observed in diet- and genetically induced obesity, fasting and aging, [96–99] as well as upon FFA treatment of cultured mature adipocytes. However, in liver and in inflammatory cells of adipose tissue, *Abhd15* expression was regulated conversely.

Furthermore, it could be shown that excess of ABHD15, evoked by overexpression, slightly increased basal glucose uptake. However, insulin stimulated glucose uptake was decreased upon *Abhd15* overexpression. Analysis of the lipid profile of *Abhd15* overexpressing adipocytes indicated a trend to reduced triglyceride accumulation, and pointed out the signal molecule phosphatidylserine 32:1 as a probable target of ABHD15. Silencing of *Abhd15* in preadipocytes on the other hand, led to increased apoptosis, and induced apoptosis in turn strongly increased *Abhd15* expression. Corresponding, proliferation was reduced in *Abhd15*-silenced cells, although no striking effects were detected concerning the cell cycle.

Consistent with the fact that *Abhd15* is dominantly expressed in adipose tissue[46,47], the results demonstrate that the proximal promoter of *Abhd15* contains a functional PPARγ binding site, localized as predicted by Lefterova et al.[55]. This adds *Abhd15* to the large group of direct and functional PPARγ targets, of which many are important adipogenic players, such as FABP4, CD36, GLUT4, APMAP, and ARXES[100,101,58,102]. Therefore, a role in lipid anabolism was proposed. If that would be the case, increased lipid accumulation in overexpressing *Abhd15,* and decreased lipid expression in *Abhd15*-silenced adipocytes would be expected. However, although silencing led to impaired adipogenesis, overexpression of *Abhd15* did not lead to increased lipid storage. Surprisingly, even a trend to decreased triglyceride content was detected with various methods of lipid analysis. Corresponding, also the triglyceride precursors, long chain acyl-CoAs showed a trend to reduction, hinting rather to a defect in lipid synthesis than to increased anabolism. The starting point for this defect could be the decreased glucose uptake detected in *Abhd15* overexpressing cells. All cell culture experiments, except the glucose uptake, were performed using 3T3-L1 cells, which are fibroblasts with the ability to differentiate into mature adipocytes[103]. For the glucose uptake however, 293A cells, which are embryonic kidney cells and therefore are not able to differentiate into mature adipocytes, were used. Due to the stable overexpression of *Glut4* and *Irs1*, these cells are capable of taking up glucose, while lipid metabolism background activities are reduced[60]. Hence, effects can be seen that would probably be too small to be detected in 3T3-L1 cells. Induction of differentiation could be seen as insulin stimulated status. Therefore, although comparing two different cell culture

models, one could propose that also in 3T3-L1 cells the insulin stimulated glucose uptake, which is important for lipid accumulation as glucose serves as substrate for metabolites used for lipid synthesis, would be slightly impaired upon *Abhd15* overexpression and therefore would lead to reduced lipid synthesis, resulting in slightly decreased long chain acyl-CoAs and finally triglyceride storage, which was shown by Oil red O staining, TLC, and HPLC-MS analysis. In any case, the question why excess of ABHD15 would lead to decreased glucose uptake upon insulin stimulation stays unresolved. Also which function of ABHD15 is activated or deactivated by its insulin stimulated phosphorylation by AKT[48] could not be solved. Interestingly, mutations of the indentified phosphorylation sites[48], did not lead to any differences in the insulin stimulated glucose uptake. On the other hand, even the opposite effect, a significantly increased glucose uptake was detected in un-stimulated, basal cells, which overexpressed the mutants T142A and S425A. A trend to increased uptake was also seen in cells overexpressing wild-type *Abhd15*, and no effect was seen in cells overexpressing mutant S442A. The mutations of threonine or serine to alanine implemented not only a sequence change, which should prevent AKT binding and subsequent phosphorylation, it also changed a polar, uncharged side chain to a hydrophobic side chain. Phosphorylation on the other side leads to a change into an extremely hydrophilic residue.[8] Hence, the conformational change due to the mutation to alanin might play a role already before phosphorylation, and might even be able to increase the function before phosphorylation, as it was shown before in other cases[104]. It is tempting to hypothesize two functions of ABHD15. The first function might need a special confirmation, for example for dimerization or preventing from dimerization. Therefore the alanine mutations T142A and S425A, leading to a conformational change, could increase the ABHD15 function, leading to significantly increased glucose uptake, in comparison to a slightly and not significant glucose uptake in wild-type *Abhd15* overexpressing cells. On the other side, the phosphorylation of ABHD15, by AKT upon insulin stimulation, did not lead to differences between ABHD15 wild-type and mutants, as all constructs, independent whether wild-type or mutant, led to a significantly reduced glucose uptake, when normalized to associated basal levels. Therefore, a phosphorylation dependent function of ABHD15, which is not involved in glucose uptake, can be suggested as a second function.

Besides the conspicuity in glucose uptake and a trend to decreased acyl-CoA and triglyceride content, *Abhd15* overexpressing cells showed another significant divergence, found by HPLC-MS analysis of *Abhd15* overexpressing 3T3-L1 cells on day 4 of differentiation. Although the significance has to be seen critically because no internal standard has been used and phosphatidylserine 32:1 is present only in very small amounts compared to other phosphatidylserines, the results will be discussed as verified, as phosphatidylserine 32:1 was decreased in a way strongly dependent on *Abhd15*

overexpression. Phosphatidylserines are important constituents of eukaryotic membranes, and are synthesized either from phosphatidylcholine or phosphatidylethanolamine precursors, and degraded back to phosphatidylethanolamine.[75] Both, phosphatidylcholine and phosphatidylethanolamine 32:1 showed a trend to reduction in *Abhd15* overexpressing cells. This suggests that excess of ABHD15 did not lead directly to this significant reduced phosphatidylserine 32:1 effect, but that ABHD15 might take part in the degradation of one acyl chain or the combination of the 32:1 acyl chains, as this trend to reduction could also be seen in phosphatidylinositol 32:1. Acyl chains of phosphatidylserines tend to consist of a saturated chain of at least 16 carbons on *sn*-1 position and an unsaturated chain of at least 18 carbons on *sn*-2 position.[105] Therefore, phosphatidylserine 32:1 most likely contains the acyl chains 14:0, 14:1, 16:0, 16:1, 18:0, and 18:1. If ABHD15 would degrade one or both of the phosphatidylserine 32:1 acyl chains, this chains should be also reduced in triglycerides. Interestingly 46:1, 46:2, 48:1, and 48:2, but not 46:0, and 48:0 showed the decreased trend upon excess of ABHD15. Further, a decrease could also be detected in 46:3 and 48:3, which would suggest an acyl chain of 16 carbons, which contains one double bond, to be the target for ABHD15. This idea was supported by the finding that lipids containing longer acyl chains, e.g. carbon chains with a length of 18 or longer, did not show any changes in the lipid profile of *Abhd15* overexpressing cells. HPLC-MS analysis can only distinguish between chain length and number of double bonds, which would explain why no significant differences could be shown, as the groups display a group of acyl chains, which also contains acyl chains differently than 16:1. What speaks against this theory is that no differences or trends at all were detected within the sphingomyeline group between control and *Abhd15* overexpressing cells. Regardless the formation of the reduced phosphatidylserine 32:1 content, this specific reduction might lead to a phenotype evoked by different *Abhd15* expression levels. Due to the distinct head group of phosphatidylserines, and the therefore negative charge under physiological conditions, they play an important role in several signaling pathways.[75] The most famous role is the delivery of the so called “eat me” signal for the clearance of apoptotic cells.[74] Therefore, the in healthy cells on the inner leaflet of the plasma membrane located phosphatidylserines, are exposed to the outer membrane by scramblases.[75] However, the determinants of phosphatidylserine exposure are not well known until now.[75,106,107] Phosphatidylserine signaling can occur in two ways. Firstly, by electrostatic interaction with membranes, which are rich in phosphatidylserine and therefore are charged negatively and therefore can lead to triggering of proteins towards the membrane. For this reason, the distribution of phosphatidylserine is important, which is maintained by various flippases, floppases, and scramblases.[75] As the phosphatidylserine 32:1, which is reduced significantly upon excess of ABHD15, represents only a small fraction of the phosphatidylserines present in the cells, it is very unlikely that this signal function of phosphatidylserines is affected. The

second way of phosphatidylserine signaling is due to stereospecifical recognition of the head group by certain proteins.[75] One of these by phosphatidylserine triggered proteins that should be mentioned in this context is AKT. Only binding to phosphatidylserine leads to fully activated AKT.[108] Further it has been shown that the AKT regulator phosphoinositide-dependent kinase-1 (PDK1) specifically binds to phosphatidylserine, and thereby is recruited to the plasma membrane, which is important for its signaling function.[109,110] Although it is not mentioned which specific phosphatidylserine serves as the signal molecule, these two signaling pathways might be influenced by the reduced content of phosphatidylserine 32:1, present in the *Abhd15* overexpressing cells. If that would be the case, *Abhd15* silencing would lead to reduced AKT activation, which in turn would mean less ABHD15 phosphorylation, which could be a feed forward signaling loop. Another signaling pathway which is possibly affected is the activation of the sphingosine kinases (SK) 1 and SK2 by phosphatidylserine binding. SKs phosphorylate sphingosine and thereby can protect cells from apoptosis.[111] If *Abhd15* expression would affect this signaling pathway by regulation of the amount of the signaling molecule phosphatidylserine 32:1, this could explain why *Abhd15* overexpressing cells showed a slightly increased cell number after 48 hours of cell growth, and *Abhd15*-silenced cells showed increased apoptosis. This was proven by the observation that firstly, *Abhd15*-silenced cells proliferated slower than control cells, shown by reduced cell counts and a colorimetric proliferation assay. Secondly, cell cycle analysis revealed no change in the S phase, but an increased SubG1 peak. Thirdly, pro-death regulation of the apoptosis marker proteins BCL-2 and BAX was observed, and fourthly, caspase 3/7 activity was increased. Finally, the low silencing efficiency of only ~30% in preconfluent cells as well as the observed loss of silencing after 2 weeks of culturing could be explained by an apoptosis-mediated “dilution” of cells with high *Abhd15*-knockdown during prolonged culturing. A probably higher amount of phosphatidylserine 32:1 in *Abhd15*-silenced cells might explain why cell cycle analysis, caspase assay, and western blot analysis of apoptosis marker proteins revealed increased apoptosis, but annexinV staining did not. AnnexinV marks all phosphatidylserines, but does not distinguish between different species of phosphatidylserines.[75] Therefore, the acyl chains might play a more important role in apoptosis signaling than it was assumed to date.

The fact that reduced expression of *Abhd15* led to increased apoptosis, let us conclude that *Abhd15* is required for cell survival, and therefore probably has an anti-apoptotic function. On the other hand, induced apoptosis highly increased *Abhd15* mRNA expression. Without knowledge of the apoptotic effect of reduced *Abhd15* expression, it could be presumed that ABHD15 might play a pro-apoptotic role. However, as it is unlikely that the decrease of a pro-apoptotic gene would lead to increased apoptosis, this increase of *Abhd15* might be an unsuccessful attempt to fight apoptosis, rather than support it. Therefore, it is tempting to

hypothesize that ABHD15 (besides being a novel putative adipogenic player) also plays a role in the control of apoptosis, and perhaps protects cells from apoptosis, at least in the investigated cell type.

Previous studies showed that apoptosis is increased in adipocytes of mice with diet-induced obesity.[31] These mice also have increased levels of FFAs[96], which per se are known to induce apoptosis[112–114]. However, the complete mechanism connecting these two characteristics of the diet-induced obesity phenotype is still elusive. The data of this thesis suggest that *Abhd15* could be a key player in this context, as we found *Abhd15* expression to be consistently decreased *in vivo* and *in vitro* upon conditions of elevated FFA levels. In adipocytes, superfluous FFAs can activate a number of different serine kinases, leading to inhibition of insulin signaling[115], and, in turn, to reduced AKT activation. AKT signaling has been shown to phosphorylate ABHD15.[46,48] As a result, high levels of FFAs might not only lead to decreased mRNA expression of *Abhd15*, but also influence the phosphorylation state of the remaining protein. For these reasons it is tempting to speculate that reduction/impairment of "protecting ABHD15" by increased FFA content leads to induced apoptosis and its further consequences, like recruitment of adipose tissue macrophages, insulin resistance, and development of fatty liver.[31]

In liver however, *Abhd15* expression seemed to be regulated by different factors. In the case of genetically obese mice, mice on HFD, and fasted mice, *Abhd15* expression was increased in liver, which means *Abhd15* was regulated contrary to adipose tissue. However, upon addition of IBMX or isoproterenol, murine liver cells did not show any effect concerning *Abhd15* expression, and the human cell model did even show decreased *Abhd15* expression. As in adipose tissue, also in liver, *Abhd15* was reduced upon ageing. However, *Abhd15* was not only partly differently expressed in liver when compared to adipose tissue, also in SVC *Abhd15* expression was increased in mice on HFD. This makes sense though, as HFD leads to a state of increased inflammation, represented by migration of monocytes from the blood into adipose tissue, where they further differentiate into macrophages. Obese mice show increased amounts of M1 macrophages, also called classically activated macrophages, while lean mice possess more M2 macrophages, also called alternately activated macrophages.[95] *Abhd15* mRNA expression was highly increased in macrophages, compared to monocytes, and further much higher *Abhd15* expression was found in M1 macrophages, when compared to M2 macrophages. M1 macrophages highly contribute to adipose tissue inflammation resulting in insulin resistance, while M2 macrophages protect from obesity and insulin resistance.[95] What function ABHD15 might have in macrophages, and also whether it is required for differentiation of monocytes into macrophages, will have to be investigated in the future.

For fibroblasts, it could be clearly shown that *Abhd15* expression is required for adipogenesis, as *Abhd15*-silenced 3T3-L1 cells were unable to increase the expression levels of adipogenic marker genes, leading to reduced lipid accumulation. As transient silencing in fully differentiated cells did not evoke any changes of the mature adipocyte phenotype, it was concluded that *Abhd15* lacks a role in the maintenance of the mature adipogenic status. In contrast, the defect started already early during differentiation, as stable silencing of *Abhd15* in 3T3-L1 cells lowered *Pparγ* expression levels as soon as 12 hours after induction of differentiation. Therefore, expression of adipogenic markers was not induced in *Abhd15* stably silenced 3T3-L1 cells, including *Abhd15* itself, leading to an improved silencing efficiency from 30% in preconfluent cells to 80% during differentiation. However, although it was shown that *Abhd15*-silenced cells showed increased apoptosis already in preconfluent status, which of course is probably the reason for the impaired differentiation capacity, there is still the conspicuous plateau in the expression profile of *Abhd15* during the time of 3-24 hours after induction of differentiation. This time perfectly covers the first round of mitotic clonal expansion.[17] Why would *Abhd15* be regulated especially during this phase of differentiation, if it would have no role in the cell cycle? However, no differences were detected in the S phase of preconfluent *Abhd15*-silenced compared to control cells. And also analysis of cell cycle marker genes using qPCR did not reveal any conclusive results that a lack of *Abhd15* would influence the cell cycle. Still some differences between silenced and control cells were noticeable. So were the proliferation activators *E2F1* and *E2F2* increased in *Abhd15*-silenced cells. Additionally the cell cycle suppressors *E2F4* and *E2F5* showed a trend to reduced expression, which means that the expression of the regulatory transcription factor family hints to increased cell growth. An explanation could be that if *Abhd15* would show this expression plateau because its expression would be negatively regulated to ensure undisturbed cell proliferation, a lack of *Abhd15* would lead to increased cell proliferation, like the expression of the *E2F* transcription factors showed. However, increased MCE would probably rather lead to a faster differentiation, not impaired, like it was observed in *Abhd15*-silenced cells. Corresponding to that, *CylinE1*, which has to be down-regulated for MCE, was expressed higher in *Abhd15*-silenced cells, and expression of *CyclinA* and *Cdk2*, both activators of MCE, were decreased. E2F activation or repressing activity depends on the release of the binding of so called pocket proteins.[81] This release occurs due to the phosphorylation by CDKs,[81] which means that in the case of *Abhd15* silencing, due to the anti-MCE expression of *Cyclins* and *Cdks*, pocket binding proteins would block E2Fs, which in turn might be overcome due to more pro-MCE expression of E2Fs. The expression of two out of three pocket proteins was slightly reduced in *Abhd15*-silenced cells, suggesting increased cell cycle activity, rather than the expected reduced one, according to impaired adipogenesis. However, this could be

either explained by the lack of *Abhd15*, which might have a cell cycle suppressing role, or more likely a compensatory effect, due to increased apoptosis[116].

To characterize a new gene/protein, a lot of experiments which can help to find one or even several functions of the protein can be performed in cell culture. Unfortunately, this technique has limits, as for instance metabolic influences that occur in the whole organism cannot be studied in individual cell lines. The common way, to find the metabolic impact of an uncharacterized protein, is to establish a mouse model, which either lacks or overproduces this protein. For this study, a conditional knockout mouse was established, and preliminary results will be discussed. The results have to be seen with caution, as firstly, mice were only in generation F4-5 and therefore not on clean background and secondly, not only exon 2 of *Abhd15* was deleted, but also parts of intron 1 and the region downstream of *Abhd15*. Therefore, within these regions, but also on the reverse strand of *Abhd15*'s exon 2, might be a so far unidentified gene, a short non coding RNA (miRNA), or a long non coding RNA (lncRNA). A lack of each one of them would probably lead to an *Abhd15*-independent phenotype, which would mislead the search for the ABHD15 function.[88] However, to date no better models than knockout mice are known to study metabolic protein functions.[88]
Due to the impaired adipogenesis of fibroblasts upon knockdown of *Abhd15*, a reduced fat amount was expected in *Abhd15*-ko mice. Especially this example showed how important a mouse model is, as *Abhd15*-ko mice definitely did not show reduced body weight on normal chow diet. In contrast, sWAT and eWAT mass were even increased, and also BAT showed a slight trend to increased mass. As no differences were detected in total body weight, mice might gain weight in other tissues. Liver could be excluded, which leaves most probably muscle or bone. Keeping that in mind, a DEXA scan or NMR could help to elucidate this phenomenon[117,118]. If the increased adipose tissue mass found in *Abhd15*-ko mice originates from adipocytes, it can be the result of either increased adipogenesis, increased cell proliferation, or decreased apoptosis.[7] Increased adipogenesis, as well as decreased apoptosis are anyway unlikely, as this would be the total opposite of which was observed in the cell culture model. Corresponding, using qPCR analysis, no differences or even trends were observed in any of the measured adipogenic marker genes, no matter whether they were marker genes for white or brown adipose tissue[11,89]. BAT even showed a slight trend to decreased *Fabp4* mRNA expression in *Abhd15*-ko mice, which might explain why BAT was the one out of three measured adipose tissues, which showed the slightest trend to increased adipose tissue mass. The increased proliferation in turn, was already observed during MCE of *Abhd15*-silenced 3T3-L1 cells. Indeed, a trend to increased *E2F1* mRNA expression was detected in adipose tissues of *Abhd15*-ko mice, when compared to direct littermates. This same trend could not be seen in liver or SVCs, which would explain why

only adipose tissue masses were increased, but not liver. However, the change in *E2F1* expression is very small, why it is unlikely that *Abhd15*-ko could influence *E2F1* expression directly. *E2F1* expression is regulated by more than one factor, including oncogenes and miRNAs[119], which makes it difficult to say at which point ABHD15 influence could take place. Interestingly, *E2F1* is the only member of the E2F family, whose overexpression leads to apoptosis, and thereby can regulate cell proliferation as well as apoptosis.[81,120–123] Although none of the apoptosis markers *p53*[93] or *Chop*[41] showed increased mRNA expression in *Abhd15*-ko mice, E2F1 might be the link between ABHD15, cell proliferation, and apoptosis, which at least were both present in *Abhd15*-silenced cells. As both of these markers are strongly regulated on protein level, and thereby mRNA levels might not bring up the whole magnitude of their regulation, it might be interesting to examine apoptosis in adipose tissues with tunnel staining. Another attribute of *Abhd15*-silenced cells, which could not be confirmed in *Abhd15*-ko mice, was that besides *Chop* also other ER stress markers were increased. The one which was mostly increased was *Atf3*. However, in none of the tissues investigated *Atf3* mRNA expression was increased, liver even showed a slightly decrease in *Atf3* expression in *Abhd15*-ko mice. Still, it should be kept in mind that perhaps another gene might have taken over the gap that the knockout of *Abhd15* left. This gap might have led to increased ER stress in 3T3-L1 cells, which in turn could have led to apoptosis. Although verification on protein level will be necessary in cells, as well as in mice, the mRNA expression profile of the slightly increased ER stress markers in *Abhd15*-silenced cells hinted to activated PERK and ATF6 arms of the UPR of ER stress. Under acute ER stress, PERK is thought to be the first, followed by ATF6, and IRE1 last, to be activated.[41] However, under prolonged ER stress, IRE1 activity is turned off, whereas PERK maintains its signaling, possibly to sensitize chronologically damaged cells to apoptosis,[35,42] reflecting the chronological ER stress due to stably knockdown of the possibly protecting agent *Abhd15*. Both, PERK and ATF6, can induce *Chop* mRNA expression.[124] However, no reports have linked ATF6 to ER stress induced apoptosis, and it seems that ATF6 signaling is purely pro-survival.[41] Quite the opposite is known about the PERK signaling pathway. After transphosphorylation, it phosphorylates the eukaryotic translation initiation factor 2-alpha (ELF2α), which leads to increased translation of mRNAs with internal ribosome entry site, like *Atf4*[43], but also lowers the steady-state levels of inhibitors of kappa-light-chain-enhancer of activated B cells (IκB)[44]. This leads to activation and translocation of NF-κB. NF-κB in turn can form a complex with PPARγ and its specific co-activator PGC-2 (PPARγ coactivator 2), which prevents PPARγ binding to DNA, and therefore can block adipogenesis.[40] ATF4 on the other hand, is known for up-regulating the transcription factors *Atf3* and *Chop*,[45] both showing, relatively small but increased mRNA expression upon *Abhd15*-knockdown in cells. CHOP is known to be one of the major elements in the decision of cell survival or death, and

is regulated on transcriptional as well as on translational level. Although mainly known for induction of gene expression of pro-apoptotic genes like *Bax*, CHOP also down-regulates pro-survival genes, like *Bcl-2*.[41] As these proteins were clearly regulated pro-apoptotically in *Abhd15*-silenced cells, their protein expression will have to be investigated in tissues of *Abhd15*-ko mice in the future.

The second gene, which showed a trend to be differently expressed in *Abhd15*-ko mice, was *Tnfα*. *Tnfα* mRNA expression was slightly increased in BAT and eWAT, especially in the adipocytes of eWAT, but no trend could be detected in sWAT and SVC. In liver even a trend to decreased expression of *Tnfα* was observed. However, if not striking, mRNA expression pattern of *Tnfα* have to be concerned with caution, as TNFα is also strongly regulated on protein level[125]. Furthermore, qPCR analysis of the M1 macrophage marker *Il-6*[95] did not reveal any differences between *Abhd15*-ko and wild-type littermates. Still, due to the regulation of *Abhd15* in monocytes and macrophages, the influence of *Abhd15* in immune cells should not be neglected, and an immune specific phenotype might influence insulin sensitivity as much as the phenotype revealed from *Abhd15*-knockdown in fibroblasts. However, since *Abhd15*-ko mice showed increased adipose tissue, someone could expect increased inflammation and insulin resistance anyway[95], and although the inflammatory status has to be investigated better, it seemed that indeed, *Abhd15*-ko mice on normal chow diet were more insulin resistant than wild-type littermates. On HFD though, *Abhd15*-ko mice did not gain weight like their wild-type littermates did, and therefore were more insulin sensitive. To investigate whether this phenotype results from the adipocyte or the macrophage phenotype, or even another tissue, qPCR analysis might give some answers. Interestingly, glucose tolerance was not influenced in *Abhd15*-ko mice, but basal glucose levels of fasted *Abhd15*-ko mice were slightly reduced in 3 out of 4 cohorts of mice. However, also the other blood parameters measured did not reveal a clear and solid phenotype. Therefore, it will be very important in the future to reduce the deviation within and between the cohorts, which should be the case as soon as the mice have a clean background.

In conclusion, the results of this thesis can show that *Abhd15* is a functional PPARγ target gene and is required for adipogenesis. In addition to its intricate regulation by FFAs, we provide evidence that *Abhd15* expression levels are tightly connected to apoptosis of fibroblasts. While decreased expression of *Abhd15* evokes apoptosis, a striking increase of *Abhd15* expression can be found upon induction of apoptosis, proposing *Abhd15* as a protective factor against apoptosis. Further, we suggest that regulation of phosphatidylserine and/or increased ER stress is the source of this phenotype, but both of them will have to be confirmed in the *Abhd15*-ko mouse model. Preliminary results of the investigation of the *Abhd15*-ko mouse model in turn indicate increased adipose tissue mass due to increased

cell proliferation. Although the direct influences will have to be investigated in the future, it could be shown that ABHD15 can influence adipogenesis, apoptosis, and cell proliferation, all three factors crucially determining adipose cell number and size. Therefore, *Abhd15* might be an intriguing new target in obesity and diabetes research.

6 Figure Legends

6 Figure Legends

Fig. 1: Scheme of ER stress response. 10
Fig. 2: Genome organization around the *Abhd15* transcription start side....24
Fig. 3: Luciferase Assay of PPARγ binding....25
Fig. 4: *Abhd15* mRNA expression in adipose tissue of genetically obese mice, upon HFD, and ageing.. 26
Fig. 5: *Abhd15* mRNA expression in adipose tissue and adipocytes upon fasting 26
Fig. 6: Palmitic acid treatment.. 27
Fig. 7: *Abhd15* mRNA expression in liver of genetically obese mice, upon HFD and ageing 27
Fig. 8: *Abhd15* mRNA expression in liver and in liver cells upon fasting. 28
Fig. 9: *Abhd15* mRNA expression in adipocytes and SVC....28
Fig. 10: *Abhd15* mRNA expression in immune cells. 29
Fig. 11: Western blot analysis of 3T3-L1 cell lysates during differentiation 30
Fig. 12: Western blot analysis of the supernatant of cultured epididymal fat pads.. 31
Fig. 13: Western blot analysis of the supernatants of cultured epididymal fat pad and liver. .32
Fig. 14: Western blot analysis of blood plasma.....33
Fig. 15: Western blot analysis with the Lienhard anti-ABHD15 antibody....34
Fig. 16: Glucose uptake of 293A cells, overexpressing *Glut4* and *Irs1*. 35
Fig. 17: Overexpression efficiency and Oil red O staining of stably *Abhd15* overexpressing 3T3-L1 cells.....36
Fig. 18: Neutral lipid TLC of lipid extracts of 3T3-L1 cells during differentiation.. 36
Fig. 19: Neutral lipid TLC of lipid extracts of biological replicates of 3T3-L1 cells at day 4 of differentiation....37
Fig. 20: Phosphatidylserine 32:1 content measured by HPLC-MS....38
Fig. 21: Phosphatidylserines content measured by HPLC-MS....39
Fig. 22: HPLC-MS analysis of lipid extracts (1).....40
Fig. 23: HPLC-MS analysis of lipid extracts (2)....41
Fig. 24: HPLC-MS analysis of the precursors or intermediates of lipid synthesis. 41
Fig. 25: *Abhd15* silencing during differentiation 42
Fig. 26: Oil red O staining and adipogenic marker gene expression of stably *Abhd15*-silenced cells 43
Fig. 27: Transient silencing of *Abhd15*....43
Fig. 28: Stable *Abhd15* silencing in preconfluent cells and during differentiation. 44
Fig. 29: *Pparγ* and *C/ebpα* mRNA expression in *Abhd15*-silenced cells. 45
Fig. 30: *C/ebpβ* and *C/ebpδ* mRNA expression in *Abhd15*-silenced cells. 46
Fig. 31: *Abhd15* mRNA expression during MCE. 46
Fig. 32: mRNA expression of *E2F* transcription factors during MCE. 47

6 Figure Legends

Fig. 33: mRNA expression of *p27*, *CyclinE1*, *CyclinA*, and *Cdk2* during MCE. 48
Fig. 34: mRNA expression of *pocket binding proteins* during MCE. 49
Fig. 35: Cell counting of *Abhd15*-silenced and overexpressing cells.....50
Fig. 36: MTS assay and cell cycle analysis of *Abhd15*-silenced cells 51
Fig. 37: Apoptosis analysis of *Abhd15*-silenced cells. 51
Fig. 38: Palmitic acid treatment of preconfluent 3T3-L1 cells. 52
Fig. 39: Relative mRNA expression of endoplasmic reticulum (ER) stress marker genes. 53
Fig. 40: Relative mRNA expression of cAMP and cGMP hydrolase *Pde3B*. 53
Fig. 41: *Abhd15-ko* mouse targeting vector 54
Fig. 42: Southern blot analysis to examine ES cell clones containing the loxP sites and the neomycin cassette. 55
Fig. 40: Southern blot analysis to indentify floxed and knockout ES cell clones. 56
Fig. 44: Weight measurement of wild-type (wt) and *Abhd15*-ko (ko) littermates.....57
Fig. 45: Tissue weight of wild-type (wt) and *Abhd15*-ko (ko) littermates. 58
Fig. 46: Measurement of FFAs in the blood plasma. 59
Fig. 47: Measurement of triglycerides in the blood plasma. 59
Fig. 48: Blood glucose levels (1).....60
Fig. 49: Blood glucose levels (2).....60
Fig. 50: GTT and ITT of cohort 1. 61
Fig. 51: GTT and ITT of cohort 2 62
Fig. 52: ITT of cohort 2 after HFD. 63
Fig. 53: GTTand ITT of cohort 3. 64
Fig. 54: GTT and ITT of cohort 4 65
Fig. 55: mRNA expression of *Abhd15* in eWAT and liver. 66
Fig. 56: qPCR analysis of BAT. 67
Fig. 57: qPCR analysis of sWAT. 69
Fig. 58: qPCR analysis of eWAT. 70
Fig. 59: qPCR analysis of adipocytes of eWAT (1). 71
Fig. 60: qPCR analysis of adipocytes of eWAT (2). 71
Fig. 61: qPCR analysis of SVCs of eWAT (1). 72
Fig. 62: qPCR analysis of SVCs of eWAT (2). 73
Fig. 63: qPCR analysis of liver (1). 74
Fig. 64: qPCR analysis of liver (2). 74
Fig. 65: qPCR analysis of liver (3). 75

7 References

7 References

1. Aballay, L. R., Eynard, A. R., Díaz, M. del P., Navarro, A. & Muñoz, S. E. Overweight and obesity: a review of their relationship to metabolic syndrome, cardiovascular disease, and cancer in South America. *Nutr. Rev.* **71,** 168–179 (2013).
2. Kopelman, P. G. Obesity as a medical problem. *Nature* **404,** 635–643 (2000).
3. Withrow, D. & Alter, D. A. The economic burden of obesity worldwide: a systematic review of the direct costs of obesity. *Obes. Rev. Off. J. Int. Assoc. Study Obes.* **12,** 131–141 (2011).
4. Hammond, R. A. & Levine, R. The economic impact of obesity in the United States. *Diabetes Metab. Syndr. Obes. Targets Ther.* **3,** 285–295 (2010).
5. Spiegelman, B. M. & Flier, J. S. Obesity and the regulation of energy balance. *Cell* **104,** 531–543 (2001).
6. Friedman, J. M. Obesity in the new millennium. *Nature* **404,** 632–634 (2000).
7. Sorisky, A., Magun, R. & Gagnon, A. M. Adipose cell apoptosis: death in the energy depot. *Int. J. Obes. Relat. Metab. Disord. J. Int. Assoc. Study Obes.* **24 Suppl 4,** S3–7 (2000).
8. Voet, D. & Voet, J. G. *Biochemistry*. (Wiley-VCH, 2011).
9. Halaas, J. L. *et al.* Weight-reducing effects of the plasma protein encoded by the obese gene. *Science* **269,** 543–546 (1995).
10. Rosen, E. D. & MacDougald, O. A. Adipocyte differentiation from the inside out. *Nat. Rev. Mol. Cell Biol.* **7,** 885–896 (2006).
11. Gregoire, F. M., Smas, C. M. & Sul, H. S. Understanding adipocyte differentiation. *Physiol. Rev.* **78,** 783–809 (1998).
12. Scherer, P. E., Williams, S., Fogliano, M., Baldini, G. & Lodish, H. F. A novel serum protein similar to C1q, produced exclusively in adipocytes. *J. Biol. Chem.* **270,** 26746–26749 (1995).
13. Fukuhara, A. *et al.* Visfatin: a protein secreted by visceral fat that mimics the effects of insulin. *Science* **307,** 426–430 (2005).
14. Steppan, C. M. *et al.* The hormone resistin links obesity to diabetes. *Nature* **409,** 307–312 (2001).
15. Yang, Q. *et al.* Serum retinol binding protein 4 contributes to insulin resistance in obesity and type 2 diabetes. *Nature* **436,** 356–362 (2005).
16. Yan, Q.-W. *et al.* The adipokine lipocalin 2 is regulated by obesity and promotes insulin resistance. *Diabetes* **56,** 2533–2540 (2007).
17. Tang, Q.-Q., Otto, T. C. & Lane, M. D. Mitotic clonal expansion: a synchronous process required for adipogenesis. *Proc. Natl. Acad. Sci. U. S. A.* **100,** 44–49 (2003).
18. Tang, Q. Q. & Lane, M. D. Adipogenesis: from stem cell to adipocyte. *Annu. Rev. Biochem.* **81,** 715–736 (2012).
19. Tontonoz, P., Hu, E. & Spiegelman, B. M. Regulation of adipocyte gene expression and differentiation by peroxisome proliferator activated receptor gamma. *Curr. Opin. Genet. Dev.* **5,** 571–576 (1995).
20. Mandrup, S. & Lane, M. D. Regulating adipogenesis. *J. Biol. Chem.* **272,** 5367–5370 (1997).
21. Rosen, E. D., Walkey, C. J., Puigserver, P. & Spiegelman, B. M. Transcriptional regulation of adipogenesis. *Genes Dev.* **14,** 1293–1307 (2000).
22. Wu, Z., Bucher, N. L. & Farmer, S. R. Induction of peroxisome proliferator-activated receptor gamma during the conversion of 3T3 fibroblasts into adipocytes is mediated by C/EBPbeta, C/EBPdelta, and glucocorticoids. *Mol. Cell. Biol.* **16,** 4128–4136 (1996).
23. Spiegelman, B. M., Hu, E., Kim, J. B. & Brun, R. PPAR gamma and the control of adipogenesis. *Biochimie* **79,** 111–112 (1997).
24. Tontonoz, P., Hu, E. & Spiegelman, B. M. Stimulation of adipogenesis in fibroblasts by PPAR gamma 2, a lipid-activated transcription factor. *Cell* **79,** 1147–1156 (1994).
25. Rosen, E. D. & Spiegelman, B. M. PPARgamma : a nuclear regulator of metabolism, differentiation, and cell growth. *J. Biol. Chem.* **276,** 37731–37734 (2001).
26. McIntyre, T. M. *et al.* Identification of an intracellular receptor for lysophosphatidic acid (LPA): LPA is a transcellular PPARgamma agonist. *Proc. Natl. Acad. Sci. U. S. A.* **100,** 131–136 (2003).

27. Tontonoz, P. *et al.* Adipocyte-specific transcription factor ARF6 is a heterodimeric complex of two nuclear hormone receptors, PPAR gamma and RXR alpha. *Nucleic Acids Res.* **22,** 5628–5634 (1994).
28. Lehrke, M. & Lazar, M. A. The many faces of PPARgamma. *Cell* **123,** 993–999 (2005).
29. Brun, R. P., Kim, J. B., Hu, E., Altiok, S. & Spiegelman, B. M. Adipocyte differentiation: a transcriptional regulatory cascade. *Curr. Opin. Cell Biol.* **8,** 826–832 (1996).
30. Zhang, Y. & Huang, C. Targeting adipocyte apoptosis: a novel strategy for obesity therapy. *Biochem. Biophys. Res. Commun.* **417,** 1–4 (2012).
31. Alkhouri, N. *et al.* Adipocyte apoptosis, a link between obesity, insulin resistance, and hepatic steatosis. *J. Biol. Chem.* **285,** 3428–3438 (2010).
32. Della-Fera, M. A., Qian, H. & Baile, C. A. Adipocyte apoptosis in the regulation of body fat mass by leptin. *Diabetes Obes. Metab.* **3,** 299–310 (2001).
33. Herold, C., Rennekampff, H. O. & Engeli, S. Apoptotic pathways in adipose tissue. *Apoptosis Int. J. Program. Cell Death* **18,** 911–916 (2013).
34. Andersen, J. L. & Kornbluth, S. The tangled circuitry of metabolism and apoptosis. *Mol. Cell* **49,** 399–410 (2013).
35. Rodriguez, D., Rojas-Rivera, D. & Hetz, C. Integrating stress signals at the endoplasmic reticulum: The BCL-2 protein family rheostat. *Biochim. Biophys. Acta* **1813,** 564–574 (2011).
36. Kirkland, R. A. & Franklin, J. L. Bax affects production of reactive oxygen by the mitochondria of non-apoptotic neurons. *Exp. Neurol.* **204,** 458–461 (2007).
37. Jones, R. G. *et al.* The proapoptotic factors Bax and Bak regulate T Cell proliferation through control of endoplasmic reticulum Ca(2+) homeostasis. *Immunity* **27,** 268–280 (2007).
38. Gregor, M. F. & Hotamisligil, G. S. Thematic review series: Adipocyte Biology. Adipocyte stress: the endoplasmic reticulum and metabolic disease. *J. Lipid Res.* **48,** 1905–1914 (2007).
39. Cnop, M., Foufelle, F. & Velloso, L. A. Endoplasmic reticulum stress, obesity and diabetes. *Trends Mol. Med.* **18,** 59–68 (2012).
40. Suzawa, M. *et al.* Cytokines suppress adipogenesis and PPAR-gamma function through the TAK1/TAB1/NIK cascade. *Nat. Cell Biol.* **5,** 224–230 (2003).
41. Szegezdi, E., Logue, S. E., Gorman, A. M. & Samali, A. Mediators of endoplasmic reticulum stress-induced apoptosis. *EMBO Rep.* **7,** 880–885 (2006).
42. Lin, J. H., Li, H., Zhang, Y., Ron, D. & Walter, P. Divergent effects of PERK and IRE1 signaling on cell viability. *PloS One* **4,** e4170 (2009).
43. Zha, B. S. & Zhou, H. ER Stress and Lipid Metabolism in Adipocytes. *Biochem. Res. Int.* **2012,** 312943 (2012).
44. Wek, R. C., Jiang, H.-Y. & Anthony, T. G. Coping with stress: eIF2 kinases and translational control. *Biochem. Soc. Trans.* **34,** 7–11 (2006).
45. Han, J. *et al.* ER-stress-induced transcriptional regulation increases protein synthesis leading to cell death. *Nat. Cell Biol.* **15,** 481–490 (2013).
46. Chavez, J. A., Gridley, S., Sano, H., Lane, W. S. & Lienhard, G. E. The 47kDa Akt substrate associates with phosphodiesterase 3B and regulates its level in adipocytes. *Biochem. Biophys. Res. Commun.* **342,** 1218–1222 (2006).
47. Walenta, E. alpha/beta-hydrolase domain containing 15 (Abhd15)- A new Player in Adipogenesis. (2010).
48. Gridley, S., Lane, W. S., Garner, C. W. & Lienhard, G. E. Novel insulin-elicited phosphoproteins in adipocytes. *Cell. Signal.* **17,** 59–66 (2005).
49. Abhydrolase domain-containing protein 15 precursor - Mus musculus (Mouse). at <http://www.uniprot.org/uniprot/Q5F2F2>
50. Nardini, M. & Dijkstra, B. W. Alpha/beta hydrolase fold enzymes: the family keeps growing. *Curr. Opin. Struct. Biol.* **9,** 732–737 (1999).
51. Lord, C. C., Thomas, G. & Brown, J. M. Mammalian alpha beta hydrolase domain (ABHD) proteins: Lipid metabolizing enzymes at the interface of cell signaling and energy metabolism. *Biochim. Biophys. Acta* **1831,** 792–802 (2013).

52. Saltiel, A. R. & Kahn, C. R. Insulin signalling and the regulation of glucose and lipid metabolism. *Nature* **414,** 799–806 (2001).
53. Degerman, E. *et al.* From PDE3B to the regulation of energy homeostasis. *Curr. Opin. Pharmacol.* **11,** 676–682 (2011).
54. Nielsen, R. *et al.* Genome-wide profiling of PPARgamma:RXR and RNA polymerase II occupancy reveals temporal activation of distinct metabolic pathways and changes in RXR dimer composition during adipogenesis. *Genes Dev.* **22,** 2953–2967 (2008).
55. Lefterova, M. I. *et al.* PPARgamma and C/EBP factors orchestrate adipocyte biology via adjacent binding on a genome-wide scale. *Genes Dev.* **22,** 2941–2952 (2008).
56. Quandt, K., Frech, K., Karas, H., Wingender, E. & Werner, T. MatInd and MatInspector: new fast and versatile tools for detection of consensus matches in nucleotide sequence data. *Nucleic Acids Res.* **23,** 4878–4884 (1995).
57. Bogner-Strauss, J. G. *et al.* Reconstruction of gene association network reveals a transmembrane protein required for adipogenesis and targeted by PPARγ. *Cell. Mol. Life Sci. CMLS* **67,** 4049–4064 (2010).
58. Bogner-Strauss, J. G. *et al.* Reconstruction of gene association network reveals a transmembrane protein required for adipogenesis and targeted by PPARγ. *Cell. Mol. Life Sci. CMLS* **67,** 4049–4064 (2010).
59. Soukas, A., Socci, N. D., Saatkamp, B. D., Novelli, S. & Friedman, J. M. Distinct transcriptional profiles of adipogenesis in vivo and in vitro. *J. Biol. Chem.* **276,** 34167–34174 (2001).
60. Liu, F. *et al.* Development of a novel GLUT4 translocation assay for identifying potential novel therapeutic targets for insulin sensitization. *Biochem. J.* **418,** 413–420 (2009).
61. Luo, Y., Liu, Y., Hou, K., Wang, S. & Wang, Y. Molecular mechanism of differentiation and apoptosis of U937 cells induced by 12-O-tetradecanoylphorbol-13-acetate. *Chin. J. Clin. Oncol.* **2,** 553–557 (2005).
62. Pabinger, S. *et al.* QPCR: Application for real-time PCR data management and analysis. *BMC Bioinformatics* **10,** 268 (2009).
63. Matyash, V., Liebisch, G., Kurzchalia, T. V., Shevchenko, A. & Schwudke, D. Lipid extraction by methyl-tert-butyl ether for high-throughput lipidomics. *J. Lipid Res.* **49,** 1137–1146 (2008).
64. Hartler, J. *et al.* Lipid Data Analyzer: unattended identification and quantitation of lipids in LC-MS data. *Bioinforma. Oxf. Engl.* **27,** 572–577 (2011).
65. Sager, G., Sandnes, D., Bessesen, A. & Jacobsen, S. Adrenergic ligand binding in human serum. *Biochem. Pharmacol.* **34,** 2812–2815 (1985).
66. Essayan, D. M. Cyclic nucleotide phosphodiesterases. *J. Allergy Clin. Immunol.* **108,** 671–680 (2001).
67. Schaeffler, A. *et al.* Fatty acid-induced induction of Toll-like receptor-4/nuclear factor-kappaB pathway in adipocytes links nutritional signalling with innate immunity. *Immunology* **126,** 233–245 (2009).
68. Schenk, S., Saberi, M. & Olefsky, J. M. Insulin sensitivity: modulation by nutrients and inflammation. *J. Clin. Invest.* **118,** 2992–3002 (2008).
69. Schipper, H. S., Prakken, B., Kalkhoven, E. & Boes, M. Adipose tissue-resident immune cells: key players in immunometabolism. *Trends Endocrinol. Metab. TEM* **23,** 407–415 (2012).
70. Oh, D. Y., Morinaga, H., Talukdar, S., Bae, E. J. & Olefsky, J. M. Increased macrophage migration into adipose tissue in obese mice. *Diabetes* **61,** 346–354 (2012).
71. Murray, P. J. & Wynn, T. A. Protective and pathogenic functions of macrophage subsets. *Nat. Rev. Immunol.* **11,** 723–737 (2011).
72. Eckl, C. New players in adipogenesis: Their localization in the cell and influence of their expression levels on lipid droplet formation and lipid composition in adipocytes. (2013).
73. Verhoven, B., Schlegel, R. A. & Williamson, P. Mechanisms of phosphatidylserine exposure, a phagocyte recognition signal, on apoptotic T lymphocytes. *J. Exp. Med.* **182,** 1597–1601 (1995).

74. Fadok, V. A. *et al.* Exposure of phosphatidylserine on the surface of apoptotic lymphocytes triggers specific recognition and removal by macrophages. *J. Immunol. Baltim. Md 1950* **148,** 2207–2216 (1992).
75. Kay, J. G. & Grinstein, S. Phosphatidylserine-mediated cellular signaling. *Adv. Exp. Med. Biol.* **991,** 177–193 (2013).
76. Tang, Q.-Q. & Lane, M. D. Activation and centromeric localization of CCAAT/enhancer-binding proteins during the mitotic clonal expansion of adipocyte differentiation. *Genes Dev.* **13,** 2231–2241 (1999).
77. Nevins, J. R. Toward an understanding of the functional complexity of the E2F and retinoblastoma families. *Cell Growth Differ. Mol. Biol. J. Am. Assoc. Cancer Res.* **9,** 585–593 (1998).
78. Patel, Y. M. & Lane, M. D. Mitotic clonal expansion during preadipocyte differentiation: calpain-mediated turnover of p27. *J. Biol. Chem.* **275,** 17653–17660 (2000).
79. Zhang, J.-W., Tang, Q.-Q., Vinson, C. & Lane, M. D. Dominant-negative C/EBP disrupts mitotic clonal expansion and differentiation of 3T3-L1 preadipocytes. *Proc. Natl. Acad. Sci. U. S. A.* **101,** 43–47 (2004).
80. Sherr, C. J. & Roberts, J. M. CDK inhibitors: positive and negative regulators of G1-phase progression. *Genes Dev.* **13,** 1501–1512 (1999).
81. DeGregori, J., Leone, G., Miron, A., Jakoi, L. & Nevins, J. R. Distinct roles for E2F proteins in cell growth control and apoptosis. *Proc. Natl. Acad. Sci. U. S. A.* **94,** 7245–7250 (1997).
82. Guo, W., Wong, S., Xie, W., Lei, T. & Luo, Z. Palmitate modulates intracellular signaling, induces endoplasmic reticulum stress, and causes apoptosis in mouse 3T3-L1 and rat primary preadipocytes. *Am. J. Physiol. Endocrinol. Metab.* **293,** E576–586 (2007).
83. Gregor, M. F. & Hotamisligil, G. S. Thematic review series: Adipocyte Biology. Adipocyte stress: the endoplasmic reticulum and metabolic disease. *J. Lipid Res.* **48,** 1905–1914 (2007).
84. Insel, P. A., Zhang, L., Murray, F., Yokouchi, H. & Zambon, A. C. Cyclic AMP is both a pro-apoptotic and anti-apoptotic second messenger. *Acta Physiol. Oxf. Engl.* **204,** 277–287 (2012).
85. Magin, T. M., McWhir, J. & Melton, D. W. A new mouse embryonic stem cell line with good germ line contribution and gene targeting frequency. *Nucleic Acids Res.* **20,** 3795–3796 (1992).
86. Sauer, B. & Henderson, N. Site-specific DNA recombination in mammalian cells by the Cre recombinase of bacteriophage P1. *Proc. Natl. Acad. Sci. U. S. A.* **85,** 5166–5170 (1988).
87. Yagi, T. *et al.* Homologous recombination at c-fyn locus of mouse embryonic stem cells with use of diphtheria toxin A-fragment gene in negative selection. *Proc. Natl. Acad. Sci. U. S. A.* **87,** 9918–9922 (1990).
88. Eisener-Dorman, A. F., Lawrence, D. A. & Bolivar, V. J. Cautionary insights on knockout mouse studies: the gene or not the gene? *Brain. Behav. Immun.* **23,** 318–324 (2009).
89. Barbera, M. J. *et al.* Peroxisome proliferator-activated receptor alpha activates transcription of the brown fat uncoupling protein-1 gene. A link between regulation of the thermogenic and lipid oxidation pathways in the brown fat cell. *J. Biol. Chem.* **276,** 1486–1493 (2001).
90. Ouchi, N., Parker, J. L., Lugus, J. J. & Walsh, K. Adipokines in inflammation and metabolic disease. *Nat. Rev. Immunol.* **11,** 85–97 (2011).
91. O'Brien, S. N., Mantzke, K. A., Kilgore, M. W. & Price, T. M. Relationship between adipose stromal-vascular cells and adipocytes in human adipose tissue. *Anal. Quant. Cytol. Histol. Int. Acad. Cytol. Am. Soc. Cytol.* **18,** 137–143 (1996).
92. Yu, X., Si, J., Zhang, Y. & Dewille, J. W. CCAAT/Enhancer Binding Protein-delta (C/EBP-delta) regulates cell growth, migration and differentiation. *Cancer Cell Int.* **10,** 48 (2010).
93. Shen, Y. & White, E. p53-dependent apoptosis pathways. *Adv. Cancer Res.* **82,** 55–84 (2001).
94. Sun, C. *et al.* SIRT1 improves insulin sensitivity under insulin-resistant conditions by repressing PTP1B. *Cell Metab.* **6,** 307–319 (2007).

95. Chawla, A., Nguyen, K. D. & Goh, Y. P. S. Macrophage-mediated inflammation in metabolic disease. *Nat. Rev. Immunol.* **11,** 738–749 (2011).
96. Ahrén, B. & Scheurink, A. J. Marked hyperleptinemia after high-fat diet associated with severe glucose intolerance in mice. *Eur. J. Endocrinol. Eur. Fed. Endocr. Soc.* **139,** 461–467 (1998).
97. Sloan, C. *et al.* Central leptin signaling is required to normalize myocardial fatty acid oxidation rates in caloric-restricted ob/ob mice. *Diabetes* **60,** 1424–1434 (2011).
98. Kanda, T. *et al.* PPARgamma in the endothelium regulates metabolic responses to high-fat diet in mice. *J. Clin. Invest.* **119,** 110–124 (2009).
99. Houtkooper, R. H. *et al.* The metabolic footprint of aging in mice. *Sci. Reports* **1,** 134 (2011).
100. Tontonoz, P. & Spiegelman, B. M. Fat and beyond: the diverse biology of PPARgamma. *Annu. Rev. Biochem.* **77,** 289–312 (2008).
101. Li, P. *et al.* Adipocyte NCoR knockout decreases PPARγ phosphorylation and enhances PPARγ activity and insulin sensitivity. *Cell* **147,** 815–826 (2011).
102. Prokesch, A. *et al.* Arxes: retrotransposed genes required for adipogenesis. *Nucleic Acids Res.* **39,** 3224–3239 (2011).
103. Green, H. & Meuth, M. An established pre-adipose cell line and its differentiation in culture. *Cell* **3,** 127–133 (1974).
104. M. Pitson, S. *et al.* A point mutant of human sphingosine kinase 1 with increased catalytic activity. *FEBS Lett.* **509,** 169–173 (2001).
105. Leventis, P. A. & Grinstein, S. The distribution and function of phosphatidylserine in cellular membranes. *Annu. Rev. Biophys.* **39,** 407–427 (2010).
106. Martin, S. J., Finucane, D. M., Amarante-Mendes, G. P., O'Brien, G. A. & Green, D. R. Phosphatidylserine externalization during CD95-induced apoptosis of cells and cytoplasts requires ICE/CED-3 protease activity. *J. Biol. Chem.* **271,** 28753–28756 (1996).
107. Nagata, S., Hanayama, R. & Kawane, K. Autoimmunity and the clearance of dead cells. *Cell* **140,** 619–630 (2010).
108. Huang, B. X., Akbar, M., Kevala, K. & Kim, H.-Y. Phosphatidylserine is a critical modulator for Akt activation. *J. Cell Biol.* **192,** 979–992 (2011).
109. Bayascas, J. R. Dissecting the role of the 3-phosphoinositide-dependent protein kinase-1 (PDK1) signalling pathways. *Cell Cycle Georget. Tex* **7,** 2978–2982 (2008).
110. Lucas, N. & Cho, W. Phosphatidylserine binding is essential for plasma membrane recruitment and signaling function of 3-phosphoinositide-dependent kinase-1. *J. Biol. Chem.* **286,** 41265–41272 (2011).
111. Stahelin, R. V. *et al.* The mechanism of membrane targeting of human sphingosine kinase 1. *J. Biol. Chem.* **280,** 43030–43038 (2005).
112. Rohana, A., Fadzilah Adibah, A. M. & Muhammad Roji, M. S. Oleate Induces Apoptosis in 3T3-L1 Adipocytes. *World Acad. Sci. Eng. Technol.* 1–4 (2011).
113. Guo, W., Wong, S., Xie, W., Lei, T. & Luo, Z. Palmitate modulates intracellular signaling, induces endoplasmic reticulum stress, and causes apoptosis in mouse 3T3-L1 and rat primary preadipocytes. *Am. J. Physiol. Endocrinol. Metab.* **293,** E576–586 (2007).
114. Kim, H.-K., Della-Fera, M., Lin, J. & Baile, C. A. Docosahexaenoic acid inhibits adipocyte differentiation and induces apoptosis in 3T3-L1 preadipocytes. *J. Nutr.* **136,** 2965–2969 (2006).
115. Capurso, C. & Capurso, A. From excess adiposity to insulin resistance: the role of free fatty acids. *Vascul. Pharmacol.* **57,** 91–97 (2012).
116. Ryoo, H. D., Gorenc, T. & Steller, H. Apoptotic cells can induce compensatory cell proliferation through the JNK and the Wingless signaling pathways. *Dev. Cell* **7,** 491–501 (2004).
117. Halldorsdottir, S., Carmody, J., Boozer, C. N., Leduc, C. A. & Leibel, R. L. Reproducibility and accuracy of body composition assessments in mice by dual energy x-ray absorptiometry and time domain nuclear magnetic resonance. *Int. J. Body Compos. Res.* **7,** 147–154 (2009).

118. Ramanadham, S. *et al.* Age-related changes in bone morphology are accelerated in group VIA phospholipase A2 (iPLA2beta)-null mice. *Am. J. Pathol.* **172,** 868–881 (2008).
119. O'Donnell, K. A., Wentzel, E. A., Zeller, K. I., Dang, C. V. & Mendell, J. T. c-Myc-regulated microRNAs modulate E2F1 expression. *Nature* **435,** 839–843 (2005).
120. Mundle, S. D. & Saberwal, G. Evolving intricacies and implications of E2F1 regulation. *FASEB J.* **17,** 569–574 (2003).
121. Johnson, D. G. The paradox of E2F1: oncogene and tumor suppressor gene. *Mol. Carcinog.* **27,** 151–157 (2000).
122. Leone, G. *et al.* Myc requires distinct E2F activities to induce S phase and apoptosis. *Mol. Cell* **8,** 105–113 (2001).
123. Saavedra, H. I. *et al.* Specificity of E2F1, E2F2, and E2F3 in mediating phenotypes induced by loss of Rb. *Cell Growth Differ. Mol. Biol. J. Am. Assoc. Cancer Res.* **13,** 215–225 (2002).
124. Pirot, P. *et al.* Transcriptional regulation of the endoplasmic reticulum stress gene chop in pancreatic insulin-producing cells. *Diabetes* **56,** 1069–1077 (2007).
125. Averill, L., Toossi, Z., Aung, H., Boom, W. H. & Ellner, J. J. Regulation of production of tumor necrosis factor alpha in monocytes stimulated by the 30-kilodalton antigen of Mycobacterium tuberculosis. *Infect. Immun.* **63,** 3206–3208 (1995).

8 Appendix

8.1 Submitted Manuscript *(PLOS ONE, PONE-D-13-25085)*

α/β-Hydrolase Domain Containing Protein 15 (ABHD15) – an Adipogenic Protein Protecting from Apoptosis

Evelyn Walenta[1], Ariane R. Pessentheiner[1], Helmut J. Pelzmann[1], Alexander Deutsch[2], Madeleine Goeritzer[3], Dagmar Kratky[3], Hubert Hackl[4], Da Young Oh[5], Andreas Prokesch[1], Juliane G. Bogner-Strauss[1#]

[1] Institute for Genomics and Bioinformatics, Graz University of Technology, Graz, Austria
[2] Division of Hematology, Medical University of Graz, Graz, Austria
[3] Institute of Molecular Biology and Biochemistry, Medical University of Graz, Graz, Austria
[4] Division of Bioinformatics, Biocenter, Innsbruck Medical University, Innsbruck, Austria
[5] Division of Endocrinology and Metabolism, Department of Medicine, University of California, San Diego, La Jolla, CA 92093, USA

[#] E-mail: juliane.bogner-strauss@tugraz.at

8 Appendix

Abstract

Our knowledge about adipocyte metabolism and development is steadily growing, yet many players are still undefined.

Here, we show that α/β-hydrolase domain containing protein 15 (Abhd15) is a direct and functional target gene of peroxisome proliferator-activated receptor gamma (PPARγ), the master regulator of adipogenesis. In line, Abhd15 is mainly expressed in brown and white adipose tissue and strongly upregulated during adipogenesis in various murine and human cell lines. Stable knockdown of Abhd15 in 3T3-L1 cells evokes a striking differentiation defect, as evidenced by low lipid accumulation and decreased expression of adipocyte marker genes. In preconfluent cells, knockdown of Abhd15 leads to impaired proliferation, which is caused by apoptosis, as we see an increased SubG1 peak, Caspase 3/7 activity, and BAX protein expression as well as a reduction in anti-apoptotic BCL-2 protein. Furthermore, apoptosis-inducing amounts of palmitic acid evoke a massive increase of Abhd15 expression, proposing an apoptosis-protecting role for Abhd15. On the other hand, in mature adipocytes physiological (i.e. non-apoptotic) concentrations of palmitic acid down-regulate Abhd15 expression. Accordingly, we found that the expression of Abhd15 in adipose tissue is reduced in physiological situations with high free fatty acid levels, like high-fat diet, fasting, and aging as well as in genetically obese mice.

Collectively, our results position Abhd15 as an essential component in the development of adipocytes as well as in apoptosis, thereby connecting two substantial factors in the regulation of adipocyte number and size. Together with its intricate regulation by free fatty acids, Abhd15 might be an intriguing new target in obesity and diabetes research.

8 Appendix

Introduction

During the last decade, obesity became one of the major pandemics and is strongly associated with several diseases, such as type 2 diabetes, liver cirrhosis, cardiovascular diseases, and certain cancers [1,2], leading to socio-economic repercussions [3,4]. Therefore, it is of extreme importance to gain a better insight into adipocyte biology and the link between adipose tissue and disturbed metabolism.

Obesity is characterized by an excessive increase in number and size of adipocytes, factors tightly regulated by the rate of proliferation of preadipocytes and the differentiation into mature adipocytes [5]. Adipogenesis is a process highly controlled through sequential activation of several genes, most of them transcription factors [6–8]. The nuclear receptor peroxisome proliferator-activated receptor gamma (PPARγ) has been postulated as the master regulator of adipogenesis and is necessary and sufficient for adipocyte differentiation[6,9,10], as many genes of the adipogenesis regulating cascade are either regulated by or regulate PPARγ [11]. Furthermore, in addition to proliferation and adipogenesis, it has been demonstrated that apoptosis of pre-adipocytes as well as mature adipocytes is a potent player in the regulation of adipose tissue mass [5]. For instance, adipocyte apoptosis is increased in diet-induced obesity, and inhibition of apoptosis protects from adipose tissue macrophage recruitment, development of fatty liver, and insulin resistance of obese animals [12]. However, the complete mechanism connecting adipogenesis and apoptosis is still elusive.

We and others utilized high throughput techniques to uncover novel players in adipogenesis [13–16]. Based on previous observations, α/β-hydrolase domain containing protein 15 (ABHD15) was found as being strongly increased during adipocyte differentiation [17]. Previous studies revealed that the insulin-activated protein kinase Akt phosphorylates ABHD15 in adipocytes and that ABHD15 associates with and regulates cyclic nucleotide phosphodiesterase 3B (PDE3B) [17–19]. ABHD15 belongs to the α/β-hydrolase family, which is characterized by a similar tertiary protein fold of α-helixes and β-sheets. However, the family members do not share obvious sequence similarities, leading to a widespread variety of enzyme subclasses, such as lipases, esterases, dehydrogenases, dehalogenases, peroxidases, and epoxide hydrolases [20]. It is therefore expected that ABHD15 possesses a hydrolytic active site but its distinct function has not been defined so far.

In this study, we demonstrate that ABHD15 is required for adipogenesis and a direct and functional target gene of PPARγ, resulting in strongly increased Abhd15 expression during murine and human adipogenesis. Additionally, we identified free fatty acids (FFAs) as negative regulators of Abhd15 expression in differentiated adipocytes as well as in physiological circumstances like in fasting or obesity. Finally, we show that Abhd15

knockdown results in increased apoptosis, whereas induction of apoptosis increases Abhd15 expression, suggesting a protective role of ABHD15 against apoptosis.

Materials and Methods

Animal studies

Mouse experiments conformed to the Guide for Care and Use of Laboratory Animals of the US National Institutes of Health and were approved by the Austrian Federal Ministry of Science and Research, Division of Genetic Engineering and Animal Experiments.
Male C57BL/6 (age mentioned in figures and text) and 4 months old male ob/ob mice were used for this study. Animals were kept on a 12/12 hours light/dark cycle and were put on either chow or high fat diet (60% calories in fat; Ssniff, Soest, Germany) with 8 weeks of age. Tissues were harvested from mice in *fed ad libitum* state or after fasting for 12 hours.

Promoter analyses

Genome organization around the Abhd15 transcription start site was visualized using the UCSC genome browser (GRCm38/mm10). Custom tracks include data from chromatin immunoprecipitation (ChIP) followed by sequencing or microarray analysis, respectively, for PPARγ at day 6 [21] and for PPARγ and C/EBPα at day 10 [22] during 3T3-L1 adipocyte differentiation, as well as for PPARγ-RXRα direct repeats 1 (DR1) motifs (similarity score > 0.90) (potential binding sites on the plus strand are shown in red and on the minus strand in blue). *In silico* promoter analysis was performed with a Perl implementation of the MatInspector algorithm [23] using a 1133 element position weight matrix (PWM) as identified before [22]. Sequence logo was generated using http://icbi.at/logo.

Cell culture, adipocyte differentiation, and lipid staining

Cells were cultured as described before [16]. 3T3-L1 adipocytes were treated with 1 µM rosiglitazone at time points and durations indicated in the text, figures and figure legends. Fully differentiated cells (day 7 after differentiation start) were treated with 0.5 mM 3-isobutyl-1-methylxanthine, 10 µM isoproterenol, or 100 µM palmitic acid in serum-free high glucose DMEM containing L-glutamine (2 mM), penicillin (50 U/mL) and streptomycin (50 µg/mL) (P/S), and harvested after 2 hours of treatment. Preconfluent cells were treated with palmitic acid concentrations as indicated in the text, figures, and figure legends for 24 hours. Palmitic acid was resolved in 90% ethanol to a stock of 50 mM and added to serum-free high glucose DMEM containing L-glutamine, P/S, and 0.5% BSA. Plates were oil red O-stained as described earlier [24]. MEFS[25,26], OP-9 [16] and SGBS [16] cells were cultured as described before.

RNA isolation, reverse transcription, and gene expression analysis

Cells were washed with PBS and harvested using an RNA isolation kit (Marcherey-Nagel, Dueren, Germany). Tissue RNA was isolated with the TRIzol® reagent (Invitrogen, Carlsbad, USA) according to the manufacturer's protocol. Expression of genes was assessed by real-time reverse transcriptase-polymerase chain reaction (RT-PCR) using an ABI Prism 7700 Sequence Detector system utilizing SYBR Green PCR master mix (Applied Biosystems, Darmstadt, Germany). Gene expression was normalized using TFIIβ for murine tissues and cells and β-actin for human cells as reference genes. Relative mRNA expression levels were calculated using averaged 2^{-ddCt} values for each biological replicate as implemented before [27].

Primer sequences:

mAbhd15 (TATGAACGTGGGTTCTTGCT, TTGGTGTGACAGAACAGGGT),

hAbhd15 (CCGTGCTGCGCTGCCGAGAGTGG, GGCTGTGGCATACCTGCTGAGGGCG),

hβ-Actin (CGCCGCATCCTCCTCTTC, GACACCGGAACCGCTCATT),

mC/ebpα (ATCTGCGAGCACGAGACGTC, TGTCGGCTGTGCTGGAAGA),

mFabp4 (CGACAGGAAGGTGAAGAGCATC, ACCACCAGCTTGTCACCATCTC),

mFasn (GCTGTAGCACACATCCTAGGCA, TCGTGTTCTCGTTCCAGGATC),

mPparγ2 (TGCCTATGAGCACTTCACAAGAAAT, CGAAGTTGGTGGGCCAGAA),

mTFIIβ (GTCACATGTCCGAATCATCCA, TCAATAACTCGGTCCCCTACAA)

Silencing of Abhd15 using short hairpin (sh)RNA lentivirus particles

One control non-targeting shRNA lentivirus and two shRNA lentiviruses directed against Abhd15 were purchased from Sigma (MISSION shRNA lentiviral particles NM_026185). 3T3-L1 cells were seeded into 6-well plates 12 hours before transduction using $3*10^4$ cells/well (30% confluence). Cells were infected over night with 5 MOI (multiplicity of infection) in standard medium containing 8 µg/ml polybrene (Sigma). After 16 hours, the infection medium was replaced with fresh medium containing 3 µg/mL puromycin (Sigma). 3T3-L1 cells were selected for stable expression for at least 5 days.

Silencing of Abhd15 via electroporation using siRNA

Control non-targeting siRNA and siRNA directed against Abhd15 were purchased from Sigma (MISSION siRNA NM_026185). 80,000 fully differentiated 3T3-L1 (day 8 after differentiation start) were electroporated per 10 µL reaction with siRNA (100 nM) using the Neon Transfection System (Invitrogen, Carlsbad, USA), at 1400 V, 20 ms, 1 pulse. Cells were harvested 2 days after transfection.

Generation of recombinant retrovirus

The coding sequence of mouse Abhd15 was amplified by PCR from mouse adipose tissue cDNA using Pfu polymerase (Thermo Scientific, Waltham, USA). The primers were designed to create *Bgl*II and *Xho*I restriction sites and the product, containing the whole open reading frame, was ligated into *Bgl*II-*Xho*I digested Murine Stem Cell Virus vector (pMSCV puro; BD Biosciences Clontech). To produce infectious, but replication-incompetent recombinant retroviruses expressing Abhd15, PhoenixEco packaging cells were transfected with pMSCV-Abhd15 using Metafectene (Biontex Laboratories, Planegg, Germany). Supernatants containing viral particles were collected 48 hours after transfection. Viral supernatants were supplemented with 8 µg/mL polybrene and added to 3T3-L1 cells (30% confluence) for infections for 18–24 hours. Cells were selected with 3 µg/mL puromycin, expanded, and seeded for differentiation experiments. The empty pMSCVpuro vector was used as control.

Western blot analysis

Control (ntc) and Abhd15-silenced (Abhd15_sil1) 3T3-L1 cells were harvested by scraping with lysis buffer (50 mM Tris-HCl pH 6.8, 10% glycerol, 2.5% SDS, 1x protease inhibitor cocktail, 1 mM PMSF) after two washing steps with PBS and benzoase (Merck, Vienna, Austria) digested. Protein concentration was determined with the BCA protein assay kit (Pierce, Rockford, USA). Protein samples were separated according to size by SDS-polyacrylamide gel electrophoresis (NuPAGE, Invitrogen). Resolved samples were transferred onto nitrocellulose or polyvinylidene difluoride membranes. Blots were incubated with an anti-rabbit polyclonal antibody against Abhd15 (1:1 kind gift from Gustav Lienhardt), against a monoclonal anti-mouse β-actin antibody (1:25,000 Sigma), or anti-rabbit polyclonal antibodies BCL-2 (1:1000), and BAX (1:1000) (Cell Signaling Technology, Danvers, MA), or against a monoclonal anti-mouse β-actin antibody (1:20,000 Santa Cruz, Heidelberg, Germany). The horseradish peroxidase-conjugated goat anti-mouse (1:3000 for Abhd15 antibody, 1:2000 for BCL-2 and BAX antibodies) and rabbit anti-mouse (1:3000 for the β-actin antibody from Sigma, 1:1000 for the β-actin antibody from Cell Signaling) antibodies (Dako, Glostrup, Denmark) were visualized by enhanced chemiluminescence detection (ECL component from Pierce Clarity™ and Western ECL Substrate from Bio-Rad, Hercules, USA) using a ChemiDoc™ MP Imaging System (Bio-Rad).

Luciferase reporter assays

Three regions upstream of the Abhd15 transcription start site (TSS) (F1 -1190-0bp, F2 -1190-530bp, and F3 -530-0bp from TSS) were cloned into luciferase reporter vectors (Promega, Madison, USA) either containing a minimal promoter (F2 into pGl4.26) or not (F1 and F3 into pGL4.21), and were cotransfected with PPARγ2 and RXRα containing pCMX expression vectors. As described before[28], renilla reporter vector pGl4.75 (Promega,

Madison, USA) was cotransfected in all experiments in a ratio of 1:50 to luciferase reporter vectors as a control for varying transfection efficiencies. Transfection into Cos7 cells was performed in 96-well plates using MetafectenePro (Biontex, Martinsired, Austria) according to the manufacturer's protocol in a ratio of MetafectenePro to DNA 3:1 (µl:µg). 100 ng of luciferase reporter vector and either 50 ng of PPARγ2 and RXRα or 100 ng of the empty pCMX as a control were used. After 48 hours cells were lysed and assayed according to the protocol provided with the Dual-luciferase assay system (Promega, Madison, USA). Luminescence read-outs were generated with a Berthold Orion II luminometer. Relative luciferase activity was calculated by referring renilla-normalized values to empty luciferase vector measurements.

Assessment of cell growth

Cells were plated at a density of 1000 cells/96-well and cultured for 72 hours. Seven replicates of the CellTiter 96 AQueous One Solution Cell Proliferation Assay (Promega, Madison, USA) were measured using 3-(4,5-dimethylthiazol-2-yl)-5-(3-carboxymethoxyphenyl)-2-(4-sulfophenyl)-2**H**-tetrazolium, inner salt (MTS). Absorbance was recorded by a BioRad spectrophotometer at 490 nm.

BrdU cell cycle analysis

$1x10^6$ cells were incubated for 1 hour at 37°C with 10 µM BrdU solution. BrdU and 7-AAD staining was performed according to the BrdU Flow kit manual (Becton Dickinson, San Diego, USA). A total of 1×10^5 events were collected on FACScan and cellular DNA content was analyzed by FlowJo software (TreeStar, Ashland, USA).

Caspase-Glo 3/7 Assay

14,500 cells/96-well (in 100 µL) were cultured for 18 hours and analyzed for caspase activation using the Caspase-Glo 3/7 assay (Promega Corporation, Madison, USA), according to the manufacturer's protocol. Luminescence was measured 30 min after adding the Caspase-Glo 3/7 reagent (Caspase-Glo substrate and buffer).

Statistical analysis

If not otherwise stated, results are mean values (±standard deviation) of at least three independent experiments. Statistical significance was determined using the two-tailed Student's *t* test.

Results

Abhd15 is a direct and functional target gene of Pparγ

In a search for new key players of adipogenesis, we surveyed published ChIP sequencing data sets that identified genome-wide PPARγ and CCAAT-enhancer-binding protein alpha (C/EBPα) binding sites in differentiating 3T3-L1 cells [21–23]. In these studies, Abhd15 possesses PPARγ and C/EBPα binding sites in its promoter region (Figure 1A). Further, motif search for peroxisome proliferator response element sequences (PPRE) revealed two putative binding sites of PPARγ and its dimerization partner retinoid X receptor alpha (RXRα), ~990 bp and ~440 bp upstream to the Abhd15 transcription start site (TSS) (Figure 1A). Together with the upregulation of Abhd15 during differentiating 3T3-L1 cells (Figure 1B), these findings suggest that Abhd15 might be regulated by PPARγ. In order to test this hypothesis, 3T3-L1 cells were exposed to the PPARγ agonist rosiglitazone (1 µM). As expected, the treatment during differentiation led to strongly increased mRNA expression of Abhd15 (Figure 1B). Furthermore, short term treatments of fully differentiated 3T3-L1 adipocytes with rosiglitazone for either 12 or 24 hours (Figure 1C), and undifferentiated cells for 6, 12, or 24 hours (Figure 1D) showed a time-dependent increased mRNA expression of Abhd15. Additionally, mouse embryonic fibroblasts (MEFs) isolated from Pparγ -/- and Pparγ +/- mice[26] were subjected to hormone-induced adipocyte differentiation. While Pparγ +/- MEFs showed significantly increased Abhd15 mRNA levels from day 0 to day 4 of differentiation, Pparγ -/- MEFs did not (Figure 1E). Moreover, the addition of rosiglitazone to Pparγ +/- MEFs increased Abhd15 expression 6-fold on day 4, whereas in Pparγ -/- MEFs rosiglitazone did not evoke any changes in expression level (Figure 1E). Finally, in order to prove the direct binding of PPARγ and its dimerization partner RXRα to the Abhd15 promoter region, luciferase reporter assays with three different sequences were performed (segments containing the 990 bp PPRE (F2), the 440 bp PPRE (F3), and one segment containing both (F1) (Figure 1F). We clearly observed Abhd15 promoter activation of the region ~440 bp upstream to the TSS, which could be further increased upon addition of rosiglitazone (Figure 1G). The region with the putative PPRE at ~990 bp seemed not to be involved in Abhd15 promoter activation (Figure 1G).

Taken together, these results indicate that Pparγ is a prerequisite for Abhd15 expression and that Abhd15 is a direct and functional PPARγ target gene.

Abhd15 expression is upregulated during adipogenesis and decreased by high FFA levels

Next, gene expression of Abhd15 was assessed in human and murine model systems of adipogenesis. In addition to its upregulation in 3T3-L1 cells (Figure 1B), Abhd15 was strongly upregulated during adipogenic differentiation of OP9 cells and MEFs (Figure 2A). A similar expression profile of the human ortholog of Abhd15 could be shown in Simpson-Golabi-Behmel syndrome (SGBS) cells (Figure 2B). In accordance to the increased expression during adipogenic differentiation, Abhd15 was mainly expressed in murine brown (BAT) and white adipose tissue (WAT), to a lower extent in liver, and hardly in skeletal (SM) and cardiac muscle (CM) (Figure 2C). Interestingly, Abhd15 mRNA expression was significantly decreased in WAT of genetically obese, leptin-deficient mice (ob/ob) compared to their wild type littermates (Figure 2D). Moreover, already after 3 days on a high fat diet (HFD), Abhd15 mRNA expression was strongly down-regulated in WAT when compared to chow-fed controls (Figure 2E). This reduction of Abhd15 mRNA expression in WAT was still evident after 15 weeks on HFD (Figure 2E). Notably, 23 weeks old mice had strongly reduced expression levels compared to 8 weeks old littermates, suggesting that Abhd15 mRNA expression is reduced in an age-dependent manner (Figure 2E). Furthermore, overnight fasting decreased Abhd15 mRNA expression levels in murine WAT and BAT (Figure 2F). Simulated fasting in mature adipocytes by short-term treatment (2 hours) of fully differentiated 3T3-L1 cells with isoproterenol or 3-isobutyl-1-methylxanthine (IBMX) also resulted in reduced Abhd15 mRNA expression (Figure 2G). Both components increase intracellular cAMP levels and thereby stimulate lipolysis [29,30].
The observations that Abhd15 mRNA expression is reduced in obese mice, in mice fed HFD, but also upon fasting indicate that increased FFAs, the common denominator in these conditions, directly diminish Abhd15 expression. In accordance, short-term treatment (2 hours) of mature adipocytes with 100 µM palmitic acid, a dose reflecting fasting levels without evoking toxic effects [31], strongly reduced Abhd15 mRNA expression (Figure 2H).

Abhd15 is required for adipogenesis

To gain more insight into its function, stable knock-down of Abhd15 in 3T3-L1 cells was performed. For this purpose, an shRNA construct targeting Abhd15, encoded by lentiviral vectors, was used to generate 3T3-L1 cells with constitutive knock-down of Abhd15 expression. After transduction and selection, the cells were grown to confluence and induced to differentiate using a standard hormonal cocktail. During differentiation, two Abhd15-targeting shRNA lentiviral constructs revealed a reduction of up to 80% compared to a non-

targeting control shRNA (ntc) on mRNA level (Figure 3A). The silencing of the stronger shRNA lentiviral construct (Abhd15_sil1) was confirmed on protein level using western blot analysis (Figure 3B). Knock-down of Abhd15 drastically reduced the formation of lipid droplets, as revealed by oil red O staining of fully differentiated 3T3-L1 cells (Figure 3C). Additionally, mRNA expression levels of several adipogenic markers, such as C/ebpα, Pparγ, fatty acid binding protein 4 (Fabp4), and fatty acid synthase (Fasn), were decreased in Abhd15-silenced compared to control cells at day 5 of differentiation (Figure 3D). However, stable overexpression of Abhd15 (Supporting Figure 1) did not induce any changes in the differentiation capacity of 3T3-L1 cells (Supporting Figure 2).

In order to investigate a potential influence of Abhd15 on mature adipocytes, Abhd15 was transiently knocked down in fully differentiated 3T3-L1 cells by means of siRNA introduced by electroporation. Although the expression level of Abhd15 was reduced by 60% in mature adipocytes (Figure 3D), neither differences in lipid accumulation (data not shown), nor changes in expression levels of C/ebpα, Pparγ, Fabp4, and Fasn could be detected (Figure 3E).

Together, these results point out that Abhd15 is a required factor for adipogenic differentiation, whereas reduced Abhd15 expression in mature adipocytes has no effect on the maintenance of the differentiated status.

Abhd15 expression is tightly connected to apoptosis

To track the origin of the differentiation defect in Abhd15-silenced 3T3-L1 cells, we closely monitored the mRNA expression of Pparγ during early differentiation. Right after induction the expected increase in Pparγ expression was reduced in Abhd15-silenced cells compared to control cells (Figure 4A), hinting at an early defect of differentiation. In 3T3-L1 cells, the first steps before terminal differentiation include growth arrest due to cell-cell contact, followed by two sequential rounds of mitosis (called mitotic clonal expansion), which are necessary for terminal differentiation [32]. Mitotic clonal expansion involves a transcription factor cascade, followed by the expression of genes responsible for the adipocyte phenotype [33]. The reduced Pparγ levels upon Abhd15 silencing started right during this phase of mitotic clonal expansion, suggesting a cell cycle defect due to reduced Abhd15 expression. Preconfluent Abhd15-silenced 3T3-L1 cells only showed a ~30% decrease in Abhd15 mRNA expression (Figure 4B), and did not show any decrease in Abhd15 expression after 2 weeks of culturing (data not shown). Nevertheless, compared to control cells the cells with reduced Abhd15 expression showed a slower proliferation rate, reflected by a decrease in cell count by 30-40% 48 hours after seeding a defined number of cells (Figure 4C). This observation

was confirmed by a colorimetric proliferation assay (MTS), revealing a reduction in proliferation of preconfluent Abhd15-silenced cells by ~20% (Figure 4D). In line with this, cells stably overexpressing Abhd15 showed a slightly increased cell proliferation (Supporting Figure 1, 3).

To get a better insight into the changed proliferation of Abhd15-silenced cells, their cell cycle was analyzed in more detail using BrdU FACScan. The analysis revealed an increased SubG1 peak, without any changes in the S phase in Abhd15-silenced 3T3-L1 cells (Figure 4E, Supporting Figure 4). As the SubG1 peak reflects apoptotic cells, whereas the S phase shows cells in the interphase, these results indicate increased apoptosis, rather than a defect in cell division, as a cause for the reduced cell number. Further, western blot analysis of B-cell lymphoma 2 (BCL-2) and BCL-2-associated X protein (BAX), both essential regulators of apotosis[34], revealed decreased protein levels of the pro-survival regulator BCL-2, and increased protein levels of the pro-apoptotic regulator BAX (Figure 4F, 4G). Finally, a caspase 3/7 assay, showing a more than 2-fold increase in caspase activity in Abhd15-silenced cells (Figure 4H), provided the last hint that apoptosis is increased in preconfluent Abhd15-silenced 3T3-L1 cells. In accordance with these findings, induced apoptosis (provoked by treatment of preconfluent 3T3-L1 cells with palmitic acid concentrations leading to conditions from non-apoptotic (100 µM) to highly apoptotic (500 µM) for 24 hours [35]) resulted in a massive increase of Abhd15 mRNA expression in a dose- dependent manner (Figure 4I).

Together these results demonstrate a connection of Abhd15 levels and apoptosis and suggest that a sufficient amount of Abhd15 is necessary to keep apoptotic signaling in check.

Discussion

In this study, we provide conclusive evidence that Abhd15 is a direct and functional target gene of PPARγ and an essential factor for adipogenesis. Interestingly, while Abhd15 expression increases during adipogenesis, it decreases in the presence of high levels of FFAs, as observed in diet- and genetically induced obesity, fasting and aging, [36–39] as well as upon FFA treatment of cultured mature adipocytes. Furthermore, we show that knockdown of Abhd15 in preadipocytes leads to increased apoptosis, and that induced apoptosis in turn strongly increases Abhd15 expression.

Our results demonstrate that the proximal promoter of Abhd15 contains a functional Pparγ binding site. This adds Abhd15 to the large group of direct and functional PPARγ targets, of which many are important adipogenic players, such as FABP4, CD36, GLUT4, APMAP, and ARXES [40,41,16,15]. Like other adipogenic and Pparγ target genes [40], the expression of Abhd15 is strongly upregulated during adipogenic differentiation. Moreover, when cells were exposed to the PPARγ agonist rosiglitazone, Abhd15 expression was increased similarly like the above mentioned adipogenic genes [40].

Abhd15 is mainly expressed in murine adipose tissues and upregulated during *in vitro* adipogenesis, pointing toward a role of ABHD15 in adipocyte development. Additionally, we clearly show that Abhd15 expression is required for adipogenesis, as Abhd15-silenced 3T3-L1 cells were unable to increase the expression levels of adipogenic marker genes, leading to reduced lipid accumulation. As transient silencing in fully differentiated cells did not evoke any changes of the mature adipocyte phenotype, we conclude that Abhd15 lacks a role in the maintenance of the mature adipogenic status. Stable silencing of Abhd15 in 3T3-L1 cells lowers Pparγ expression levels as soon as 12 hours after induction of differentiation. Therefore, expression of adipogenic markers was not induced in Abhd15 stably silenced 3T3-L1 cells, including Abhd15 itself, leading to an improved silencing efficiency from 30% in preconfluent cells to 80% during differentiation. Searching for a cause for the differentiation defect prior to Pparγ induction, we observed that Abhd15-silenced cells proliferated slower than control cells, shown by reduced cell counts and a colorimetric proliferation assay. Cell cycle analysis revealed no change in the S phase, but an increased SubG1 peak. These observations, together with pro-death regulation of the apoptosis marker BCL-2 and BAX, and increased caspase 3/7 activity, hint to apoptosis as causal for the proliferation defect. Hence, the low silencing efficiency of only ~30% in preconfluent cells as well as the observed loss of silencing after 2 weeks of culturing could be explained by an apoptosis-mediated “dilution” of cells with high Abhd15 knockdown during prolonged culturing. On the other hand, induced apoptosis highly increased Abhd15 mRNA expression, which let us conclude that

Abhd15 (besides being a novel putative adipogenic player) also plays a role in the control of apoptosis and probably protects cells from apoptosis, at least in the investigated cell type. Previous studies showed that apoptosis is increased in adipocytes of mice with diet-induced obesity [12]. These mice also have increased levels of FFAs [36], which per se are known to induce apoptosis [42–44]. However, the complete mechanism connecting these two characteristics of the diet-induced obesity phenotype is still elusive. Our data suggest that Abhd15 could be a key player in this context, as we found Abhd15 expression to be consistently decreased *in vivo* and *in vitro* upon conditions of elevated FFA levels. In adipocytes, superfluous FFAs can activate a number of different serine kinases, leading to inhibition of insulin signaling [45] and, in turn, to reduced Akt activation. Akt signaling has been shown to phosphorylate Abhd15 [17,18]. As a result, high levels of FFAs might not only lead to decreased mRNA expression of Abhd15, but also influence the phosphorylation state of the remaining protein. For these reasons it is tempting to speculate that reduction/impairment of "protecting Abhd15" by increased FFA content leads to induced apoptosis and its further consequences, like recruitment of adipose tissue macrophages, insulin resistance, and development of fatty liver [12].

In conclusion, our results show that Abhd15 is a functional PPARγ target gene and required for adipogenesis. In addition, we provide evidence that Abhd15 expression levels are tightly connected to apoptosis. While decreased expression of Abhd15 evokes apoptosis, a striking increase of Abhd15 expression can be found upon induction of apoptosis, proposing Abhd15 as a protective factor against apoptosis. Together with its intricate regulation by FFAs, Abhd15 might be an intriguing new target in obesity and diabetes research, as it impacts on adipogenesis and apoptosis, both factors crucially determining adipose cell number and size.

Acknowledgements

We want to thank C. Neuhold, T. Schreiner, and F. Stoeger for technical assistance. Pparγ -/- and Pparγ +/- MEFs were kind gift from E. Rosen[26], and PPARγ2 and RXRα containing pCMX expression vectors were kindly provided by M. Schupp. We also want to thank M. Maris for critically reviewing the manuscript and for fruitful discussions. Our thanks also go to J.M. Olefsky for giving E. Walenta the opportunity to work in his lab for one year during her graduate studies. Additionally, we want to thank G. Lienhardt for the Abhd15 antibody.

8 Appendix

References

1. Aballay LR, Eynard AR, Díaz M del P, Navarro A, Muñoz SE (2013) Overweight and obesity: a review of their relationship to metabolic syndrome, cardiovascular disease, and cancer in South America. Nutr Rev 71: 168–179. doi:10.1111/j.1753-4887.2012.00533.x.
2. Kopelman PG (2000) Obesity as a medical problem. Nature 404: 635–643. doi:10.1038/35007508.
3. Withrow D, Alter DA (2011) The economic burden of obesity worldwide: a systematic review of the direct costs of obesity. Obes Rev Off J Int Assoc Study Obes 12: 131–141. doi:10.1111/j.1467-789X.2009.00712.x.
4. Hammond RA, Levine R (2010) The economic impact of obesity in the United States. Diabetes Metab Syndr Obes Targets Ther 3: 285–295. doi:10.2147/DMSOTT.S7384.
5. Sorisky A, Magun R, Gagnon AM (2000) Adipose cell apoptosis: death in the energy depot. Int J Obes Relat Metab Disord J Int Assoc Study Obes 24 Suppl 4: S3–7.
6. Tontonoz P, Hu E, Spiegelman BM (1995) Regulation of adipocyte gene expression and differentiation by peroxisome proliferator activated receptor gamma. Curr Opin Genet Dev 5: 571–576.
7. Mandrup S, Lane MD (1997) Regulating adipogenesis. J Biol Chem 272: 5367–5370.
8. Rosen ED, Walkey CJ, Puigserver P, Spiegelman BM (2000) Transcriptional regulation of adipogenesis. Genes Dev 14: 1293–1307.
9. Spiegelman BM, Hu E, Kim JB, Brun R (1997) PPAR gamma and the control of adipogenesis. Biochimie 79: 111–112.
10. Tontonoz P, Hu E, Spiegelman BM (1994) Stimulation of adipogenesis in fibroblasts by PPAR gamma 2, a lipid-activated transcription factor. Cell 79: 1147–1156.
11. Rosen ED, MacDougald OA (2006) Adipocyte differentiation from the inside out. Nat Rev Mol Cell Biol 7: 885–896. doi:10.1038/nrm2066.
12. Alkhouri N, Gornicka A, Berk MP, Thapaliya S, Dixon LJ, et al. (2010) Adipocyte apoptosis, a link between obesity, insulin resistance, and hepatic steatosis. J Biol Chem 285: 3428–3438. doi:10.1074/jbc.M109.074252.
13. Prokesch A, Hackl H, Hakim-Weber R, Bornstein SR, Trajanoski Z (2009) Novel insights into adipogenesis from omics data. Curr Med Chem 16: 2952–2964.
14. Hakim-Weber R, Krogsdam A-M, Jørgensen C, Fischer M, Prokesch A, et al. (2011) Transcriptional regulatory program in wild-type and retinoblastoma gene-deficient mouse embryonic fibroblasts during adipocyte differentiation. Bmc Res Notes 4: 157. doi:10.1186/1756-0500-4-157.
15. Prokesch A, Bogner-Strauss JG, Hackl H, Rieder D, Neuhold C, et al. (2011) Arxes: retrotransposed genes required for adipogenesis. Nucleic Acids Res 39: 3224–3239. doi:10.1093/nar/gkq1289.
16. Bogner-Strauss JG, Prokesch A, Sanchez-Cabo F, Rieder D, Hackl H, et al. (2010) Reconstruction of gene association network reveals a transmembrane protein required for adipogenesis and targeted by PPARγ. Cell Mol Life Sci Cmls 67: 4049–4064. doi:10.1007/s00018-010-0424-5.
17. Chavez JA, Gridley S, Sano H, Lane WS, Lienhard GE (2006) The 47kDa Akt substrate associates with phosphodiesterase 3B and regulates its level in adipocytes. Biochem Biophys Res Commun 342: 1218–1222. doi:10.1016/j.bbrc.2006.02.091.
18. Gridley S, Lane WS, Garner CW, Lienhard GE (2005) Novel insulin-elicited phosphoproteins in adipocytes. Cell Signal 17: 59–66. doi:10.1016/j.cellsig.2004.05.013.
19. Saltiel AR, Kahn CR (2001) Insulin signalling and the regulation of glucose and lipid metabolism. Nature 414: 799–806. doi:10.1038/414799a.
20. Nardini M, Dijkstra BW (1999) Alpha/beta hydrolase fold enzymes: the family keeps growing. Curr Opin Struct Biol 9: 732–737.
21. Nielsen R, Pedersen TA, Hagenbeek D, Moulos P, Siersbaek R, et al. (2008) Genome-wide profiling of PPARgamma:RXR and RNA polymerase II occupancy reveals temporal activation of distinct metabolic pathways and changes in RXR dimer composition during adipogenesis. Genes Dev 22: 2953–2967. doi:10.1101/gad.501108.

22. Lefterova MI, Zhang Y, Steger DJ, Schupp M, Schug J, et al. (2008) PPARgamma and C/EBP factors orchestrate adipocyte biology via adjacent binding on a genome-wide scale. Genes Dev 22: 2941–2952. doi:10.1101/gad.1709008.
23. Quandt K, Frech K, Karas H, Wingender E, Werner T (1995) MatInd and MatInspector: new fast and versatile tools for detection of consensus matches in nucleotide sequence data. Nucleic Acids Res 23: 4878–4884.
24. Soukas A, Socci ND, Saatkamp BD, Novelli S, Friedman JM (2001) Distinct transcriptional profiles of adipogenesis in vivo and in vitro. J Biol Chem 276: 34167–34174. doi:10.1074/jbc.M104421200.
25. Hansen JB, Petersen RK, Larsen BM, Bartkova J, Alsner J, et al. (1999) Activation of peroxisome proliferator-activated receptor gamma bypasses the function of the retinoblastoma protein in adipocyte differentiation. J Biol Chem 274: 2386–2393.
26. Rosen ED, Hsu C-H, Wang X, Sakai S, Freeman MW, et al. (2002) C/EBPalpha induces adipogenesis through PPARgamma: a unified pathway. Genes Dev 16: 22–26. doi:10.1101/gad.948702.
27. Pabinger S, Thallinger GG, Snajder R, Eichhorn H, Rader R, et al. (2009) QPCR: Application for real-time PCR data management and analysis. BMC Bioinformatics 10: 268. doi:10.1186/1471-2105-10-268.
28. Bogner-Strauss JG, Prokesch A, Sanchez-Cabo F, Rieder D, Hackl H, et al. (2010) Reconstruction of gene association network reveals a transmembrane protein required for adipogenesis and targeted by PPARγ. Cell Mol Life Sci Cmls 67: 4049–4064. doi:10.1007/s00018-010-0424-5.
29. Sager G, Sandnes D, Bessesen A, Jacobsen S (1985) Adrenergic ligand binding in human serum. Biochem Pharmacol 34: 2812–2815.
30. Essayan DM (2001) Cyclic nucleotide phosphodiesterases. J Allergy Clin Immunol 108: 671–680. doi:10.1067/mai.2001.119555.
31. Schaeffler A, Gross P, Buettner R, Bollheimer C, Buechler C, et al. (2009) Fatty acid-induced induction of Toll-like receptor-4/nuclear factor-kappaB pathway in adipocytes links nutritional signalling with innate immunity. Immunology 126: 233–245. doi:10.1111/j.1365-2567.2008.02892.x.
32. Tang Q-Q, Otto TC, Lane MD (2003) Mitotic clonal expansion: a synchronous process required for adipogenesis. Proc Natl Acad Sci U S A 100: 44–49. doi:10.1073/pnas.0137044100.
33. Tang QQ, Lane MD (2012) Adipogenesis: from stem cell to adipocyte. Annu Rev Biochem 81: 715–736. doi:10.1146/annurev-biochem-052110-115718.
34. Rodriguez D, Rojas-Rivera D, Hetz C (2011) Integrating stress signals at the endoplasmic reticulum: The BCL-2 protein family rheostat. Biochim Biophys Acta 1813: 564–574. doi:10.1016/j.bbamcr.2010.11.012.
35. Guo W, Wong S, Xie W, Lei T, Luo Z (2007) Palmitate modulates intracellular signaling, induces endoplasmic reticulum stress, and causes apoptosis in mouse 3T3-L1 and rat primary preadipocytes. Am J Physiol Endocrinol Metab 293: E576–586. doi:10.1152/ajpendo.00523.2006.
36. Ahrén B, Scheurink AJ (1998) Marked hyperleptinemia after high-fat diet associated with severe glucose intolerance in mice. Eur J Endocrinol Eur Fed Endocr Soc 139: 461–467.
37. Sloan C, Tuinei J, Nemetz K, Frandsen J, Soto J, et al. (2011) Central leptin signaling is required to normalize myocardial fatty acid oxidation rates in caloric-restricted ob/ob mice. Diabetes 60: 1424–1434. doi:10.2337/db10-1106.
38. Kanda T, Brown JD, Orasanu G, Vogel S, Gonzalez FJ, et al. (2009) PPARgamma in the endothelium regulates metabolic responses to high-fat diet in mice. J Clin Invest 119: 110–124. doi:10.1172/JCI36233.
39. Houtkooper RH, Argmann C, Houten SM, Cantó C, Jeninga EH, et al. (2011) The metabolic footprint of aging in mice. Sci Reports 1: 134. doi:10.1038/srep00134.
40. Tontonoz P, Spiegelman BM (2008) Fat and beyond: the diverse biology of PPARgamma. Annu Rev Biochem 77: 289–312. doi:10.1146/annurev.biochem.77.061307.091829.

41. Li P, Fan W, Xu J, Lu M, Yamamoto H, et al. (2011) Adipocyte NCoR knockout decreases PPARγ phosphorylation and enhances PPARγ activity and insulin sensitivity. Cell 147: 815–826. doi:10.1016/j.cell.2011.09.050.
42. Rohana A, Fadzilah Adibah AM, Muhammad Roji MS (2011) Oleate Induces Apoptosis in 3T3-L1 Adipocytes. World Acad Sci Eng Technol: 1–4.
43. Guo W, Wong S, Xie W, Lei T, Luo Z (2007) Palmitate modulates intracellular signaling, induces endoplasmic reticulum stress, and causes apoptosis in mouse 3T3-L1 and rat primary preadipocytes. Am J Physiol Endocrinol Metab 293: E576–586. doi:10.1152/ajpendo.00523.2006.
44. Kim H-K, Della-Fera M, Lin J, Baile CA (2006) Docosahexaenoic acid inhibits adipocyte differentiation and induces apoptosis in 3T3-L1 preadipocytes. J Nutr 136: 2965–2969.
45. Capurso C, Capurso A (2012) From excess adiposity to insulin resistance: the role of free fatty acids. Vascul Pharmacol 57: 91–97. doi:10.1016/j.vph.2012.05.003.

Figure Legends

Figure 1. Abhd15 is a direct and functional PPARγ target gene.

A. Genome organization around the Abhd15 transcription start side (TSS) of 3T3-L1 cells during differentiation with ChIP data of peroxisome proliferator-activated receptor gamma (PPARγ) (day 6 and day 10) and CCAAT-enhancer-binding protein alpha (C/EBPα) (day 10) binding, and Pparγ-Retinoid X receptor (RXRα) direct repeat motif analysis. The data suggest putative PPARγ-RXRα binding ~990 bp and ~440 bp upstream at to the Abhd15 TSS. **B-D.** Abhd15 mRNA levels of 3T3-L1 cells upon PPARγ agonist rosiglitazone (Rosi) treatments. Cells were treated with 1 µM Rosi (**B**) during differentiation, (**C**) for 12 and 24 hours on day 7 of differentiation, and (**D**) for 6, 12, and 24 hours before induction of differentiation, all leading to increased Abhd15 expression. **E.** Abhd15 mRNA expression in Pparγ -/- and Pparγ +/- mouse embryonic fibroblasts (MEFs). Abhd15 is hardly expressed in Pparγ -/- MEFs and can only be further increased upon addition of Rosi (1 µM) in Pparγ +/- MEFs. **F.** Sequence map of the sequences containing either one (F2 and F3) or two (F1) of the putative PPARγ-RXRα binding sites, evaluated in figure A, used for the luciferase assay. **G.** 3 regions of interest located upstream of the Abhd15 gene were cloned into luciferase reporter vectors (named pGL4.21-F1, pGL4.26-F2, pGL4.21-F3) and cotransfected with either Pparγ/Rxrα expressing vectors or an empty vector (pCMX) into Cos7 cells. The luciferase activity of pGL4.21-F1 and pGL4.21-F3, both containing the putative PPARγ-RXRα binding site ~440 bp upstream to the TSS, were significantly increased when compared to pCMX-transfected cells. Addition of Rosi to cells cotransfected with pGL4.21-F1 or pGL44.21-F3 and Pparγ/Rxrα, again significantly increased luciferase activity.

Data is presented as mean ± SD from at least three independent experiments. Statistical significance was determined using the two-tailed Student's t test. *p<0.05, **p<0.01, ***p<0.001.

Figure 2. Abhd15 expression is regulated during adipogenesis and decreased by elevated free fatty acid levels.

A-B. Abhd15 mRNA expression is increased during adipocyte differentiation of (**A**) OP9 cells, mouse embryonic fibroblasts (MEFs), and (**B**) human Simpson-Golabi-Behmel syndrome (SGBS) cells. **C.** Abhd15 mRNA is highly expressed in brown and white adipose tissue (BAT and WAT), to a lower extent in liver (Liv), and hardly in skeletal (SM) and cardiac muscle (CM) of wild-type mice in the fed state. **D.** Abhd15 mRNA expression is decreased in WAT and BAT of genetically obese mice (ob/ob) compared to wild type (wt) mice. **E.** Mice fed a high fat diet (HFD, 60% calories in fat) show a decreased Abhd15 mRNA expression in WAT already after 3 days, but still after 15 weeks on this diet. Additionally, aging strongly

decreases Abhd15 mRNA levels. **F.** Abhd15 mRNA expression is regulated depending on the nutritional status in mouse tissues. Upon fasting, the expression is decreased in both BAT and WAT. **G.** Simulated fasting of fully differentiated 3T3-L1 cells (day 7 of differentiation) with IBMX (0.5 mM) and isoproterenol (10 µM) for 2 hours resulted in reduced Abhd15 mRNA expression. **H.** Treatment of fully differentiated 3T3-L1 cells (day 7 of differentiation) with palmitic acid (100 µM) strongly reduces Abhd15 mRNA expression.
Data is presented as mean ± SD from at least three independent experiments. Statistical significance was determined using the two-tailed Student's t test. *p<0.05, **p<0.01.

Figure 3. Abhd15 expression is required for adipogenesis

A-D. 3T3-L1 cells were infected with lentiviral particles coding for Abhd15 shRNA (Abhd15_sil) or using a non-target shRNA as control (ntc), selected for puromycin resistance, expanded as a mixed population and differentiated. **A.** Silencing efficiency during adipogenesis of two knock-down lentiviruses against Abhd15, determined by qPCR assay. **B.** Protein was harvested at day 4 of differentiation of control (ntc) and Abhd15-silenced 3T3-L1 cells (Abhd15_sil1) and subjected to western blotting using the anti-Abhd15 antibody. β-actin served as loading control. Abhd15 protein expression is decreased in Abhd15-silenced 3T3-L1 cells compared to control cells. n=2 **C.** Silencing of Abhd15 impairs adipogenesis, indicated by the strongly decreased amount of neutral lipids on day 7 of differentiation, stained with Oil red O. **D.** Stable silencing of Abhd15 in 3T3-L1 cells shows high influences on the expression levels of various important adipogenic genes on day 5 of differentiation (Cebpα, Pparγ, fatty acid binding protein 4 (Fabp4), fatty acid synthase (Fasn)). **E.** Transient silencing of Abhd15 by electroporation of siRNAs on day 8 of differentiation did not show any effects onto the mRNA levels of adipogenic genes in fully differentiated 3T3-L1 fibroblasts (day 10).
Data is presented as mean ± SD from at least three independent experiments if not otherwise stated. Statistical significance was determined using the two-tailed Student's t test. *p<0.05, **p<0.01, ***p<0.001.

Figure 4. Abhd15 expression is tightly connected to apoptosis

A-H. 3T3-L1 cells were infected with lentiviral particles coding for Abhd15 shRNA (Abhd15_sil) using a non-target shRNA as control (ntc), selected for puromycin resistance, and expanded as a mixed population. **A.** After inducing 3T3-L1 cells to differentiate, Pparγ mRNA expression did not increase to the same extent in Abhd15-silenced cells as in control cells. **B.** Silencing efficiency of Abhd15 on mRNA level in preconfluent cells reached ~30%. **C.** Cell proliferation is reduced in Abhd15-silenced preconfluent 3T3-L1 cells, shown by the decreased cell number compared to control cells 48 hours after seeding. **D.** The colorimetric

proliferation assay (MTS) showed a reduction in proliferation of preconfluent Abhd15-silenced cells by ~20 %. **E.** Analysis of preconfluent 3T3-L1 cells, using BrdU FACScan, showed a strongly elevated SubG1 peak, pointing towards increased apoptosis. **F-G.** Western blot (**F**) and relative WB signal (**G**) of the essential regulators of apoptosis B-cell lymphoma 2 (BCL-2) and BCL-2-associated X protein (BAX). The protein expression of the pro-survival regulator BCL-2 was decreased, while the protein level of the pro-apoptotic regulator BAX increased. n=2 **H.** Increased Caspase 3/7 activity could be measured in preconfluent Abhd15-silenced 3T3-L1 cells, proofing increased apoptosis. **I.** 24 hours treatment of preconfluent 3T3-L1 cells with palmitic acid concentrations, reaching from non-apoptotic (100 μM) to apoptosis-inducing (500 μM) [43], increased Abhd15 mRNA expression dose dependently.
Data is presented as mean ± SD from at least three independent experiments if not otherwise stated. Statistical significance was determined using the two-tailed Student's t test. *p<0.05, **p<0.01, ***p<0.001.

Supporting Figure. 1.-3. 3T3-L1 cells were infected with lentiviral particles obtained from phoenix cells transfected with either empty pMSCVpuro vector (pMSCVpuro) or a vector containing the Abhd15 gene (pMSCV-Abhd15). After transduction, 3T3-L1 cells were selected with puromycin and expanded as a mixed population **1.** Relative mRNA expression of Abhd15 in preconfluent 3T3-L1 cells stably overexpressing Abhd15 compared to control cells. **2.** Overexpression of Abhd15 does not affect adipogenesis when compared to control cells, indicated by similar neutral lipid staining on day 7 of differentiation. **3.** Cell proliferation was slightly increased in Abhd15 overexpressing preconfluent 3T3-L1 cells, shown by an upwards trend in the cell number 48 hours after seeding. **4.** 3T3-L1 cells were infected with lentiviral particles coding for Abhd15 shRNA (Abhd15_sil) using a non-target shRNA as control (ntc), selected for puromycin resistance and expanded as a mixed population. Analysis of the certain stages of cell division, using BrdU FACScan, revealed no differences in the S phase peak between preconfluent Abhd15-silenced 3T3-L1 and control cells.
Data is presented as mean ± SD from at least three independent experiments.

Figure 1

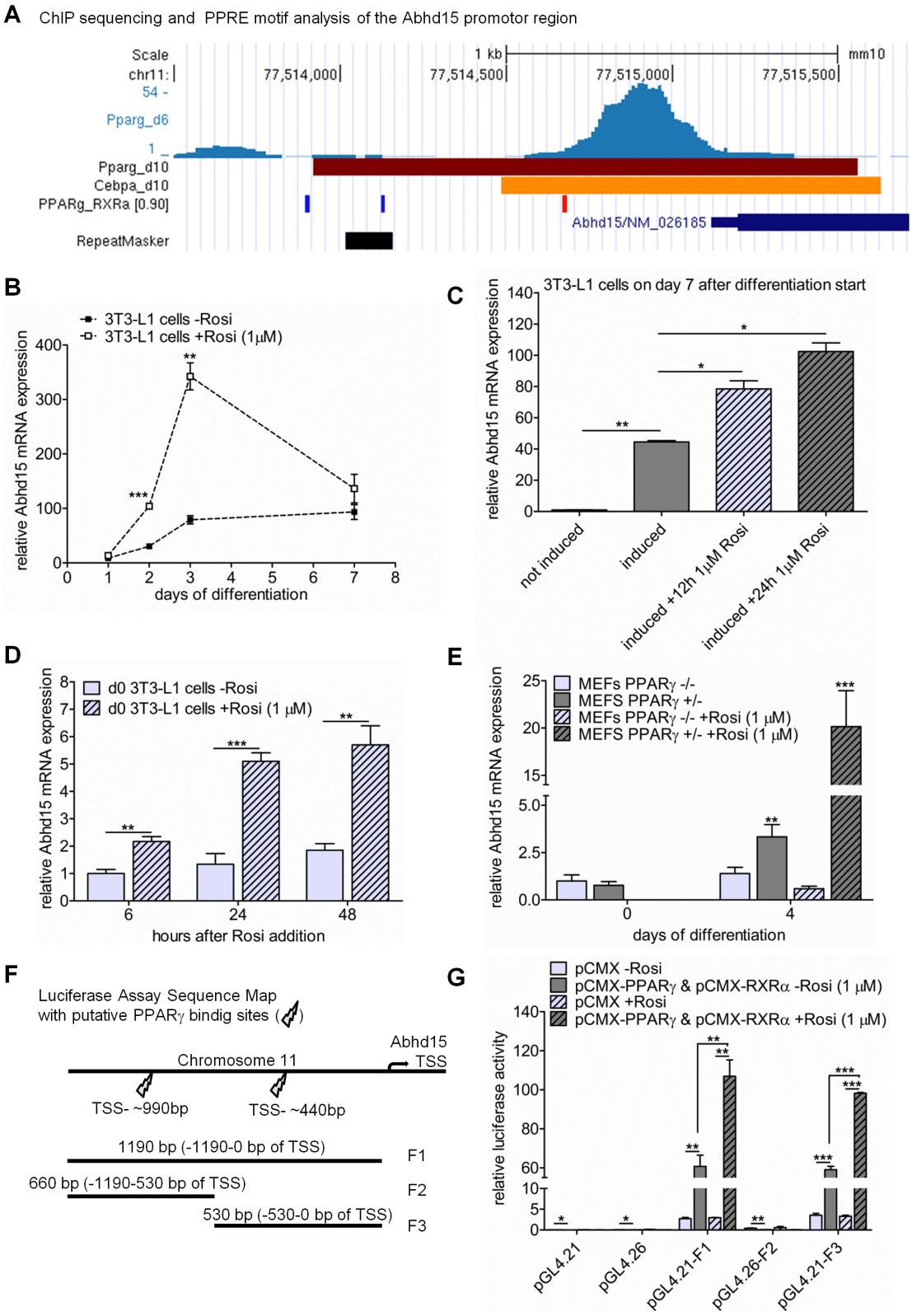
A
ChIP sequencing and PPRE motif analysis of the Abhd15 promotor region
Scale
chr11:
77,514,000
1 kb
77,514,500
77,515,000
77,515,500
mm10
Pparg_d6
Pparg_d10
Cebpa_d10
PPARg_RXRa [0.90]
Abhd15/NM_026185
RepeatMasker
B
3T3-L1 cells -Rosi
3T3-L1 cells +Rosi (1μM)
relative Abhd15 mRNA expression
days of differentiation
C
3T3-L1 cells on day 7 after differentiation start
relative Abhd15 mRNA expression
not induced
induced
induced +12h 1μM Rosi
induced +24h 1μM Rosi
D
d0 3T3-L1 cells -Rosi
d0 3T3-L1 cells +Rosi (1 μM)
relative Abhd15 mRNA expression
hours after Rosi addition
E
MEFs PPARγ -/-
MEFS PPARγ +/-
MEFs PPARγ -/- +Rosi (1 μM)
MEFS PPARγ +/- +Rosi (1 μM)
relative Abhd15 mRNA expression
days of differentiation
F
Luciferase Assay Sequence Map
with putative PPARγ bindig sites
Chromosome 11
Abhd15
TSS
TSS- ~990bp
TSS- ~440bp
1190 bp (-1190-0 bp of TSS)
F1
660 bp (-1190-530 bp of TSS)
F2
530 bp (-530-0 bp of TSS)
F3
G
pCMX -Rosi
pCMX-PPARγ & pCMX-RXRα -Rosi (1 μM)
pCMX +Rosi
pCMX-PPARγ & pCMX-RXRα +Rosi (1 μM)
relative luciferase activity
pGL4.21
pGL4.26
pGL4.21-F1
pGL4.26-F2
pGL4.21-F3

Figure 2

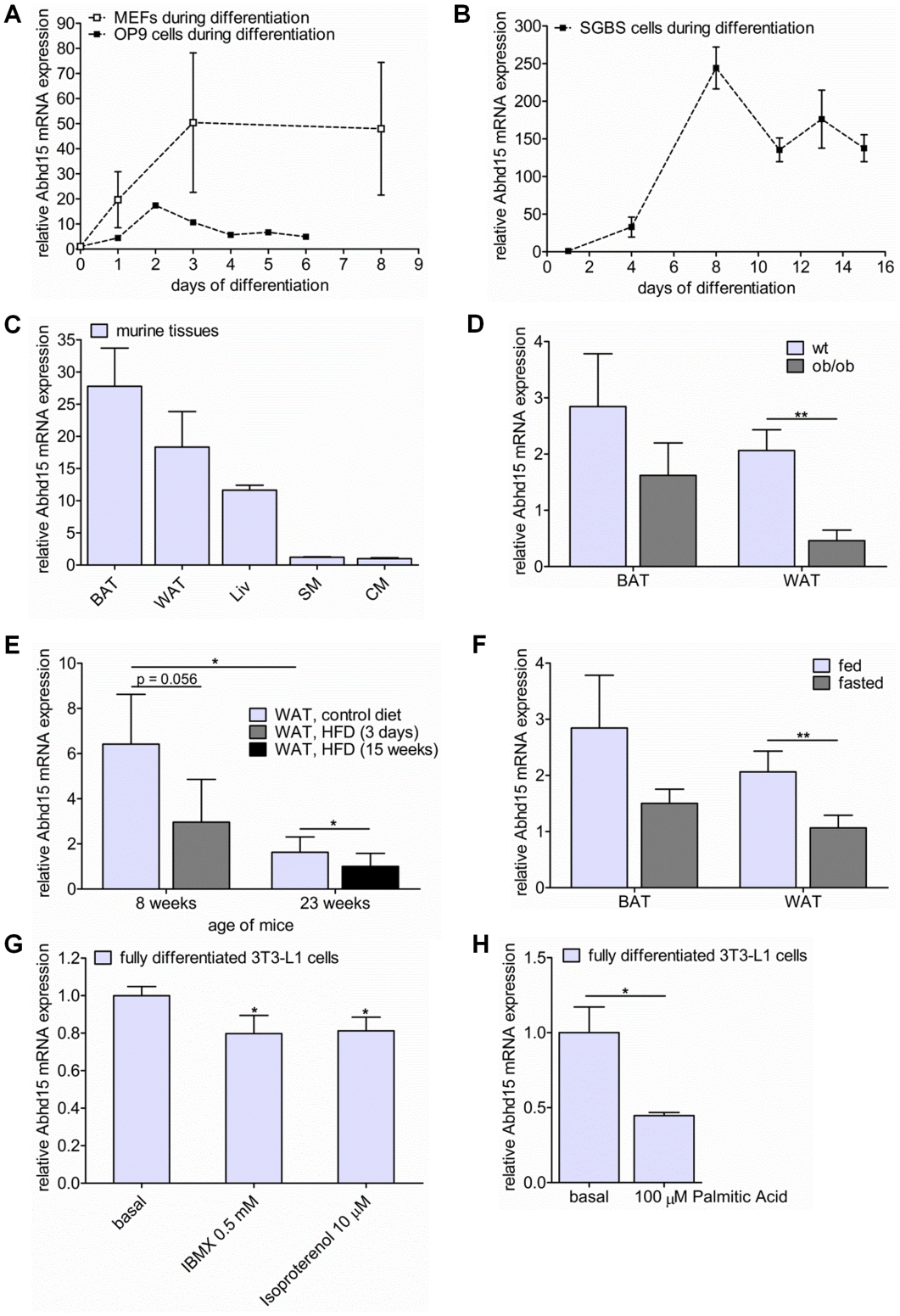
A
MEFs during differentiation
OP9 cells during differentiation
relative Abhd15 mRNA expression
days of differentiation
B
SGBS cells during differentiation
relative Abhd15 mRNA expression
days of differentiation
C
murine tissues
relative Abhd15 mRNA expression
BAT
WAT
Liv
SM
CM
D
wt
ob/ob
relative Abhd15 mRNA expression
**
BAT
WAT
E
p = 0.056
*
*
WAT, control diet
WAT, HFD (3 days)
WAT, HFD (15 weeks)
relative Abhd15 mRNA expression
8 weeks
23 weeks
age of mice
F
fed
fasted
relative Abhd15 mRNA expression
**
BAT
WAT
G
fully differentiated 3T3-L1 cells
relative Abhd15 mRNA expression
*
*
basal
IBMX 0.5 mM
Isoproterenol 10 µM
H
fully differentiated 3T3-L1 cells
relative Abhd15 mRNA expression
*
basal
100 µM Palmitic Acid

Figure 3

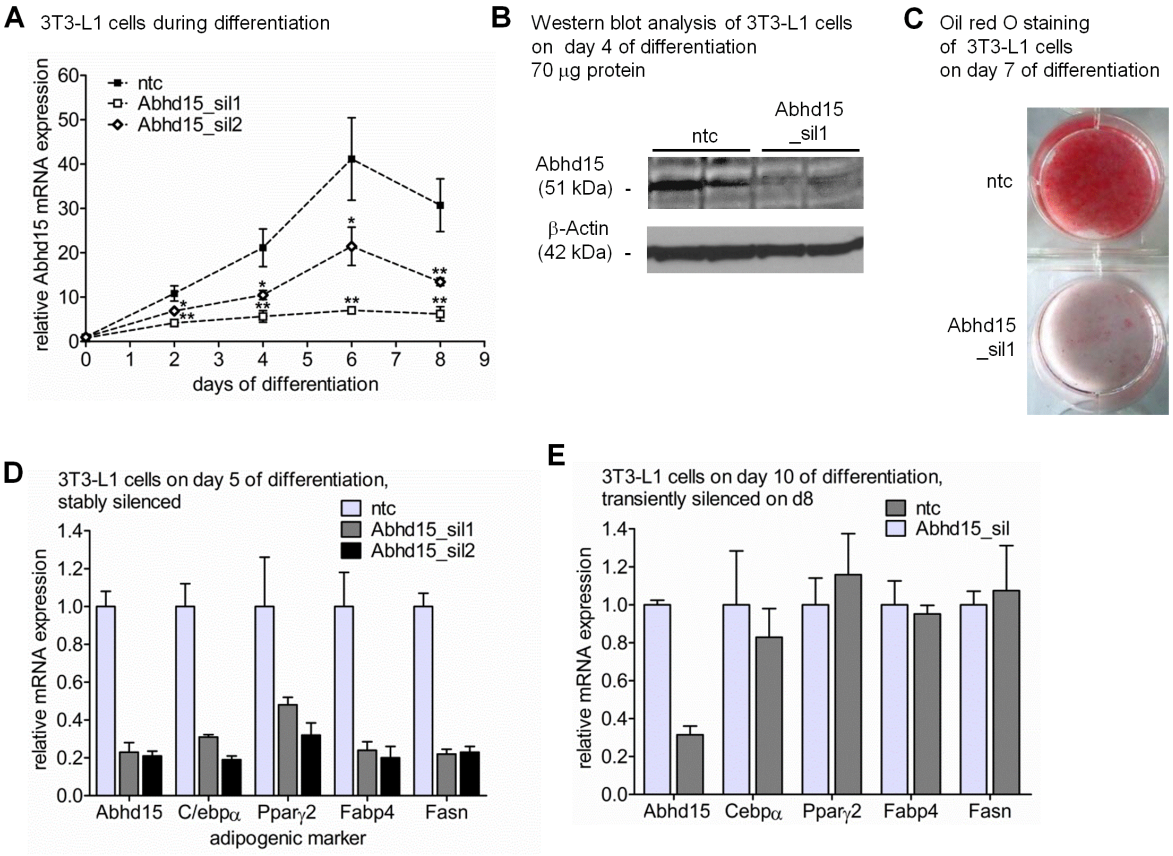
A
3T3-L1 cells during differentiation
ntc
Abhd15_sil1
Abhd15_sil2
relative Abhd15 mRNA expression
days of differentiation
B
Western blot analysis of 3T3-L1 cells
on day 4 of differentiation
70 µg protein
ntc
Abhd15 _sil1
Abhd15 (51 kDa)
β-Actin (42 kDa)
C
Oil red O staining
of 3T3-L1 cells
on day 7 of differentiation
ntc
Abhd15 _sil1
D
3T3-L1 cells on day 5 of differentiation,
stably silenced
ntc
Abhd15_sil1
Abhd15_sil2
relative mRNA expression
Abhd15
C/ebpα
Pparγ2
Fabp4
Fasn
adipogenic marker
E
3T3-L1 cells on day 10 of differentiation,
transiently silenced on d8
ntc
Abhd15_sil
relative mRNA expression
Abhd15
Cebpα
Pparγ2
Fabp4
Fasn

Figure 4

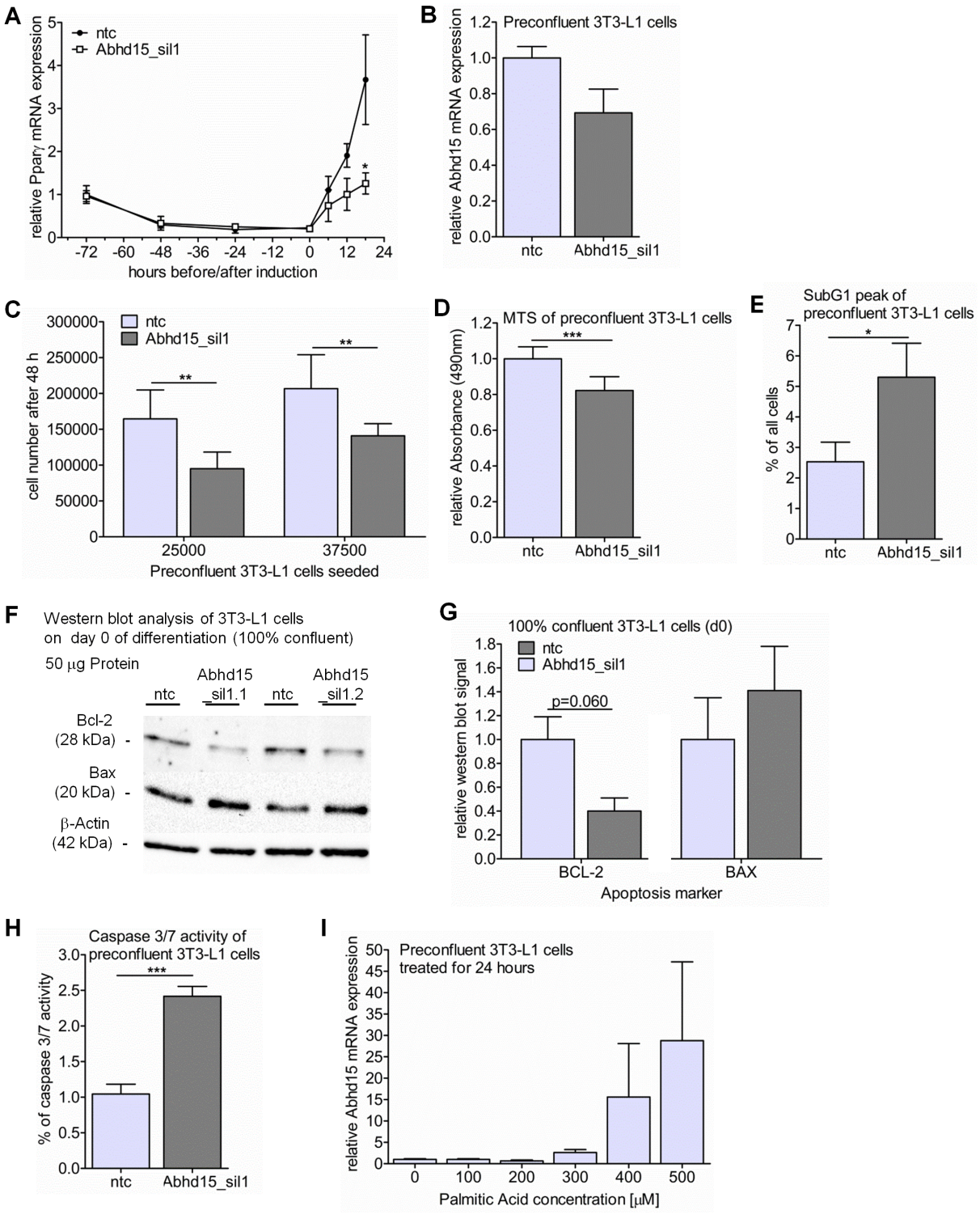
A
ntc
Abhd15_sil1
relative Pparγ mRNA expression
hours before/after induction
B
Preconfluent 3T3-L1 cells
relative Abhd15 mRNA expression
C
cell number after 48 h
Preconfluent 3T3-L1 cells seeded
D
MTS of preconfluent 3T3-L1 cells
relative Absorbance (490nm)
E
SubG1 peak of preconfluent 3T3-L1 cells
% of all cells
F
Western blot analysis of 3T3-L1 cells on day 0 of differentiation (100% confluent)
50 µg Protein
Bcl-2 (28 kDa)
Bax (20 kDa)
β-Actin (42 kDa)
G
100% confluent 3T3-L1 cells (d0)
p=0.060
relative western blot signal
BCL-2
BAX
Apoptosis marker
H
Caspase 3/7 activity of preconfluent 3T3-L1 cells
% of caspase 3/7 activity
I
Preconfluent 3T3-L1 cells treated for 24 hours
relative Abhd15 mRNA expression
Palmitic Acid concentration [µM]

8 Appendix

Supporting Figure